

Understanding cell division and its
regulation in the human pathogenic
bacterium, *Vibrio parahaemolyticus*

Dissertation

Zur Erlangung des akademischen Grades

Des Doktors der Naturwissenschaften

(Dr.rer.nat.)

dem Fachbereich Biologie
der Philipps-Universität Marburg
vorgelegt

von

SAMADA MURALEEDHARAN

aus Indien

Marburg (Lahn), October 2018

Die Untersuchungen zur vorliegenden Arbeit wurden von Oktober 2014 bis September 2018 am Max-Planck-Institut für terrestrische Mikrobiologie unter der Leitung von Dr. Simon Ringgaard durchgeführt.

Vom Fachbereich Biologie der Philipps-Universität Marburg als Dissertation angenommen am _____._____.2018

Erstgutachter: Dr. Simon Ringgaard

Zweitgutachter: Prof. Dr. Martin Thanbichler

Weitere Mitglieder der Prüfungskommission:

Prof. Dr. Knut Drescher

Prof. Dr. Uwe Maier

Tag der mündlichen Prüfung: 28.11.2018

Die während der Promotion erzielten Ergebnisse wurden zum Teil in folgenden Originalpublikationen veröffentlicht:

Muraleedharan, S., Freitas, C., Mann, P., Glatter, T. and Ringgaard, S. (2018).

A cell length-dependent transition in MinD-dynamics promotes a switch in division-site placement and preservation of proliferating elongated *Vibrio parahaemolyticus* swarmer cells. *Molecular Microbiology* 109(3): 365-384

Unpublished work:

Muraleedharan, S., Heering, J. & Ringgaard, S. ParA-like protein, ParC regulates cell division in swarmer cells of *Vibrio parahaemolyticus* (in preparation).

അച്ചുൻ

TABLE OF CONTENTS

TABLE OF CONTENTS	1
TABLE OF FIGURES	3
ABSTRACT	5
ZUSAMMENFASSUNG	7
1. CHAPTER I	9
INTRODUCTION	9
1.1. Bacterial cell division	11
1.2. FtsZ: the central component of divisome	12
1.3. Cell constriction: FtsZ ring or the PG synthetic machinery?	13
1.4. Chromosome organization - a brief comparison.....	14
1.5. Chromosome replication and its effect on cell division	16
1.6. Negative regulation by Nucleoid Occlusion (NO)	18
1.7. Negative regulation of FtsZ by the Min system	20
1.8. Negative regulation of FtsZ by MipZ	25
1.9. Positive regulation of FtsZ by PomZ	27
1.10. Other known regulators of Z-ring placement.....	27
1.11. Involvement of ParA/MinD-like proteins in cell division.....	28
1.12. ParA-like protein ParC and chemotaxis.....	30
1.13. Cell division in <i>Vibrios</i>	33
1.14. <i>Vibrio parahaemolyticus</i> : a model for cell division	35
1.15. Scope of the research	37
2. CHAPTER II	39
RESULTS.....	39
2.1. Part I-Understanding the classical regulators of cell division.....	41
2.2. Part II-Cell type specific regulation of cell division by ParC in <i>Vibrio parahaemolyticus</i>	72
3. CHAPTER III	85
DISCUSSION	85
3.1. FtsZ forms distinct localization patterns in the swimmer cells	87
3.2. Daughter cells of the swimmer cell cycle inherit replicating chromosomes...	87
3.3. Min, NO and their role in division of swimmer cells	89
3.4. Cell division in swarmer cells	90
3.5. Role of Min and NO in division of swarmer cells	92
3.6. Ensuring the preservation of long swarmer cells.....	94

3.7. A model summarizing the processes leading to an asymmetric cell division in swarmer cells.....	95
3.8. Cell type specific regulation of cell division by ParC in swarmer cells.	97
3.9. Conclusions and outlook	100
4. CHAPTER IV.....	103
MATERIALS AND METHODS.....	103
4.1. Chemicals, equipment and software.....	105
4.2. Media, buffers and solutions.....	107
4.3. Microbiological Methods	108
4.4. Molecular cloning	109
4.5. Microscopic methods.....	120
4.6. Biochemical methods	123
REFERENCES	129
ACKNOWLEDGEMENTS	141
CURRICULUM VITAE.....	143
ERKLÄRUNG	145
EINVERSTÄNDNISERKLÄRUNG.....	147

TABLE OF FIGURES

Figure 1: Spatial organization of bacterial chromosomes.....	15
Figure 2: Nucleoid occlusion.....	20
Figure 3: Spatial and temporal regulation of Z-ring assembly by the Min system.....	22
Figure 4: Regulation of FtsZ localization by MipZ in <i>Caulobacter crescentus</i>	26
Figure 5: In <i>V. cholerae</i> , localization of ParB1 is governed by ParA1 which in turn is localized by HubP.	33
Figure 6: <i>Vibrio parahaemolyticus</i> swimmer cell and swarmer cell.	36
Figure 7: Sequence conservation of FtsZ, SlmA, and MinD in <i>V. parahaemolyticus</i> in comparison to other bacterial model organisms.	42
Figure 8: Polar FtsZ localization transitions to mid-cell upon the onset of cell division in swimmer cells of <i>V. parahaemolyticus</i>	43
Figure 9: Schematic depicting the consensus sequence (sequence logo) of <i>parS1</i> and <i>parS2</i> centromere sites and their location on <i>V. parahaemolyticus</i> chromosome 1 and 2, respectively.	44
Figure 10: Specific DNA binding properties of ParB1 and ParB2.....	45
Figure 11: Proper ParB1 localization in <i>V. parahaemolyticus</i> swimmer cells is dependent on ParA1.....	46
Figure 12: Segregation of chromosome II is not likely dependent on ParA1 in swimmer cells of <i>V. parahaemolyticus</i>	48
Figure 13: A cell length-dependent switch in the positioning of the Z-ring and division site in swarmer cells.	49
Figure 14: MinCDE system regulates cell division in both swimmer cells and swarmer cells of <i>V. parahaemolyticus</i>	52
Figure 15: Min system regulates the LD site divisions.	53
Figure 16: Absence of SlmA exerts significant elongation in swimmer cells when deleted alone and severe elongation on deletion together with Min system.	54
Figure 17: The Min-system regulates cell division and the proper transition from mid-cell to non-mid-cell LD-site division in swarmer cells.	55
Figure 18: Effect of <i>minCDE</i> deletion and <i>slmA</i> deletion in FtsZ localization in swarmer cells.....	57
Figure 19: Pole-to-pole MinD oscillation in swimmer cells of <i>V. parahaemolyticus</i>	58
Figure 20: A cell length-dependent switch from pole-to-pole to multi-node standing-wave oscillation of MinD.....	59
Figure 21: Localization dynamics of YFP-MinD in artificially elongated planktonic cells..	60
Figure 22: The LD-division site is positioned at the utmost pole-proximal MinD-node.....	62

Figure 23: Equidistant segregation of the chromosomal origins in polyploid swarmer cells.	63
Figure 24: Cell length-dependent switch in the site of complete chromosome segregation correlates with the position of the division site.	65
Figure 25: Formation of multiple division sites in artificially elongated planktonic cells correlates with positions of complete chromosome segregation.	67
Figure 26: The FtsZ protein level of swarmer cells is similar to that of planktonic cells..	67
Figure 27: Overexpression of FtsZ results in the formation of multiple Z-rings in swarmer cells, reduced swarmer cell length and swarming behavior.	68
Figure 28: All cells from swarm flares have initiated the swarm program independent of their length.	69
Figure 29: Asymmetric division results in the formation of progeny cells with distinct swimming capabilities and drives population heterogeneity.....	71
Figure 30: ParC exerts specific developmental regulation of cell division.	73
Figure 31: ParC prevents polar localization of FtsZ in swarmer cells.....	74
Figure 32: Deletion of <i>parC</i> does not affect cell division in swimmer cells.	76
Figure 33: An ATP-driven ParC cycle is required for its regulation of FtsZ localization. ..	78
Figure 34: Intracellular localization of ParC is regulated by its ATPase cycle and DNA binding.	80
Figure 35: ParC's ATPase cycle and DNA binding determines its effects on polar FtsZ.	81
Figure 36: ParC actively prevents polar division events through direct interaction with FtsZ.....	83
Figure 37: Cell division in swarmer cells of <i>Vibrio parahaemolyticus</i>	96
Figure 38: Development cycle of <i>Vibrio parahaemolyticus</i>	101

ABSTRACT

Bacteria undergo a well-orchestrated cell division process with a highly regulated placement of the division site in order to generate progeny cells with complete hereditary information. Thus, bacteria have evolved mechanisms to govern the spatio-temporal dynamics and localization of cell division proteins in accordance with the cell cycle. Cell division needs to be particularly tightly regulated in differentiating bacteria where changes between different cell morphologies increases the complexity of the process. *Vibrio parahaemolyticus* exists as swimmer and swarmer cells, specialized for growth in liquid and on solid environments, respectively. Swarmer cells are highly elongated by a probable regulated inhibition of cell division. But, these cells still need to divide in order to proliferate and expand the colony. The regulators that facilitate the drastically different cell sizes between the two cell types and the factors that control their cell divisions are unknown. Here we show that swarmer cells of all lengths undergo cell divisions, but the placement of the division site is cell length-dependent. The short swarmer cells divide at mid-cell whereas the long swarmer cells divide at a non-mid-cell (pole-proximal) division site. We show that the transition to non-mid-cell positioning of the division site is cell length-dependent. Our research reveals that *V. parahaemolyticus* uses the Min system to mark the length-dependent (LD) division site in the swarmer cells. Through microscopy experiments we demonstrate that the dynamics of the division regulator MinD switches from a pole-to-pole oscillation in short swarmer cells to a multi-node standing-wave oscillation in long swarmer cells. Additionally, the regulation of FtsZ levels restricts the number of divisions to one per cell cycle and the nucleoid occlusion determinant SlmA ensures sufficient free FtsZ to sustain Z-ring formation by preventing sequestration of FtsZ into division deficient clusters over the nucleoid. We also show that, in spite of several Min minima that arise during a standing wave oscillation of MinD, the cell divides at the utmost pole-proximal Min minimum. By limiting the number of division events to one per cell, *V. parahaemolyticus* promotes the preservation of long swarmer cells and permits swarmer cell division without the need for dedifferentiation. Additionally, we show that the ParA-like ATPase, ParC, that has previously been described to be the cell pole-determinant in *Vibrios*, also regulates the localization of the major cell division protein FtsZ in swarmer cells, and thereby prevents polar division events. Altogether, this work sheds light to the study of cell division in the di-morphic pathogenic bacterium, *V. parahaemolyticus*. For the first time, we demonstrate a cell length-dependent division site placement in naturally occurring bacteria by employing Min oscillation. The identification of ParC as a protein of dual-function ties together the spatio-temporal regulation of diverse

ABSTRACT

processes such as bacterial chemotaxis, cell pole development and regulation of cell division.

ZUSAMMENFASSUNG

Bakterien durchlaufen einen hochgradig organisierten Zellteilungsprozess bei welchem die Platzierung der Zellteilungsmaschinerie präzise reguliert ist. Dadurch wird sichergestellt, dass Tochterzellen mit vollständigen Erbinformationen erzeugt werden. So haben Bakterien Mechanismen entwickelt, um die räumlich-zeitliche Dynamik und Lokalisation von Zellteilungs-Proteinen in Übereinstimmung mit dem Zellzyklus zu steuern. Die Zellteilung muss bei der Differenzierung von Bakterien besonders stark reguliert werden, wenn Veränderungen zwischen verschiedenen Zellmorphologien die Komplexität des Prozesses erhöhen. *Vibrio parahaemolyticus* existiert als Schwimmer- und Schwärmerzelle, spezialisiert auf das Wachstum in flüssiger bzw. fester Umgebung. Schwärmerzellen sind vermutlich durch eine regulierte Hemmung der Zellteilung während der Differenzierung stark verlängert. Dennoch müssen sich diese Zellen teilen, um die Kolonie zu vermehren und zu erweitern. Die Regulatoren, welche die drastisch unterschiedlichen Zellgrößen zwischen den beiden Zelltypen (Schwimmer und Schwärmer) ermöglichen und die Faktoren, die ihre Zellteilung steuern, sind unbekannt. Hier zeigen wir, dass Schwärmerzellen jeglicher Zelllängen Teilungen durchlaufen, jedoch die Platzierung der Teilungsstelle zelllängenabhängig ist. Kurze Schwärmerzellen teilen sich in der Mitte der Zelle, während lange Schwärmerzellen die Teilungsstelle näher am Zellpol platzieren (Pol-proximal). Wir zeigen, dass der Übergang zur Pol-proximalen Platzierung der Teilungsstelle zelllängenabhängig ist. Unsere Forschung zeigt außerdem, dass *V. parahaemolyticus* das Min-System verwendet, um die längenabhängige (LD) Teilungsstelle in den Schwärmerzellen zu markieren. Durch mikroskopische Experimente zeigen wir, dass die Dynamik des Teilungsregulators MinD von einer Pol-zu-Pol-Schwingung in kurzen Schwärmerzellen zu einer Multi-Knoten-Stehwellenschwingung in langen Schwärmerzellen wechselt. Zusätzlich beschränkt die Regulierung des FtsZ-Spiegels die Anzahl der Teilungen auf eine pro Zellzyklus. Hinzukommend verhindert SlmA die Z-Ring-Bildung über dem Nukleoid, indem es freie FtsZ Moleküle sequestriert und deren Polymerisation unterbindet. Wir zeigen auch, dass sich die Zelle trotz mehrerer Min-Minima, die bei einer Stehwellenschwingung von MinD entstehen, am äußersten, polgelegenen Min-Minimum teilt. Durch die Begrenzung der Anzahl der Teilungsereignisse auf ein Ereignis pro Zellteilung, fördert *V. parahaemolyticus* den Erhalt langer Schwärmerzellen und ermöglicht die Schwärmerzellteilung ohne Dedifferenzierung. Darüber hinaus zeigen wir, dass die ParA-ähnliche ATPase, ParC, die zuvor als Zellpoldeterminant in *Vibrios* beschrieben wurde, auch die Lokalisation des Zellteilungs-Proteins FtsZ in Schwärmerzellen reguliert und damit Zellteilungsereignisse in Polnähe verhindert. Wir demonstrieren zum ersten Mal

ZUSAMMENFASSUNG

eine zelllängenabhängige Platzierung des Zellteilungsapparates in natürlich vorkommenden Bakterien. Die Identifizierung von ParC als Protein mit Doppelfunktion verbindet die räumlich-zeitliche Regulation verschiedener Prozesse wie bakterielle Chemotaxis, Zellpolentwicklung und Regulation der Zellteilung.

CHAPTER I

INTRODUCTION

1.1. Bacterial cell division

Bacterial cell division broadly consists of a chromosome replication and segregation step, and a septum formation and a cell body separation step (cytokinesis). Unlike in eukaryotes, both these steps occur simultaneously in bacteria. DNA replication and segregation stay highly coordinated with the cell separation as accurate inheritance of complete genetic material is essential for proper colony maintenance. The division of the mother cell is achieved by a macromolecular protein complex called the divisome. FtsZ, a tubulin homologue, assembles into a ringlike structure, called the Z-ring, at the incipient division site and acts as the central component of the divisome (Bi & Lutkenhaus, 1991; Erickson, 1995). The Z-ring acts as a scaffold and recruits the downstream cell division proteins resulting in the formation of the structure known as the divisome or septal ring (Aarsman et al., 2005; Gamba et al., 2009).

Divisome formation has been thoroughly studied in *Escherichia coli* and following are some of the proteins that have been discovered to play diverse and important functions to sustain the divisome. Several Z-ring associated proteins like ZapA, ZapB, ZapC and ZapD are involved in promoting lateral interactions of FtsZ protofilaments (Durand-Heredia et al., 2011; Gueiros-filho & Losick, 2002; Hale et al., 2011). FtsA - an actin homologue (Dai & Lutkenhaus, 1992) and ZipA - an inner membrane protein (Hale & De Boer, 1997) act to associate FtsZ with the inner membrane. The Z-ring is stabilized by FtsA and ZipA (the proto-ring), which then recruits FtsK, the DNA translocase that sorts chromosomal DNA to the daughter cells (Begg et al., 1995; Bigot et al., 2005). Other important proteins that are recruited include the penicillin-binding proteins (PBPs) like PBP3 in *E. coli*, the FtsW and FtsN. The peptidoglycan synthase PBP3 generates the peptidoglycan (PG) required for the establishment of the division septum (Pogliano et al., 1997). Although a flippase activity was earlier proposed for FtsW (Mohammadi et al., 2011), it was later proved that the transport of PG precursors across the cytoplasmic membrane was in fact carried out by MurJ (Sham et al., 2014). FtsN, one of the late recruits to the divisome, activates the PG synthesis through its interaction with PBP3, thereby resulting in recruitment of the other enzymes leading to constriction of the septum (Addinall et al., 1997; Gerding et al., 2009; Rico et al., 2010).

Formation of the divisome is an important hierarchical process during cell division and hence needs to be highly coordinated. Therefore, regulating cell division largely also points towards a spatio-temporal regulation of divisome formation and hence that of FtsZ.

1.2. FtsZ: the central component of divisome

Identification of FtsZ resulted from a search to find out the reason behind filamentation of *E. coli* cells on DNA damage (van de Putte et al. 1964). Several *fts* (filamentous growth is thermosensitive) genes and others were identified following this study. Subsequently the *ftsZ* locus was also identified, which was later suggested to be a bacterial cytoskeletal protein (Bi & Lutkenhaus, 1991; Lutkenhaus et al., 1980).

FtsZ was discovered to be a homologue to eukaryotic cytoskeletal protein tubulin subsequently by three research groups (De Boer et al., 1992; Mukherjee et al., 1993; RayChaudhuri & Park, 1992). A conserved sequence of GGGTGTG in FtsZ is almost like the G/AGGTGSG sequence (also known as the tubulin signature sequence) in all tubulins that is involved in GTP binding. With the resolution of the structures of the two proteins, FtsZ and tubulin, their homology was confirmed (Löwe & Amos, 1998; Nogales et al., 1998).

FtsZ is a cytoplasmic protein. It is a GTPase and can polymerize in a head to tail fashion forming filaments (protofilaments) which can further bundle to form polymers of higher order structures. Based on sequence homology across species, FtsZ is broadly divided into four regions – (i) a poorly conserved N-terminal peptide, (ii) the highly conserved core, (iii) the C-terminal linker (CTL) and (iv) a C-terminal conserved peptide (CTC). The function of the variable N-terminal segment is not exactly determined. The conserved core consists of the tubulin signature motif and is the region responsible for GTP binding and hydrolysis. This leads to the polymerization of FtsZ into filaments. The core has been shown to consist of two segments – (a) The N-terminal (Nt) core consisting of the GTP binding site and binds the bottom of the adjacent monomer of the FtsZ protofilament and (b) the C-terminal (Ct) core that binds the top of the adjacent monomer (Oliva et al., 2004). The CTC is the binding site for several regulators of FtsZ like Clp proteins (Williams et al., 2014) as well for the membrane anchors that tether this cytoplasmic protein to the inner membrane, like FtsA (Din et al., 1998) and SepF (Duman et al., 2013; Król et al., 2012). The region between the GTPase domain and the CTC is CTL, an unstructured region. It displays a broad range of length and is described to be important for the polymer structure and dynamics through its regulation of lateral interaction of the protofilaments (Buske & Levin, 2013; Sundararajan & Goley, 2017). Also, an intact CTL in *C. crescentus* ensures a proper peptidoglycan synthesis whereas deletions of different lengths of this region leads to defective peptidoglycan synthesis and an eventual cell lysis (Sundararajan et al., 2015).

1.3. Cell constriction: FtsZ ring or the PG synthetic machinery?

Extensive studies have been carried out to identify the force generator that constricts the parent cell. FtsZ is a GTPase and the energy released from GTP hydrolysis can be converted to mechanical energy. Additionally, FtsZ can polymerize and a biological polymer can generate force using its physical properties like stiffness, curvature (Jensen et al., 2015) and polymerization-depolymerization ability. When reconstituted in liposomes, FtsZ linked to membrane tethering sequences could result in indentations on the liposomes (Osawa et al., 2008, 2009). Using FtsA to direct FtsZ to the membrane resulted in complete fission of the liposomes and this prompted the conclusion that FtsZ in the presence of GTP and FtsA can probably orchestrate the cell constriction (Osawa & Erickson, 2013). These studies pointed towards FtsZ-ring being the force generator.

However, in later experiments it was shown that the change in FtsZ assembly, its GTPase activity or amount of FtsZ in the Z-ring failed to alter the constriction rate (Coltharp et al., 2016). Further, FtsZ mutants with reduced GTPase activity still formed Z-rings and continued to be functional for cell division, which resulted in viable cells (Lu et al., 2001). Taken together, these evidences point against FtsZ being the sole force generator for cell constriction. Additionally, L-forms (cell wall deficient bacteria) of *B. subtilis* was shown to propagate indefinitely without the expression of FtsZ (Leaver et al., 2009). Although in the rod-shaped *B. subtilis* a complete *ftsZ* deletion could not be achieved, its respective L-form survived the deletion of *ftsZ*. Thus, suggesting that constriction by the Z-ring alone is insufficient and requires cell wall synthesis in wild-type cells (Leaver et al., 2009).

It has long been known that the factors that affect PG, like impairment of FtsI (PBP3) activity or use of penicillin, results in cell division defects leading to filamentous cells (Schwarz et al., 1969; Spratt, 1975). Suggesting, an importance for the peptidoglycan synthesis in cell division. Additionally, long constriction periods observed in *E. coli* with mutations in FtsI, FtsQ (Huls et al., 1999; Taschner et al., 1988) and by overexpression of FtsN (Aarsman et al., 2005); premature initiation of constriction by mutants of FtsL and FtsB (Liu et al., 2015; Tsang & Bernhardt, 2015) and hyperactive constrictions in *C. crescentus* through mutations of FtsW and FtsI (Modell et al., 2014) - all supported the idea that the PG metabolic enzymes drive cell constriction. These observations suggest that PG synthesis and not FtsZ is the plausible candidate for the rate determining constrictive force for cell septation. In the subsequent breakthrough studies, the link between PG synthesis and constriction rate was established (Bisson Filho et al., 2016; Yang et al., 2016). It was established in *E. coli* and *B. subtilis*, that the GTPase driven

treadmilling of FtsZ directs the cell wall synthesis machinery. In *E. coli*, the rate of septal synthesis is independent on FtsZ treadmilling (Yang et al., 2016) whereas in *B. subtilis* FtsZ treadmilling rates control the rate of peptidoglycan synthesis as well as the rate of cell division (Bisson Filho et al., 2016).

Division of L-forms

If not mediated by neither FtsZ nor PG, how do L-forms divide? Novel proliferation mechanisms were revealed on time-lapse imaging of L-forms (Gilpin & Nagy, 1976; Leaver et al., 2009). The cells were shown to undergo shape perturbations through formation of protrusions, which eventually resolved into several round progenies (Leaver et al., 2009). This L-form reproduction mechanism was later shown not to depend on any of the well-characterized cytoskeletal systems, but on membrane fluidity (Mercier et al., 2012). Such modes of propagation is hence suggested to be an early mode of proliferation used by primitive cells before the existence of cell wall (Leaver et al., 2009).

1.4. Chromosome organization - a brief comparison

The genetic material in the cell is maintained in a conserved arrangement that are also replicated in progeny cells following cell division. The spatial organization of the bacterial chromosome can be broadly categorized into: (1) chromosomes arranged longitudinally in an *ori-ter* fashion and (2) chromosomes arranged in a transverse fashion with the left and right chromosomal arms lying in the two halves of the cell. Chromosome organization in *C. crescentus*, whose origin is tethered to the pole, follows pattern (1) (Figure 1A) (Viollier et al., 2004). Following initiation of replication, one of the two replicated origins (*ori*) migrate to the opposite pole followed by the rest of the replicating DNA, gradually positioning the terminus (*ter*) at the mid-cell/future division site (Schofield et al., 2010; Shebelut et al., 2010). This ensures the conservation of the *ori-ter* arrangement in the following generations. *Vibrio cholerae*'s chromosome I (ChrI) (David et al., 2014; Fiebig et al., 2006; Fogel & Waldor, 2005) and *Myxococcus xanthus* chromosome (Harms et al., 2013) also follow the same arrangement (Figure 1B). Additionally, ChrII of *V. cholerae*, which is not tethered to the pole at the origin but aligns in an *ori-ter* manner, suggests that tethering at the poles is not a prerequisite for this type of chromosome alignment.

Chromosome organization in slow growing *B. subtilis* presents a variation from these established patterns. At the time of birth of a daughter cell, the origins stay at the cell poles in a longitudinal arrangement following an *ori-ter-ori* pattern. However, following initiation

of replication at the poles, the newly replicated origins move to the center of the two cell halves followed by a rearrangement of the non-replicated chromosomal arms such that it adopts a ‘*left-replicated oris-right*’ pattern.

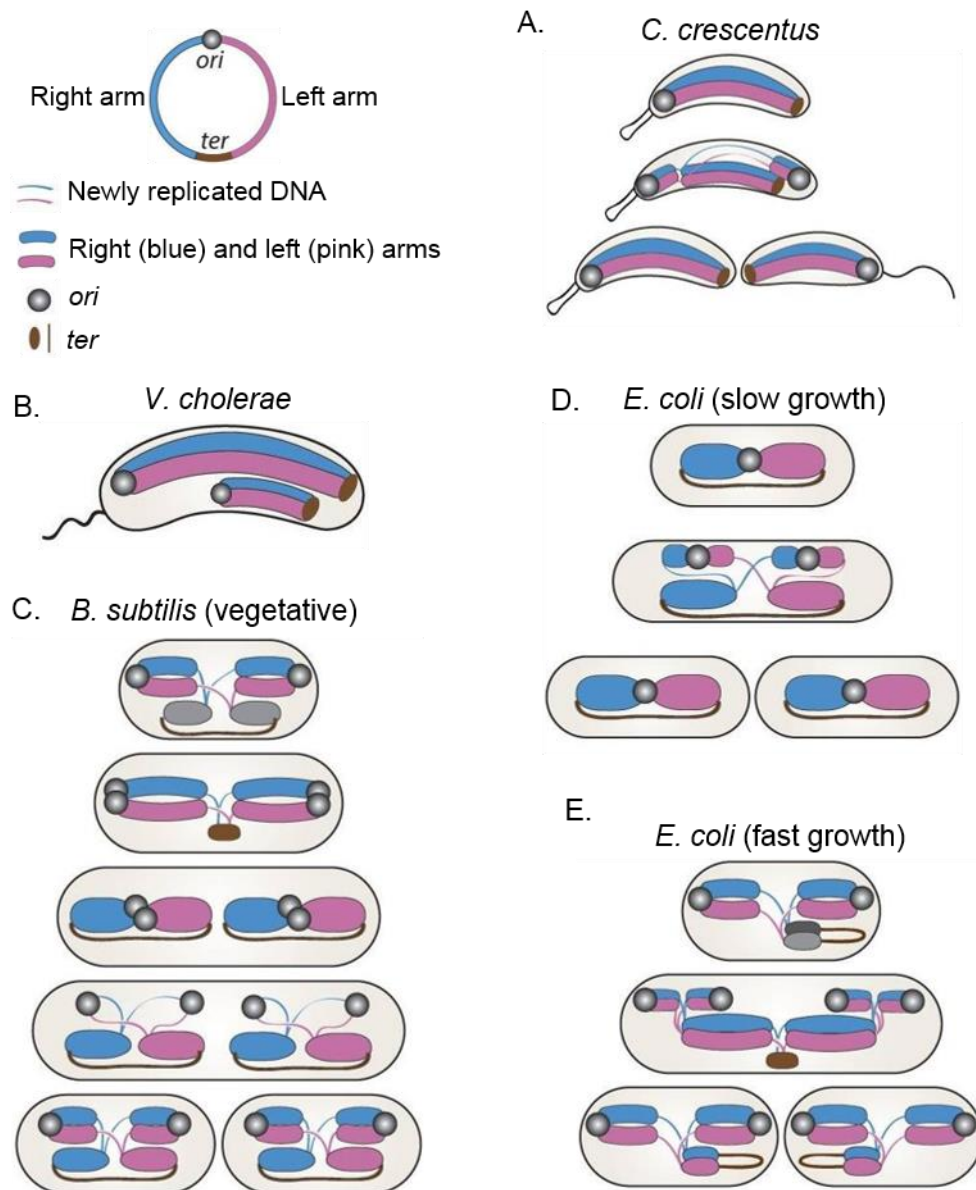


Figure 1: Spatial organization of bacterial chromosomes. Chromosome organization in *C. crescentus* (A), *V. cholerae* (B), *B. subtilis* during vegetative growth (C), *E. coli* under slow growing conditions (D) and *E. coli* under fast-growing conditions (E). Replication origins are represented by grey circles and termini by brown lines and ovals. The left and right chromosomes are represented by thick pink and blue lines or blobs, respectively, and newly synthesized DNA are shown in thin lines of the respective colors. Figure modified from Wang and Rudner 2014.

Subsequently, the replicated origins segregate to the peripheries of the respective nucleoid, adopting a final longitudinal alignment (Figure 1C) (Wang et al., 2014). Similarly, *E. coli* also exhibits both chromosome arrangements under different growth conditions. While in slow growth medium, *E. coli* adopts a *left-ori-right* pattern (Nielsen et al., 2006;

Wang et al., 2006), whilst fast growth, which provides multifork replication conditions, an *ori-ter* pattern is observed (Figure 1D and E) (Youngren et al., 2014). These findings give enough indications that the chromosome organization in a bacterial cell also depends on the growth conditions of the cell in addition to the proteins with which the segregating DNA interacts.

Arjes *et al.* confirmed for the first time that there exists a direct link between DNA replication and cell division through the concept of 'point of no return' (PONR). Inhibiting cell division in *B. subtilis* and *Staphylococcus aureus* led to an arrest in new rounds of DNA replication initiation and vice-versa (Arjes et al., 2014), suggesting that cell division and DNA replication are not only coordinated but also represent a coupled set of events.

1.5. Chromosome replication and its effect on cell division

Unlike in eukaryotes where the different stages of cell division, DNA replication, segregation, and cell body separation are all regulated through checkpoints, generally in prokaryotic organisms, they occur simultaneously. In bacteria growing under high nutrient conditions, replicated chromosomes start a second round of replication even before the first division completes. The lack of spatio-temporal distinction in the various stages of prokaryotic cell division imparts more complexity in the regulation of this process. The exact mechanism of how bacteria accomplish coupling of the chromosome replication and the segregation together with the septum formation and cell separation is yet to be completely determined.

DNA replication begins with binding of the ATPase, DnaA, to the origin of replication, *oriC*. This binding results in the subsequent assembly of several other components resulting in a nucleo-protein complex that melts and unwinds the double helix, and thus loading of the replication machinery (Duderstadt et al., 2010; Katayama et al., 2010). DNA synthesis occurs bi-directionally by two replication forks, until it encounters the terminus region (*ter*) where subsequent de-catenation and resolution of the replicated chromosomes occur (Bussiere & Bastia, 1999).

The segregation of the replicating chromosomes is important to ensure proper cell division. The different types of active DNA segregation machineries found in bacteria share the three common components: an NTPase, a DNA-binding protein and a specific DNA sequence to which the DNA binding protein binds. The partition system ParABS is the most studied of all and it had been originally discovered associated with plasmid

segregation. This system consists of the Walker-type ATPase ParA, the DNA-binding protein ParB that binds to *parS*, which are specific *cis*-acting sites located in the *oriC* region (Gerdes et al., 2010; Surovtsev & Jacobs-Wagner, 2018). ParA interacts with the ParB-*parS* complex and segregates the newly replicated origin. In *B. subtilis*, the components for the ParABS system are Soj (ParA) and Spo0J (ParB), which binds to the *parS* sites (Ireton et al., 1994). Spo0J binds to *parS* and spreads on to the neighboring DNA forming complex nucleo-protein clusters. Spo0J also recruits the structural maintenance of chromosome (SMC) complexes to the origin (Gruber & Errington, 2009; Sullivan et al., 2009). SMC foci are lost on Spo0J deletion or in the absence of the *parS* sites. Ectopic positioning of the *parS* sites lead to mistargeting of SMC to these regions, resulting in chromosome organization and segregation defects (Sullivan et al., 2009). An absence of the segregation system leads to varying defects in different bacteria. In *B. subtilis*, the absence of Soj-Spo0J system leads to minor defects in segregation (Lee & Grossman, 2006; Wang et al., 2014), whereas the ParABS system is crucial for chromosome partitioning in *C. crescentus* (Toro et al., 2008). The multi-chromosomal bacterium *V. cholerae* harbors two distinct partitioning systems, ParABS1 and ParABS2, dedicated to the segregation of Chromosome 1 and Chromosome 2, respectively (Fogel & Waldor, 2006; Yamaichi et al., 2006).

In most species cell division is mainly dependent on the assembly of FtsZ, the key component of the septal ring. One of the processes that has not yet been completely understood is how the assembly of FtsZ (and hence the divisome) is in concert with the replication and segregation of chromosomes. The link between DNA replication and cell division was obtained through studies in *B. subtilis*, where it was discovered that septation began only after 70% of the chromosome replicated. Additionally, a block in replication resulted in the mispositioning of the Z-ring. In the research by Moriya et al, it was established that the earlier the block occurred at the replication initiation stage, the likelihood of a mid-cell positioned Z-ring decreased. The resulting proposed model linked the progression of DNA replication initiation to the proper positioning of the Z-ring (Moriya et al., 2010). Although what positioned FtsZ to the mid-cell or the future division site remained unanswered, it was proposed early on to be a nucleoid dependent mechanism.

Studies on chromosome architecture categorized the *E. coli* chromosome into different macrodomains (MD). A macrodomain is defined as a region of the chromosome with an approximate size of 1Mbps, which is physically isolated from the rest of the chromosome. The four proposed MDs in *E. coli* include one surrounding the replication origin (*ori* MD), another surrounding the replication terminus region (*ter* MD) and two flanking the *ter* MD from the left (Left MD) and the right (Right MD) (Niki et al., 2000; Valens et al., 2004). The

ter MD is organized by the DNA-binding protein MatP (macrodomain Ter protein) that binds to the *matS* sequences at the terminus region (Mercier et al., 2008). In addition to its role in compaction of the terminus region, MatP is also attributed the function of Z-ring positioning. The association of the *ter* region to the Z-ring is established through the linkage of ZapA, ZapB, and MatP. This so called *ter* linkage consists of a network of ZapB filaments that extends from nucleoid to the Z-ring, to which FtsZ is linked via ZapA. ZapB is also linked to the DNA at the replication terminus region via MatP (Mercier et al., 2008). Taken together, on initiation of replication, the *ter* region repositions to the middle of the cell and this explains how replication initiation is linked to the Z-ring positioning, eventually facilitating the orchestration of DNA replication and divisome formation (Espeli et al., 2012).

1.6. Negative regulation by Nucleoid Occlusion (NO)

To prevent the incomplete inheritance of a chromosome, the divisions over the nucleoid is inhibited by a phenomenon called nucleoid occlusion (NO) (Mulder & Woldringh, 1989; Woldringh, 1989). In *E. coli* nucleoid occlusion is effected through SlmA (Bernhardt & De Boer, 2005). The cell division regulation by nucleoid occlusion in *B. subtilis* is effected by Noc (Wu & Errington, 2004).

1.6.1. Nucleoid occlusion by SlmA

SlmA, by binding to specific sequences on the chromosome (SlmA binding sequences, SBS), prevents FtsZ from forming the Z-ring over the nucleoid (Cho et al., 2011a) (**Figure 2**). This in turn prevents cell constrictions that might lead to chromosome guillotining. SlmA contains an N-terminal TetR-like helix-turn-helix (HTH) motif that is considered to bind DNA facilitating its localization over the nucleoid (Bernhardt & De Boer, 2005). In *E. coli*, distribution of SlmA adopted a cell cycle dependent pattern. In newborn cells with a single nucleoid, SlmA localized on the nucleoid, mostly concentrating on the pole-proximal regions. In older cells with clearly segregated nucleoid, SlmA distributes over the two separated lobes of the nucleoid. Further, SlmA's association to the DNA as well as its capacity to mediate nucleoid occlusion was attributed to the HTH motif of the protein (Bernhardt & De Boer, 2005).

Several models were proposed on the mechanism by which SlmA regulates the positioning of the Z-ring. The initial proposal was that SlmA bound to the DNA competes with the membrane anchors of FtsZ in FtsZ binding, thus preventing Z-ring formation (Bernhardt &

De Boer, 2005). This study also suggested that, alternatively, SlmA might be involved in an active depolymerization of FtsZ filaments when bound to DNA. However, no evidence for SlmA's destabilization effect on FtsZ was obtained.

In subsequent investigations, evidences were found for SlmA's action to disassemble FtsZ filaments *in vitro* (Cho et al., 2011a). Untagged SlmA blocked the assembly of FtsZ polymers. SlmAT33A in *E. coli* created an aminoacid substitution in the conserved HTH motif resulting in a protein variant that failed to associate to DNA. As a result, SlmAT33A localized diffusively throughout the cell. In spite of its localization along the entire cell length, the non-DNA binding SlmAT33A did not lead to a complete block in cell division (Cho et al., 2011a). Thus, DNA binding of SlmA was concluded to activate its antagonistic effect on FtsZ. The identification of the specific SlmA binding DNA sequences (SBS) aided in proving this hypothesis. In the presence of SBS DNA fragment, SlmA robustly inhibited FtsZ polymerization at very low concentrations. Additionally, inhibition of FtsZ polymerization was achieved by SlmA-SBS by increasing FtsZ's GTPase activity. In an FtsZ GTPase mutant, SlmA failed to extend this effect. SBSs were also confirmed to induce SlmA-SlmA and SlmA-FtsZ interactions (Cho et al., 2011b). Altogether, it was concluded that, SBS binding promotes oligomerization of SlmA, which inhibits FtsZ polymerization by preventing FtsZ-FtsZ interactions.

However, in a parallel study it was also proposed that SlmA induces formation of antiparallel FtsZ protofilaments that are unable to effectively assemble to form the Z-ring (Tonthat et al., 2011).

Nonetheless, the most recent study of Du and Lutkenhaus, confirmed that SlmA binds to SBS when it comes in contact with the FtsZ filaments and leads to its breakage. Studies analyzing the effect of mutations in the C-terminal tail of FtsZ confirmed the importance of this region of FtsZ for its interaction with SlmA. Additionally, an interaction between FtsZ and SlmA was also established, which triggers the filament disassembly (Du & Lutkenhaus, 2014). Although binding of SlmA to the SBSs is confirmed to be important for SlmA's activity, both processes of SlmA binding on DNA and SlmA's inhibitory effect on FtsZ are separable as a non-DNA-binding mutant of SlmA can still partially inhibit division.

1.6.2. Nucleoid occlusion by Noc

Noc is a DNA-binding protein that forms nucleo-protein complexes on binding to palindromic sequences (Noc binding sequences, NBS) spread along the entire chromosome with exception to the near terminus regions (Wu et al., 2009). Noc, like SlmA, is not essential for the organism but it is synthetically lethal together with a Min deletion. A

double deletion leads to random FtsZ clusters and thus resulting in an inability to form a complete Z-ring at any location due to insufficient availability of FtsZ. Similar to SlmA in *E. coli*, the absence of Noc binding near the terminus might be essential for timing the chromosome segregation and cell separation events.

Structurally, the N-terminus of Noc has been found to be important for its membrane binding although it is a weak binding. Additionally, it was shown that DNA binding of Noc is a pre-requisite for its membrane association, thus ensuring that cell division is inhibited only in regions of the nucleoid. Unlike SlmA, both membrane association and DNA binding are required for Noc's function (Adams et al., 2015). Interaction analysis failed to establish any direct interaction between Noc and FtsZ or any other divisome protein.

Taken together, one of the earliest models proposed for the action of Noc holds reasonable. The nucleo-protein complexes formed by Noc by binding to NBS on the chromosomal DNA, which then associates to the cell periphery, presents a steric hindrance for the establishment of the divisome complex (Figure 2B)(Adams et al., 2015).

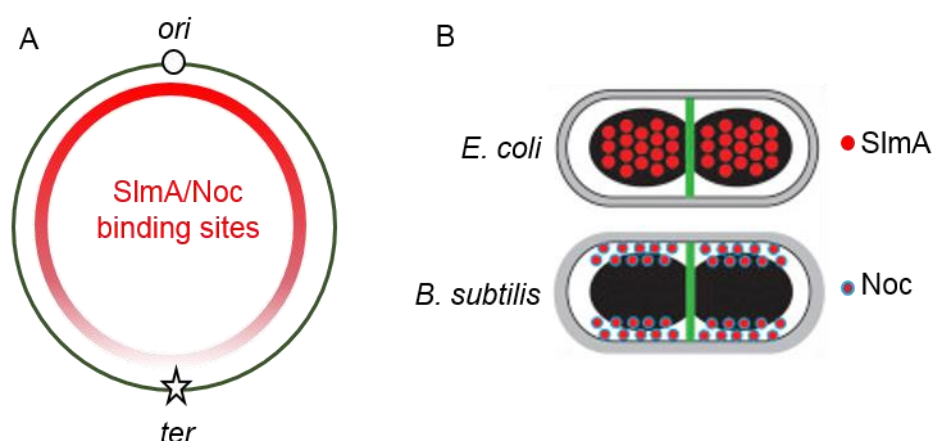


Figure 2: Nucleoid occlusion. (A) Distribution of SlmA/Noc binding sites. In red is represented the density of SlmA/Noc binding sites. Lesser the intensity of red, fewer the binding sites or binding of SlmA. Nucleoid occlusion is facilitated by this asymmetry in DNA binding of SlmA/ Noc. (B) Negative regulation of FtsZ ring (in green) positioning by the activity of nucleoid occlusion protein SlmA and Noc in *E. coli* and *B. subtilis* respectively. Figure modified from Surovtsev and Jacobs-Wagner 2018.

1.7. Negative regulation of FtsZ by the Min system

Apart from regulation on the chromosome level by nucleoid occlusion, a large number of proteins across several bacteria have been discovered to be involved in regulating the placement of FtsZ. This regulation is achieved either by directing FtsZ to the site of future cell division or by inhibiting its polymerization everywhere else other than at the correct division site. The earliest system discovered was the Min system, which has been

thoroughly studied in *E. coli* and *B. subtilis* (Figure 3). In both bacteria, the Min system prevents the occurrence of divisions in regions close to the poles, thereby acting as the spatial inhibitory system for division site selection in addition to nucleoid occlusion. Deletion of the Min system results in divisions closer to the poles giving rise to non-viable mini-cells (de Boer et al., 1989).

The Min system in *E. coli* consists of three proteins: MinC, the inhibitor of FtsZ polymerization; MinD, the ATPase that binds MinC and localizes to the membrane; and MinE, the stimulator of MinD's ATPase activity. The ATPase MinD and its activator MinE drives the spatial organization of the Min complex. Recent studies show that MinE's ability to undergo MinD-dependent conformational switching, confers the required robustness to the Min system to form a spatio-temporal protein pattern (Denk et al., 2018; Park et al., 2017). Upon ATP-binding, MinD dimerizes and attaches to the cytoplasmic membrane through its amphipathic helix (Szeto et al., 2003). MinC is the FtsZ-interacting protein and has a very low FtsZ inhibitory activity by itself (Zhou & Lutkenhaus, 2005). MinC gets activated upon binding to the membrane bound MinD (Hu & Lutkenhaus, 2003). The binding of MinD to ATP causes the MinCD complex to attach to the cytoplasmic membrane where it prevents the polymerization of FtsZ. MinE binds the MinCD complex, stimulates the ATPase activity of MinD, thereby dissociating the MinCD complex from the membrane (Loose et al., 2008; Lutkenhaus et al., 2012) and releasing it to the cytoplasm. Subsequently, the cytoplasmic MinD binds ATP, rebinds MinC and reattaches the membrane at the farther pole. The cumulative effect results in the oscillation of the MinCD complex from pole-to-pole followed by a circular trail of MinE triggering this oscillation (Raskin & de Boer, 1999a) resulting in a time-averaged minimum of the MinCD complex at the mid-cell where subsequently the Z-ring establishes (Figure 3A). Z-rings are prevented from forming at the cell poles as they experience a time-averaged MinCD maximum (Figure 3). Therefore, a deletion of the Min system leads to polar divisions and mini-cell formation due to the polymerization of FtsZ into Z-rings near the cell poles.

Unlike in *E. coli*, the Min system is not oscillatory in *B. subtilis* (Figure 3B). This is because of the absence of MinE. Instead, DivIVA is the topological factor in this bacterium. DivIVA localizes to the cell poles and to the division site in the later stages of cell division. DivIVA's localization has been attributed to its intrinsic ability to target itself to regions of negative curvatures (Edwards et al., 2000). DivIVA recruits MinCD to the poles. MinJ, an integral membrane protein, also recruited by DivIVA, facilitates the interaction of DivIVA with the inhibitor complex MinCD. Earlier it was thought to be stably recruited to the cell poles to prevent polar accumulation of FtsZ and hence divisions at the poles (Bramkamp et al., 2008). In subsequent studies it was shown that instead of preventing polar accumulation

of FtsZ, MinC interacted with and destabilized polar FtsZ polymers (Gregory et al., 2008). Thus, preventing an immediate new cell division in the regions close to the newly formed cell pole.

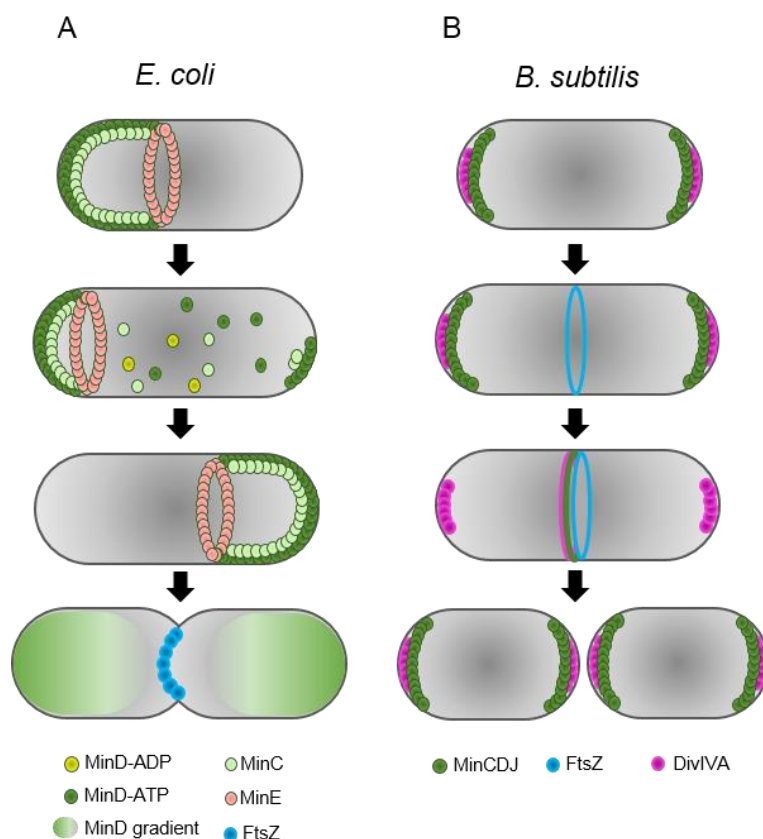


Figure 3: Spatial and temporal regulation of Z-ring assembly by the Min system. (A) The MinCDE system in *E. coli* is oscillatory. MinD-ATP (dark green circles) binds to the membrane and recruits MinC (yellow circles). MinE (pink circles) binds to MinD and activates ATP hydrolysis, releasing MinD-ADP (light green circles) and MinC off the membrane. Nucleotide exchange in the cytoplasm reactivates the membrane affinity of MinD and it assembles at the membrane farther from MinE concentration (the opposite pole in short cells). The oscillation of MinCD creates a region of minimal concentration at the mid-cell where FtsZ polymerizes into a ring (blue band) and results in the formation of the divisome. (B) The MinCDJ system in *B. subtilis* is dynamic in a different way. In new born cells, DivIVA (purple circles) recruits MinCDJ complex to the incipient division site (dark green circles). Following the separation of the nucleoid at the future division site, the Z- ring (blue ring) forms at mid-cell. At this time point, MinC, ensures the prevention of formation of a second Z-ring adjacent to it. Following septation, MinCDJ redistributes to both the poles transiently.

1.7.1. MinC's mode of action on FtsZ

The molecular details of MinC's inhibitory effect over FtsZ polymerization was addressed through studies in *E. coli*. In vitro, MinC was found to prevent FtsZ polymerization without affecting the GTPase activity of FtsZ. MinC, even at higher molar concentrations, was not observed to affect the GTPase activity of FtsZ. However, incubation of increasing concentrations of MinC with FtsZ for sedimentation assay decreased the amount of FtsZ

recovered in the pellet post centrifugation (Hu et al., 1999). Thus indicating the inhibitory effect of MinC on FtsZ polymer formation.

MinC has two functional domains, N-terminal MinC^N and C-terminal MinC^C (Hu & Lutkenhaus, 2000). Similar to the full length MinC, sedimentation assays also showed that MinC^N is capable of inhibiting FtsZ polymerization. However, this inhibitory effect on polymerization is not exerted by MinC^C (Hu & Lutkenhaus, 2000). Expression of MinC^C alone in a Δmin strain did not recover the *min* deletion phenotype. However, it did not lead to any additional phenotype other than the slight elongations and mini-cells as found in a Δmin strain. Instead, the sole expression of MinC^N resulted in extensive cell elongation. Thus, concluding that the inhibitory role of MinC over cell division is predominantly by the N-terminal domain (Hu & Lutkenhaus, 2000). Later it was clarified that, although a native expression of MinC^C did not change the phenotype of the cells, an overexpression did. Thus suggesting a cell division inhibitory function for the MinC^C domain as well (Shiomi & Margolin, 2007). Later, by visualizing FtsZ polymers formed using electron microscopy, the effect of MinC^C on FtsZ polymerization was studied. In the presence of MinC^C, FtsZ protofilaments were long but did not form thick bundles. Thus, MinC^C does not depolymerize the filaments but prevents their lateral assembly. Furthermore, in the presence of full length MinC, in addition to reduced bundling of the filaments, it also resulted in shorter and curved filaments, which was speculated to be the effect of MinC^N on FtsZ polymers (Dajkovic et al., 2008).

Follow up studies in this direction shed more insights into FtsZ-MinC interaction. Mutational analysis of FtsZ and the following study on its interaction with MinC led to strains harbouring FtsZ point mutants that are resistant to the effect of either MinC^C or MinC^N. This established that different regions of FtsZ are susceptible to the two domains of MinC and the inhibitory effect of MinC over FtsZ is exerted through several mechanisms (Shen & Lutkenhaus, 2010). MinC^C localizes to the FtsZ polymer through its interaction with the C-terminal region of FtsZ (Shen & Lutkenhaus, 2009). This region of FtsZ is also the one which interacts with FtsA and ZipA, the proteins that stabilize and tether the Z-ring to the membrane. Therefore, MinC competes with FtsA and ZipA to bind the C-terminal region of FtsZ resulting in subsequent destabilization of the Z-ring (Shen & Lutkenhaus, 2009). Point mutation on FtsZ that alters the interface between two FtsZ subunits conferred resistance to the inhibitory effect of MinC^N (Shen & Lutkenhaus, 2010). Thus, confirming the earlier findings that the N-terminal domain of MinC (MinC^N) weakens the interaction between FtsZ subunits, thus weakening the longitudinal interaction leading to shorter polymers.

Although a clear mechanistic understanding of MinCD inhibition of FtsZ ring formation is yet to be reached, the current comprehension is as follows. The C-terminal domain MinC^C, that is responsible for MinC's dimerization and interaction with MinD, also interacts with the C-terminal peptide of FtsZ, bringing them together. Once this proximity is attained, the N-terminal domain of MinC, MinC^N, gets positioned at the interface of two FtsZ subunits regardless of the nucleotide present at the interphase (GTP or GDP). If the FtsZ dimer interphase is occupied by GTP, strong FtsZ-FtsZ interactions makes the interphase less available for MinC. However, if it is instead occupied by GDP, MinC^N accesses this site resulting in chopping of the FtsZ filament (Park et al., 2018; Shen & Lutkenhaus, 2010).

1.7.2. Implications of an oscillatory Min system

Self-organized protein patterns serve the function of providing spatial cues for positioning of other downstream proteins thereby aiding in cellular functions (Frey et al., 2018; Kretschmer & Schwille, 2016). The oscillatory Min system that sets up as a result of diffusion-reaction dynamics is one such well-studied protein pattern (Schweizer et al., 2012). Since first visualized in *E. coli*, MinCDE oscillations have been reported in several other organisms. The biochemical nature of this system, and the factors contributing to the parameters of its oscillation, has been thoroughly investigated in *in vivo* and *in vitro* systems (Kretschmer & Schwille, 2016; Zieske & Schwille, 2014). Computational modelling studies on this system also helped to obtain a step-by-step understanding of these oscillations. Studies on cell division during the oscillation suggested an unequal inheritance of the Min components by the daughter cells (Sengupta & Rutenberg, 2007; Tostevin & Howard, 2006). This can lead to daughter cells with unprecise division site placements in the following divisions. However, a study addressing MinD oscillation in dividing cells suggested that by changing the oscillatory pattern at the time of division, the parent cell ensures an equal distribution of Min proteins between the two daughter cells (Juarez & Margolin, 2010). Thus, in elongated pre-divisional cells, the pattern of pole-to-pole oscillation of MinD changes to a wave pattern with a maximum at mid-cell in addition to the two poles. This was then noted as 'double pole-to-pole' oscillation, which are now known as the standing wave pattern with multiple nodes. Initially it was advocated that the mid-cell MinD maximum was the result of the Min components recognizing an unknown membrane determinant at the septum. Through studies of Min oscillation in artificially elongated *E. coli* cells (Raskin & de Boer, 1999c), deformed mutant cells (Varma et al., 2008), and vesicles of different shapes (Zieske & Schwille, 2013, 2014), it was confirmed that alterations in the Min wave pattern can be established by the shape or dimension of the cell or vesicle it is contained in. As we report in this study, the capacity of Min waves is utilized in naturally occurring filamentous swarmer cells of *V. parahaemolyticus*. In these

long cells the self-organized localization of Min proteins assumes the pattern similar to that observed in artificially elongated *E. coli* cells. This multi-node standing wave pattern acts as a scale and makes available several MinCD minima, which could then be used as possible sites for septum placement.

The Min system is quite widespread among bacteria. However, bacteria that have evolved with genomes lacking orthologues of the Min system or nucleoid occlusion systems also exist. *C. crescentus* is one such interesting bacterium with neither of the previously described divisome placement regulators. MipZ, a ParA-like protein, was described to control the spatial regulation of septum placement in *C. crescentus* (Thanbichler & Shapiro, 2006).

1.8. Negative regulation of FtsZ by MipZ

C. crescentus lacks both the Min system and the nucleoid occlusion proteins. In a newborn *C. crescentus* cell, FtsZ initially localizes to the new pole (Figure 4A). As soon as the cell enters the S-phase, FtsZ undergoes a rapid shift towards the mid-cell (Figure 4B-D) and remains there until the division is completed. Here, the positioning of FtsZ and hence the regulation of cell division is carried out by yet another ParA-like ATPase, MipZ. The synchronization of DNA replication and cell division in this bacterium is carried out by this gradient forming protein (Thanbichler & Shapiro, 2006).

The cell-cycle dependent dynamics of FtsZ localization in *C. crescentus* is regulated by MipZ, which is an inhibitor of Z-ring formation and localizes consistently to the flagellated pole (old pole) in swarmer cells. MipZ forms a gradient with a maximum at the old pole, extending towards the non-flagellated pole (new pole) with a minimum concentration at this site. FtsZ localizes to this site of minimum MipZ concentration. Following the transition to a stalked cell, MipZ forms a bi-polar gradient. In consequence, the mid-cell experiences the lowest concentration of MipZ. This transitioning kicks off the polar FtsZ and repositions it at the mid-cell. Here FtsZ polymerizes to form the Z-ring. MipZ being a direct inhibitor of FtsZ, Z-ring formation is prevented elsewhere along the cell length. The bi-polar localization of MipZ is retained until the completion of the cell division where it forms a swarmer cell with MipZ at the flagellated pole and a stalked cell with MipZ at the stalk pole (Thanbichler & Shapiro, 2006).

MipZ exerts its inhibitory effect by interacting directly with FtsZ, thereby stimulating FtsZ's GTPase activity. Like the other ParA-like proteins, MipZ can switch between monomeric

and dimeric state depending on ATP binding. The ATP-dependent conformation of MipZ determines its interaction partner, interacting with either the DNA segregation system or the cell division machinery. MipZ monomers interact with ParB while it is solely the MipZ dimers that interacts with and inhibits FtsZ (Kiekebusch & Thanbichler, 2014).

The pole of highest MipZ concentration is also the region of localization of ParB. The DNA-partitioning protein ParB associated with the chromosomal origin, is anchored to the pole through its interaction with the landmark protein PopZ. Following initiation of DNA replication, the duplicated origins segregate to the opposite poles by the ParABS chromosome segregation system. PopZ, which gradually forms a second focus at the new pole, anchors the segregated origin to this pole (Bowman et al., 2010; Ebersbach et al., 2008). MipZ's change in localization occurs in synchronization with the ParB-*parS* complex and is maintained through a MipZ-ParB interaction. (Kiekebusch et al., 2012; Thanbichler & Shapiro, 2006) (Figure 4).

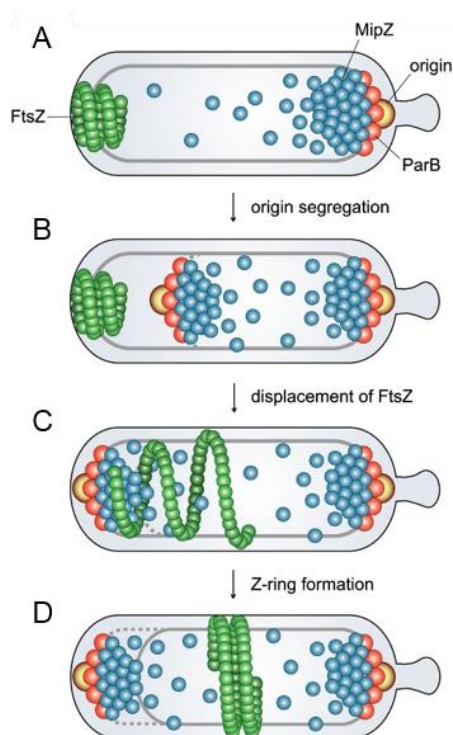


Figure 4: Regulation of FtsZ localization by MipZ in *Caulobacter crescentus*. A detailed description is provided in the main text. Figure adapted from Thanbichler and Shapiro 2006.

ParB-*parS* complex located at the cell pole recruits MipZ monomers to these sites and stimulates their ATP-dependent dimerization. Thus formed MipZ dimers get released from ParB into the cytosol where they bind nonspecifically to the chromosomal DNA. As bound proteins are less mobile compared to the unbound ones, most DNA bound MipZ dimers localize to the pole-proximal region. The polar release of MipZ dimers together with reduced movement of bound dimers on the chromosome results in the development of

MipZ's polar and bi-polar concentration gradients. The intrinsic ATPase activity of MipZ results in ATP hydrolysis triggering the formation of MipZ monomers from the dimers. These monomers, then undergo nucleotide exchange in the cytoplasm and are again recaptured by ParB-*parS* complex at the poles (Kiekebusch et al., 2012).

1.9. Positive regulation of FtsZ by PomZ

PomZ is the ParA/MinD-like P-loop ATPase in *Myxococcus xanthus* required for its cell division. PomZ localizes to the mid-cell prior to FtsZ and this localization is FtsZ independent. Deletion of *pomZ* results in mini-cells and elongated cells. In PomZ's absence, the cells form fewer Z-rings. Additionally, the Z-rings that form are not restricted to mid-cell positions (Treuner-Lange et al., 2013). Thus, suggesting PomZ as a positive regulator of FtsZ in *M. xanthus*. In later studies, PomX and PomY, two genes flanking PomZ, were also found to be important for cell division in Myxobacteria. The three proteins together establish the proper positioning of division site.

Like many other ParA-like ATPases, PomZ dimerizes on ATP binding and associates non-specifically to DNA. PomX and PomY triggers ATPase activity of PomZ causing PomZ monomerization. The resultant diffusing PomZ monomers undergo quick nucleotide exchange forming ATP bound dimers and rebinds DNA. Nucleoid bound PomZ associates the PomXY cluster to the nucleoid where it remains very dynamic. The motion of this cluster is dependent PomZ's ATP hydrolysis that is stimulated by PomXY. The net effect of PomXY acting as a sink of PomZ and the nucleoid as its source, set up a PomZ diffusive flux that determines the directionality of PomXY cluster motion. When the cluster is off-centre, it moves toward direction of higher concentration of PomZ, that is, towards the mid-cell. The flux on either side equalizes when the clusters is at the mid-cell where it eventually stabilizes and triggers Z-ring formation (Schumacher et al., 2017). The PomXYZ system thus presents an example of a ParA-like protein together with its ATPase activating components, resulting in a random walk on the nucleoid ultimately marking the site for divisome formation through positive regulation of FtsZ.

1.10. Other known regulators of Z-ring placement

While a variety of bacteria have mechanisms of negative regulation to direct the division machinery to the correct site, several others, like *M. xanthus*, have resorted to direct

recruitment by positive regulator proteins. The first evidence for positive regulation was provided by studies on *Streptomyces* (Willemse et al., 2011).

Streptomyces are filamentous Gram-positive bacteria that lack all the canonical regulators: Min, Noc and SulA. This is not surprising as in these bacteria cell division is dispensable for cell growth. In *Streptomyces*, SsgA and SsgB play the role of pinpointing the cell division site by recruiting FtsZ to the septum site. During sporulation SsgB recruits FtsZ to the division site and localization of SsgB in turn is controlled by SsgA. Unlike the previously studied models for cell divisions, where FtsZ preceded the recruitment of cell division proteins, in *Streptomyces* septa formation is dependent of SsgA and SsgB and not vice-versa (Willemse et al., 2011).

Furthermore, the phosphorylation regulated cell division in *Streptococcus pneumoniae*, another bacterium that lacks the Min and nucleoid occlusion proteins, presents an entirely diverse mechanism of Z-ring placement. The Serine/Threonine kinase StkP localizes to the mid-cell in *S. pneumoniae* after FtsA, but prior to DivIVA, and phosphorylates DivIVA. Mutations in StkP resulted in elongated cells, confirming that StkP signaling is essential in regulating cell division of *S. pneumoniae* (Beilharz et al., 2012).

Later studies reported the discovery of a phosphorylation target of StkP in *S. pneumoniae*, whose phosphorylated and non-phosphorylated forms are important for proper Z-ring formation and dynamics. This mid-cell anchored protein, MapZ, that shares sequence similarity with no other proteins, acts as a marker for the cell division site. In newborn cells, MapZ co-localizes as a ring along with the FtsZ-ring at the mid-cell. As the cells elongate, MapZ forms a double band at the mid-cell position with the Z-ring in between them. As peptidoglycan insertion begins at mid-cell, the newly formed MapZ rings gets pushed away to the right and left. This is followed by the appearance of a MapZ ring at the ongoing constriction site and splitting of the FtsZ ring that begins migrations to the attain co-localization with the MapZ rings at the future division sites of the future daughter cells. Therefore MapZ arrives and leaves the equator of the cell earlier than FtsZ and its position marks the site for upcoming division events (Fleurie et al., 2014; Holečková et al., 2014).

1.11. Involvement of ParA/MinD-like proteins in cell division

Decades of research in various cell division model organisms have added evidence for an extensive involvement of ParA/MinD-like ATPases in several aspects of cell division. These proteins are members of a large family of P-loop ATPases (Leipe et al., 2002). MinD

and ParA subfamilies of these ATPases are widespread among bacteria. The ATP-bound state of these proteins form a dimer that can then bind to the DNA or the cell membrane, because the dimerization brings together two half sites that form a binding site with a high affinity for surfaces and protein partners. Usually the partner proteins of these ATPases activate the ATP hydrolysis, thereby functioning as an ATPase activating protein (AAP) (Wu et al., 2011). ATP binding and hydrolysis is regulated by a spatially restricted AAP, which in turn sets up a self-organized localization pattern of these ParA/MinD proteins. For instance, the MinCDE system as described in *E. coli*, where MinD is the ATPase and MinE is the AAP. In certain other MinD/ParA related proteins, dimerization upon ATP binding do not lead to membrane binding, but only to other proteins. In such cases, the cell employs a landmark protein that act as the recruiter of these ATPases. For example, MinD in *B. subtilis* gets specifically recruited to the incipient division site and transiently to the poles through its interaction with DivIVA (Eswaramoorthy et al., 2011).

Irrespective of the localization pattern, ParA/MinD-like proteins are responsible for maintaining a wide variety of cellular functions. A vast number of functions ensure the equal distribution of cellular components between the mother and the daughter cells, thereby aiding proper cell division. Two ATPases, MipZ and ParA, are employed by *C. crescentus* for proper cell division. Both MipZ and ParA bind non-specifically to the nucleoid, but the timing of their bindings and their localization patterns are different. Interestingly, in this case both the proteins are regulated spatially by the same AAP, ParB. For ParA, ParB acts as the ATPase activating protein, thereby removing ParA from the nucleoid. Therefore, hydrolysis of ParA bound to the nucleoid results in a receding gradient and a chasing motion of the origin bound ParB from one pole to the other. This effectively results in segregation of the replicated DNA to the opposite cell pole. On the other hand, for MipZ, ParB is a recruiter of monomers and facilitates its dimerization. The dimers thus formed are capable of nonspecific DNA binding (Kiekebusch et al., 2012). As explained earlier, the initial uni-polar and eventual bi-polar gradient of MipZ results in the spatial and temporal regulation of FtsZ positioning and hence division of *C. crescentus* (Thanbichler & Shapiro, 2006).

As described earlier, chromosomal ParA proteins are responsible for the segregation of chromosomes. Different types (depending on the nucleotide hydrolyzing enzyme) of such proteins are also involved in the segregation of plasmids. The first type employs ParA like ATPases, the second type consists of an actin-like protein, and the third consists of GTPases. While the latter two form filaments that segregate plasmids, the ParA-like proteins function similar to the chromosomal ParA proteins with the exception of their polar tethering. ParA binds non-specifically to the nucleoid until it interacts with ParB. When

plasmid-bound ParB encounters ParA on the nucleoid, it stimulates the ATP activity of ParB and causes its removal from the nucleoid. The remaining nucleoid-bound ParA acts as a pull for the ParB, pulling the bound plasmid together with it (Hatano et al., 2007; Ringgaard et al., 2009). The ParA-free zone that develops behind the trailing plasmid gets re-filled with ParA-ATP dimers. On plasmid duplication, the two ParB-*parS* complexes get pulled to opposite directions by the two ParA clouds (Surovtsev et al., 2016).

1.12. ParA-like protein ParC and chemotaxis

1.12.1. ParC-ParP system

Those ParA proteins that are not associated with a partner protein which regulates its ATPase activity are called orphan ParAs. They follow restricted localization in the cell and usually ensure the inheritance of key proteins by both daughter cells upon division. In *V. cholerae* (Ringgaard et al., 2011) and *V. parahaemolyticus* (Ringgaard et al., 2014), a ParA-like protein, ParC (partitioning chemotaxis) was discovered to be important for the polar recruitment of chemotaxis signaling arrays. It is a member of a separate clade of ParA-like proteins, which are encoded within the chemotaxis operon.

In *Vibrios*, chemotactic signaling arrays are localized to the old flagellated pole in newborn cells. As the cell grows, a second focus is recruited to the new pole, resulting in a bi-polar localization (Ringgaard et al., 2011). This localization pattern ensures that upon cell division each daughter cell inherits a signaling array at its old pole, indicating a cell cycle dependent maturation of the poles. Through localization studies, it was ascertained that ParC is responsible for cell-cycle dependent polar localization of the chemotaxis proteins. ParC followed a similar sub-cellular localization pattern as that of the chemotaxis proteins. It localized to the old pole in newborn cells and later was recruited also to the new pole with progression of the cell cycle (Ringgaard et al., 2011). Although the pattern of localization of ParC and chemotaxis proteins were similar, co-localization studies confirmed that ParC gets recruited to the new pole prior to chemotaxis proteins.

ParC was clarified to be the guiding factor or recruiter for chemotaxis protein localization through analyzing the position of chemotaxis foci in $\Delta parC$ background. In the absence of ParC, chemotaxis proteins are no longer directed to the poles and instead localize randomly along the cell length. For instance, deletion of ParC in *V. cholerae* resulted in a population with 25% of the cells with mislocalized CheW1 (a chemotaxis protein) compared to the <2% in the wild-type background in *V. cholerae*. Although, cell divisions

in wild-type cells occurred only after a bi-polar localization of the chemotaxis proteins, this was not the case in $\Delta parC$. As a result, not every daughter cell inherits a chemotaxis cluster (Ringgaard et al., 2011, 2014).

ParC's role in positioning the chemotaxis proteins, however, takes place through its interaction with ParP. In the genome, *parP* is encoded adjacent to *parC*. The localization pattern of ParP is also similar to that of ParC and the chemotaxis proteins, with newborn cells inheriting a single focus at the old pole and later acquiring a bi-polar pattern as the cell grows (Ringgaard et al., 2014). Through co-localization and time-lapse experiments in *V. parahaemolyticus*, Ringgaard *et al.* confirmed that while ParP arrived at the poles prior to chemotaxis proteins, ParC and ParP arrived simultaneously at this site. However, localization of ParP is dependent on ParC. On deletion of ParC, about a quarter fraction of the cell population positioned ParP foci randomly and the cells divided prior to ParP's bi-polar localization resulting in another quarter fraction of cell population without any inherited ParP foci. Although absence of both ParC and ParP affected the polar distribution of chemotaxis proteins, ParP was also found to promote gradual accumulation of chemotaxis arrays at the poles by preventing dissociation of CheA from the chemotactic signalling complex (Ringgaard et al., 2014). Further, ParP prevents dissociation of CheA, ParC and itself from the cell poles (Alvarado et al., 2017; Ringgaard et al., 2014). ParC targets ParP to the poles, Furthermore, in the absence of ParP, a fraction of ParC diffuses in the cytoplasm in addition to forming polar foci. Altogether, ParC and ParP together establish the right positioning of stable chemotactic clusters. While ParC establishes the site of localization, ParP ensures the sequestering and stability of the proteins forming the chemotactic cluster (Ringgaard et al., 2014).

ParC, posses an intrinsic ATPase activity, which is comparable to the other ParA-like proteins. Mutation analysis of ParC was used to determine the effect of ParC's ATPase activity in its ability to recruit chemotaxis proteins. Amino acid substitutions introduced into the ATP-binding motif of ParC resulted in protein variants devoid of specific functions. ParCK15Q is predicted to prevent ATP binding and is locked in the apo-monomeric form. ParCG11V is in the ATP-bound monomeric form, unable to dimerize and hydrolyze ATP (Ringgaard et al., 2011). These variants of ParC localized differently compared to the wild-type ParC. While ParCK15Q diffused throughout the cell, ParCG11V formed non-polar foci in addition to the uni-polar and bi-polar foci. Neither of the variants could restore the normal distribution of chemotaxis proteins in a $\Delta parC$ background (Ringgaard et al., 2011). By affecting the positioning of chemotaxis proteins, deletion of *parC* disrupts the co-localization of chemotaxis clusters with the flagellar machinery, thus resulting in reduced chemotaxis and altered swimming behavior (Ringgaard et al., 2011).

Additionally, absence of ParP also resulted in reduced chemotaxis and swimming of the cells. ParC has also been suggested to be important for motility in non *Vibrios*. For instance, deletion of ParC in *Pseudomonas aeruginosa* results in a similar reduction of swimming motility as observed in *V. parahaemolyticus* (Reinhardt & Bardy, 2018).

1.12.2. HubP, the polar hub, positions ParC

As mentioned earlier, ParC follows a cell cycle dependent polar localization. It forms uni-polar and bi-polar foci depending on the age of the cell. In *V. cholerae* and *V. parahaemolyticus*, ParC is directed to the cell pole by the polar landmark protein HubP. On deletion of *hubP*, cells harboured either non-polar ParC foci or both polar and non-polar foci. Chemotaxis protein CheY3 was also found to be mislocalized together with mislocalized ParC in the $\Delta hubP$ strain (Yamaichi et al., 2012). The formation of non-polar ParC foci and mislocalization of downstream chemotaxis proteins in a $\Delta hubP$ background emphasizes the role of HubP in chemotaxis. Although ParC-ParP system is the chemotaxis cluster targeting system in *Vibrios*, HubP is the pole organizing protein that positions ParC to its destined location (Yamaichi et al., 2012).

When discovered, YFP-HubP was reported to be bi-polarly localized in new born *V. cholerae* cells (Yamaichi et al., 2012). However, later studies expressing HubP-sfGFP from its native locus confirmed a uni-polar foci at the old pole that in later stages of cell cycle attains a bi-polar localization, which is similar to the localization pattern of ParC (Galli et al., 2017).

HubP, in addition to positioning ParC, is also involved in the localization of FlhG and ParA1, two other ParA-like proteins. For instance, in wild-type *V. cholerae*, ParA1 formed uni-polar or bi-polar foci together with a gradient-like diffused localization (Figure 5A). In the absence of HubP, ParA1 no longer forms the polar foci and instead is entirely diffused (Figure 5B). HubP facilitates proper chromosome segregation by directing ParA1 to the poles (Yamaichi et al., 2012). ParA1 in turn binds the origin-bound ParB1, thereby tethering the origins to the cell poles (Figure 5C). Therefore, in a $\Delta hubP$ strain, where ParA1 is no longer polar, ParB1 also remain unattached to the poles (Figure 5D). Consequently, the localization of ParB1 in $\Delta parA1$ and $\Delta hubP$ strains resemble each other (Figure 5D and Figure 5E).

Furthermore, the placement of the flagellum is also regulated by HubP through FlhG. FlhG localizes uni-polarly or bi-polarly in wild-type *V. cholerae* cells. However, it becomes diffused or forms a non-polar focus in a $\Delta hubP$ strain. While $\Delta flhG$ results in an 80% increase in multiple flagella formation, $\Delta hubP$ leads to only a minor increase of 6%. Hence,

in spite of HubP's effect on localization of FlhG, the mislocalization does not alter the negative regulation exerted by FlhG on flagella formation. On the contrary, in *Vibrio alginolyticus*, HubP is directly involved in the regulation of the number of polar flagella where deletion of HubP leads to a significant increase in the fraction of cells with multiple flagella (Takekawa et al., 2016).

Altogether, HubP in *Vibrios* is an important pole organizing landmark protein that regulates positioning of wide variety of proteins and thereby regulating diverse processes. HubP, by regulating ParC positioning, impacts the chemotaxis of this group of bacteria.

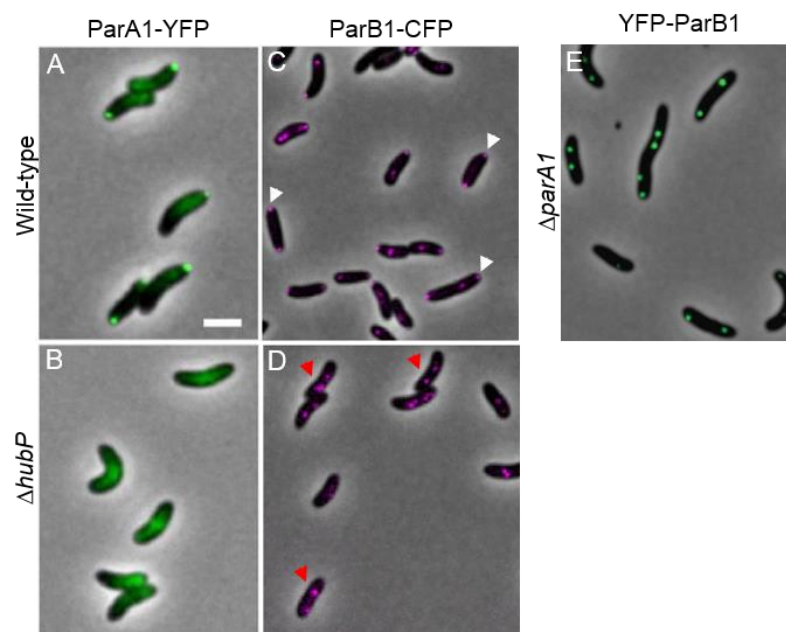


Figure 5: In *V. cholerae*, localization of ParB1 is governed by ParA1 which in turn is localized by HubP. (A-D) Subcellular localization of ParA1-YFP and ParB1-CFP in wild-type and $\Delta hubP$ *V. cholerae* swimmer cells. ParB1 in wild-type are attached to the poles (C, white arrows). On deletion of *hubP*, this anchoring is lost (D, red arrows). This mislocalization is similar to that in the $\Delta parA1$ strain in panel B. Scale bar 2 μm . (Yamaichi et al., 2012) (E) Localization of YFP-ParB1 in $\Delta parA1$ background. The ParB1 foci are not anchored to the cell poles. Scale bar 1 μm . (Fogel & Waldor, 2006).

1.13. Cell division in *Vibrios*

Even though cell division is well studied in a several organisms including *E. coli*, *B. subtilis*, and *C. crescentus*, they have in common that their genome is present as a single chromosome. Most information regarding cell division in multi-chromosomal bacteria is derived from studies of *V. cholerae*, a close relative of *V. parahaemolyticus*. However, unlike *V. cholerae*, *V. parahaemolyticus* undergoes a dimorphic life cycle.

V. cholerae encodes homologues of most genes that are known for replication, segregation, and cell division in *E. coli*. Some distinct differences between them are the

presence of HubP, the polar landmark protein that acts as a recruiter for several important proteins (Yamaichi et al., 2012) and the presence of the chromosome partitioning system. As described earlier, chromosome arrangement in *V. cholerae* is *ori-ter* and the ParABS system takes care of the alignment. The positioning and segregation of the terminus region is orchestrated by an ortholog of MatP that binds to the *matS* sequences encoded on the *ter1* and *ter2* regions (Demarre et al., 2014; Mercier et al., 2008) and keeps it coordinated with the divisome through the interaction of MatP ortholog to the divisome component (Espeli et al., 2012).

Although *V. cholerae* encodes for most of the cell division proteins also found in *E. coli*, the relative timing of various cell division steps is considerably different. The cell division protein, FtsZ, localizes to the cell pole at the beginning of the cell cycle in spite of the presence of an oscillating Min system. The uni-polar FtsZ in the new polar cells later relocalized to the mid-cell position. This relocalization occurs at around 50% of the cycle. The remaining late cell division proteins localize to the Z-ring at around 80% of the cell cycle and the constriction proceeds in the last 10% (Galli et al., 2016a, 2017). *V. cholerae* encodes for all the 3 components of the oscillating Min system. In spite of an oscillating Min, deletion of MinCD on its own only leads to mild mini-cell formation. Also, it only barely affects the localization pattern of FtsZ. However, deletion of *slmA* abolishes polar FtsZ in *V. cholerae*.

V. cholerae also encodes for SlmA, which is known to directly inhibit FtsZ polymerization when bound to specific binding motifs in chromosomal DNA (Bernhardt & De Boer, 2005). The SBS in *V. cholerae* are distributed on the origin proximal region of both the chromosomes. The ectopically expressed fluorescently tagged SlmA localizes over chromosomal DNA in *V. cholerae*. In a new born *V. cholerae* cell, where the chromosomal origin and terminus are located at the old pole and new pole respectively, SlmA located over the entire chromosomal region with exception of the cellular region with the terminus (the new pole). As the cell grows and the replicated chromosomes segregate, the termini positions to the mid-cell. At this stage SlmA localizes like a gradient extending from both the poles leaving a SlmA free-zone at the mid-cell. Therefore, SlmA localization throughout the cell cycle is mutually exclusive to the positioning of FtsZ. Altogether, suggesting that in *V. cholerae* nucleoid occlusion mediated by SlmA is the major cell division regulating component (Galli et al., 2016a). Additionally, earlier studies addressing the chromosome segregation choreography of Chr1 and Chr2 of *V. cholerae* shows that the SlmA bound DNA is excluded from the mid-cell only in the late stages of cell cycle (Demarre et al., 2014; Galli et al., 2016a). This explains the late Z-ring formation at the SlmA-absent region in *V. cholerae* cell.

Unlike the synthetic lethality of *min slmA* deletion in *E. coli*, this double deletion strain of *V. cholerae* is viable. The effect of the Min deletion in perturbing cell division increases when the cellular chromosome arrangement is compromised, suggesting that nucleoid occlusion has a major role in regulating the placement of the division site in *V. cholerae* (Galli et al., 2016a).

1.14. *Vibrio parahaemolyticus*: a model for cell division

An organism that undergoes dimorphic differentiation is *Vibrio parahaemolyticus*, a Gram-negative γ -proteobacterium that is found in estuarine, marine and coastal environments. It is an important human pathogen, which has emerged as the most common cause of seafood-borne acute gastroenteritis world-wide (Letchumanan et al., 2014). The cell biology of *V. parahaemolyticus* is a very interesting field because of the bacterium's ability to exhibit a dimorphic lifestyle. In liquid environments it exists as a swimmer cell propelled by a single polar flagellum (Figure 6). In media of higher viscosity, where the motion of the polar flagellum becomes increasingly hindered, the swimmer cells differentiate into long swarmer cells. Furthermore, long swarmer cells from the periphery resume division and become short in a few minutes once they come in contact with a liquid environment (Shinoda & Okamoto, 1977).

Additionally, the differentiation to the swarmer cell cycle induces a second motility system that results in the formation of hundreds of lateral flagella (Figure 6). There are considerable differences between the polar and lateral flagella. The single polar flagellum is covered by a membrane (sheath) that is assumed to be the extension of the outer cell membrane while the lateral flagella are unsheathed (McCarter, 1999). The polar flagellum is propelled by the energy of sodium motive force. The two flagella do not share even a single structural component and are employed by the organism in entirely different niches even though the polar flagellum is constitutively present. In addition to aiding motility, the polar flagellum is suggested to act as a surface sensor, as conditions that slow down the rotation of the polar flagellum lead to induction of differentiation to swarmer cells (Belas et al., 1986; McCarter et al., 1988). However, further evidence also suggests that obstruction of the polar flagellar rotation cannot act as the sole trigger for initiation of the swarm program. Limitation of iron in the growth medium was also shown to act as a second signal for this regulation (McCarter & Silverman, 1989).

Swarming is a form of motility that bacteria employs to move rapidly on surfaces. It is assayed by inoculating a liquid culture of swimmer cells on hard agar surfaces (for

example, heart infusion agar). When spotted onto a hard agar surface, the cells differentiate, swarm out from the site of inoculation forming a swarm colony. Cell elongation is one of the initial events during the differentiation of *V. parahaemolyticus* cells into swarmer cells. During the swarmer life cycle these cells can reach lengths greater than 50 μm . These long cells can swarm together rapidly and expand over surfaces. As the progression of the swarm colony proceeds, the long cells that are not part of the expanding periphery any longer dedifferentiate to form short cells and those that comprise the fast-expanding outer periphery remain elongated. For the swarm colony to continue the expansion of the colony, swarmer cells must undergo a regulated division such that the population of long swarmer cells are not lost.

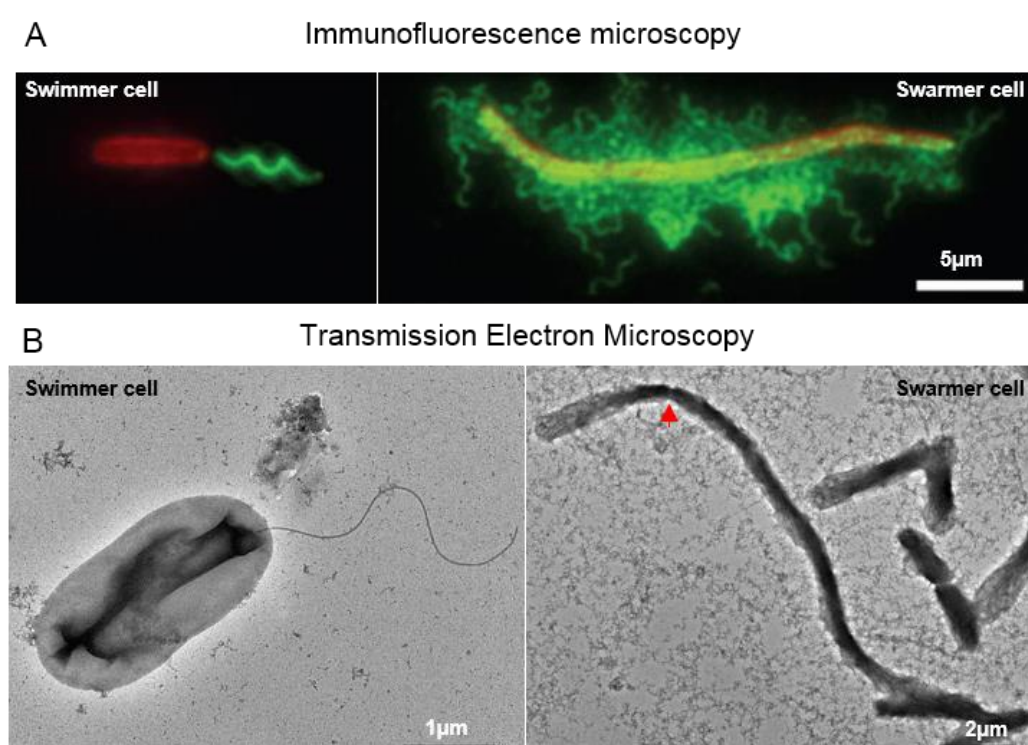


Figure 6: *Vibrio parahaemolyticus* swimmer cell and swarmer cell. (A) A swimmer cell grown in liquid culture and a swarmer cell grown on a surface were fixed and stained with the membrane dye FM 4-64 (in red) and the anti-polar flagellin antiserum (in swimmer cell) or the anti-lateral flagellin antiserum (in swarmer cell). Figure adapted from Gode-Potratz et al. 2011. (B) The left panel is a transmission electron micrograph of swimmer cell with a uni-polar flagellum and the right panel shows swarmer cells of different lengths. The longest cell is undergoing a non-mid-cell division (red arrow).

How the bacterium regulates the cell elongation and chromosome segregation to enable its differentiation to swarmer cells remain uninvestigated. At what position in the long swarmer cells the divisome establishes and what regulators determine this placement also remain unaddressed. Furthermore, the mechanisms that ensure swarmer division without diminishing the long swarmer cell population are unknown.

1.15. Scope of the research

Many bacteria, including species of *Serratia* (Alberti & Harshey, 1990), *Aeromonas* (Kirov et al., 2002), *Salmonella* (Harshey, 1994), *Proteus* (Rather, 2005), and *Vibrio* (Sar et al., 1990), differentiate between two developmentally distinct cell types – a free living swimmer cell found in liquid environments and a swarmer cell that is specialized for attachment and movement across solid surfaces (McCarter, 2004). An organism that undergoes such differentiation is *Vibrio parahaemolyticus*. *V. parahaemolyticus* swimmer cells are optimized for swimming in liquid environments and exist as short rod-shaped cells with a single polar flagellum to propel themselves forward. When swimmer cells encounter a solid surface, differentiation into a swarmer cell is triggered by the physical contact. Swarmer cells are optimized for movement on solid surfaces or through viscous environments, enabling *V. parahaemolyticus* to rapidly colonize surfaces (Gode-Potratz et al., 2011; Makino et al., 2003; McCarter, 1999, 2004, 2010; McCarter & Silverman, 1990; Stewart & McCarter, 2003). Swarmer cells express a second motility system, resulting in a multitude of lateral flagella, which are essential for swarming behavior and for surface and cell-cell contact in order to coordinate movement across surfaces (Baumann & Baumann, 1977; Böttcher et al., 2016; McCarter, 2004). One of the initial events of differentiation is inhibition of cell division. Consequently, swarmer cells are typically highly elongated compared to planktonic swimmer cells (Baumann & Baumann, 1977; Böttcher et al., 2016; McCarter, 2004). However, in order for the swarm colony to expand, swarmer cells must divide and proliferate and thus rely on a mechanism that allows for cell division without diminishing the long swarmer population. It is not clear how cell division, chromosome segregation and chromosome organization are regulated in *V. parahaemolyticus*. Furthermore, it is not clear how chromosome segregation is coordinated with cell elongation during differentiation. Also, the mechanisms that ensure swarmer division without diminishing the long swarmer cell population are unknown.

Thus, here we aim to study i) the mechanisms regulation cell division, ii) chromosome organization and iii) how chromosome organization is coordinated with cell division in *V. parahaemolyticus*. These aims will be with a special focus on how these processes are regulated and coordinated with the cell cycle during the swarming life style of this bacterium.

CHAPTER II

RESULTS

2.1. Part I-Understanding the classical regulators of cell division

2.1.1. *V. parahaemolyticus* encodes the general division determinants FtsZ, MinCDE and SlmA

The genome of the multi-chromosomal *V. parahaemolyticus* encodes for homologues of the major cell division effectors and regulator proteins, namely FtsZ, SlmA, and the MinCDE components, which are the same as for the mono-chromosomal *E. coli*, a well-studied model organism for bacterial cell division.

An alignment of FtsZ, SlmA, and MinD of *V. parahaemolyticus* against the corresponding proteins from *V. cholerae*, *E. coli*, *C. crescentus*, *B. subtilis*, and *M. xanthus* was carried out. *V. parahaemolyticus* FtsZ (FtsZ_{V.p}) displayed 91% and 79% sequence similarity with FtsZ of *V. cholerae* and *E. coli*, respectively. The tubulin-like signature motif is conserved in FtsZ_{V.p} as described for other bacterial model organisms (Figure 7A, in yellow). The asparagine (N) and aspartic acid (D) residues that have been shown in *E. coli* to be essential for FtsZ's GTPase activity are all conserved in FtsZ_{V.p} (Figure 7A, in blue) (Wang et al., 1997). The C-terminal core, established to be important for FtsZ's interaction with FtsA and/or ZipA (Figure 7A, in green) are also conserved in FtsZ_{V.p} (Ma & Margolin, 1999). This region also includes the residues important for FtsZ's interaction with SlmA (Schumacher & Zeng, 2016).

SlmA_{V.p} displayed 89% and 66% sequence similarity with that of SlmA_{V.c} and SlmA_{E.c}, respectively. Furthermore, SlmA_{V.p} has conserved residues for all positions described in SlmA_{E.c} for its interaction with FtsZ C-terminal domain (CTD) through hydrophobic interactions (Figure 7B, in yellow), salt bridges (Figure 7B, in blue) and hydrogen bonds (Figure 7B, in green) (Schumacher & Zeng, 2016). The sequence of MinD_{V.p} is 88% similar to that of MinD_{V.c} and 78% to that of MinD_{E.c}. In MinD_{V.p}, the 16th Lysine residue in the Walker A motif (Figure 7C, in red), previously described to be important for MinD_{E.c} dimerization, is also conserved. Moreover, the Arginine-Aspartic acid-Lysine residues, which are essential for the pole-to-pole oscillation as shown in studies with *E. coli* (Szeto et al., 2005), are conserved in MinD_{V.p} (Figure 7C, in purple). Residues in MinD_{E.c} that interact with ATP are also conserved in MinD_{V.p} (Figure 7C, indicated by an asterisk). Additionally, as studies in *E. coli* showed, the residues found to be important for (i) MinD's interaction with MinE (Figure 7C, in blue); (ii) MinD's interaction with MinC, and (Figure 7C, in red) (iii) MinD's interaction with MinC and MinE (Figure 7C, in grey) (Wu et al., 2011)

RESULTS

are all conserved in MinD_{V.p.}. The C-terminal amphipathic helix involved in the membrane-binding of MinD is also conserved in *V. parahaemolyticus* (Figure 7C, in violet).

In conclusion, *V. parahaemolyticus* encodes for the main cell division determinants and regulators FtsZ, SlmA and MinD

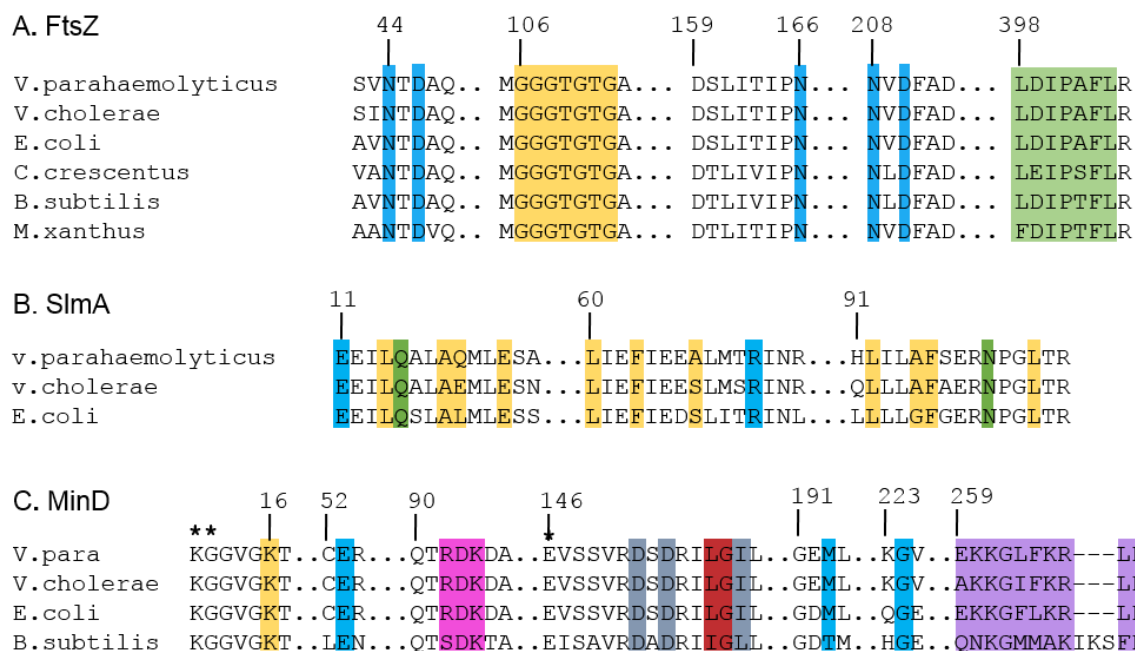


Figure 7: Sequence conservation of FtsZ, SlmA, and MinD in *V. parahaemolyticus* in comparison to other bacterial model organisms. (A) Tubulin-like motif in yellow; asparagine and aspartic acid residues important for GTPase activity in blue; C-terminal region required for FtsA, ZipA and SlmA interaction in green. (B) Residues of SlmA that interact with FtsZ through hydrophobic interactions (in yellow), salt bridges (in blue), and hydrogen bonds (in green). (C) MinD residues that are important for ATP interaction (marked with asterisks), MinE interaction (in blue), MinC interaction (in grey), and with both MinE and MinC (in red). Lysine in MinD is important for its dimerization (in yellow), residues that are important for MinD's pole-to-pole oscillation (in purple), and the C-terminal amphipathic helix (in violet).

2.1.2. Localization dynamics of FtsZ in *V. parahaemolyticus* swimmer cells

It is not ascertained that sequence or structural conservation of proteins across species guarantee similarities in cellular localization pattern or in its functions. Hence, we set to study the localization of FtsZ in *V. parahaemolyticus*. Thus, an N-terminal YFP tagged fusions of the early cell division protein FtsZ was ectopically expressed in addition to the native *ftsZ* allele in wild-type *V. parahaemolyticus*.

YFP-FtsZ localized to one pole of the new born swimmer cells in *V. parahaemolyticus* (Figure 8A, red arrows). This pattern is distinctly different in *E. coli*, where FtsZ localizes strictly to the mid-cell (Galli et al., 2016a). The localization of FtsZ in *V. parahaemolyticus* was similar to that reported in *V. cholerae* (Galli et al., 2016a; Srivastava et al., 2006).

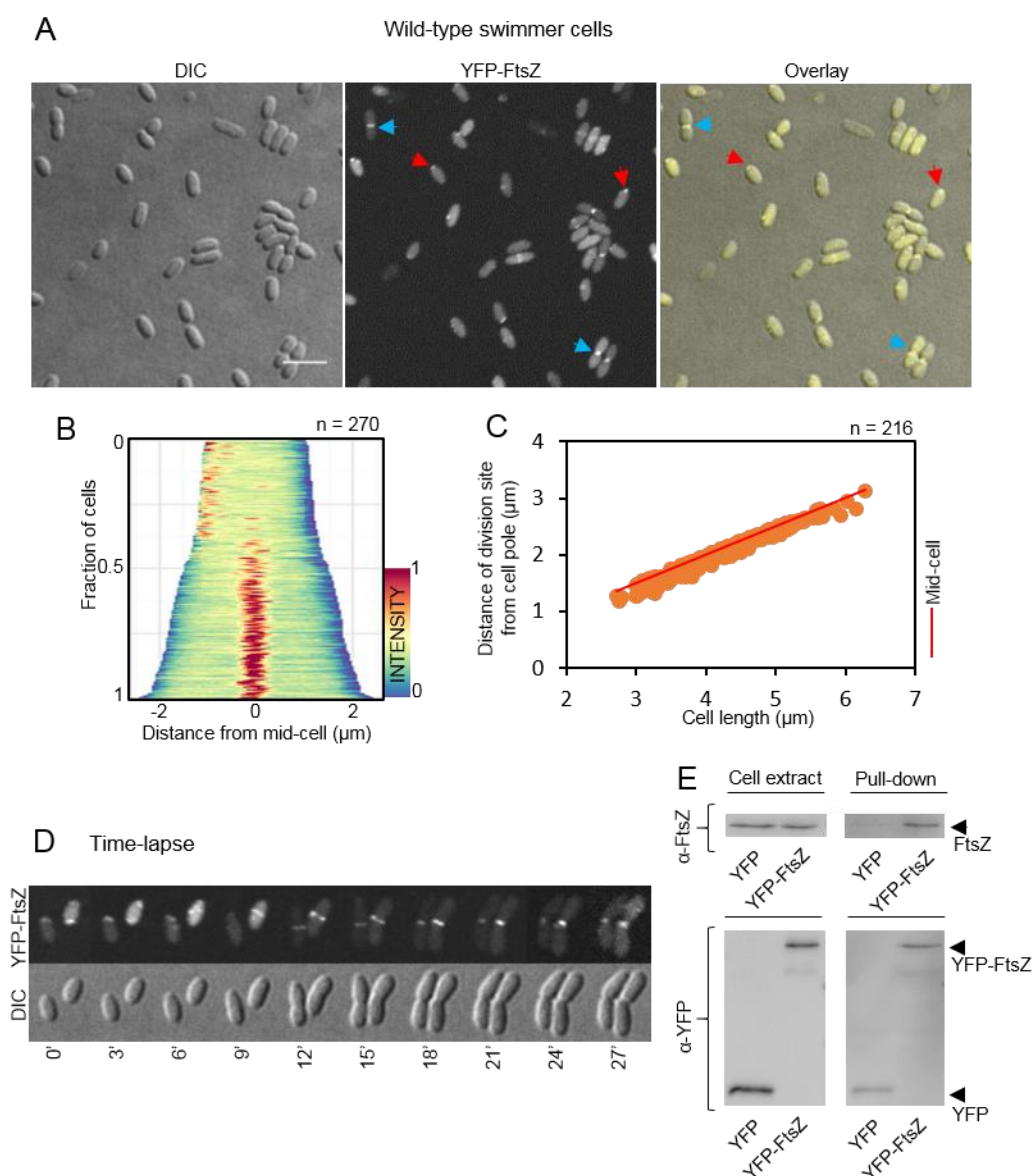


Figure 8: Polar FtsZ localization transitions to mid-cell upon the onset of cell division in swimmer cells of *V. parahaemolyticus*. (A) Fluorescence microscopy showing the intracellular localization of YFP-FtsZ in wild-type *V. parahaemolyticus* swimmer cells. Red arrows show uni-polar FtsZ and blue arrows indicate mid-cell Z-ring. (B) Demographic analysis indicating the position and intensity of fluorescence of YFP-FtsZ along the cell length in a population of swimmer cells. (C) Graph depicting the distance of division sites from the cell pole as a function of cell length. (D) Time-lapse fluorescence microscope showing the dynamic localization of YFP-FtsZ in new born swimmer cells until the next division event. (E) Co-immunoprecipitation experiment using beads with attached α -YFP antibodies on wild-type *V. parahaemolyticus* cells expressing YFP (negative control) or YFP-FtsZ, respectively. Cell extracts before incubation with α -YFP beads and precipitated α -YFP beads, were analyzed by Western blot using α -FtsZ antibodies to test for the co-purification of FtsZ protein.

Additionally, FtsZ also localized as a prominent ring-like structure at mid-cell (Z-rings) (Figure 8A, blue arrows). To further understand the localization pattern of FtsZ during the cell cycle we performed a demographic analysis. This, showed that in short young cells FtsZ localized as a focus a one cell pole. As cells became longer the localization of FtsZ shifted to mid-cell (Figure 8B, C), indicating a cell-cycle dependent localization of FtsZ. To

RESULTS

further explore this localization pattern we followed the dynamics of YFP-FtsZ from parent cell to the daughter cells by time lapse microscopy. YFP-FtsZ was observed as a single focus at one of the poles in the short cell (Figure 8D at 0'). As the cell elongated, the polar FtsZ focused disappeared and a classical Z-ring was formed at mid-cell (Figure 8D). This ring persisted until the entire division was completed and the two new daughter cells inherited a focus each at their respective new poles. Therefore, from the time-lapse it became evident that the single focus observed in the short cells is present at the new pole. Importantly, co-immunoprecipitation assays indicated that YFP-FtsZ interacted with native FtsZ (Figure 8E) and YFP-FtsZ localized to and marked the positioning of future division sites as would be expected for functional FtsZ protein. Altogether, this suggests that the YFP-FtsZ fusion protein is partially functional and can be used as a marker for studying the regulation and localization of FtsZ.

Thus, the swimmer cells of *V. parahaemolyticus* undergo binary cell divisions with symmetric placement of the division sites like *E.coli* or *V. cholerae*. We further decided to investigate the positioning of the chromosomes by visualizing the origins of the two chromosomes.

2.1.3. *OriI* localizes to both cell poles whereas *oriII* is not tethered within the cells

It is essential for cell survival that each daughter cell inherits a complete copy of the genome after completion of cell division. The genome of *V. parahaemolyticus* is divided between chromosome 1 and chromosome 2. In *V. cholerae* the ParAB1 and ParAB2 systems are responsible for proper segregation of *ori1* and *ori2* of chromosome 1 and 2, respectively (Yamaichi et al., 2007b).

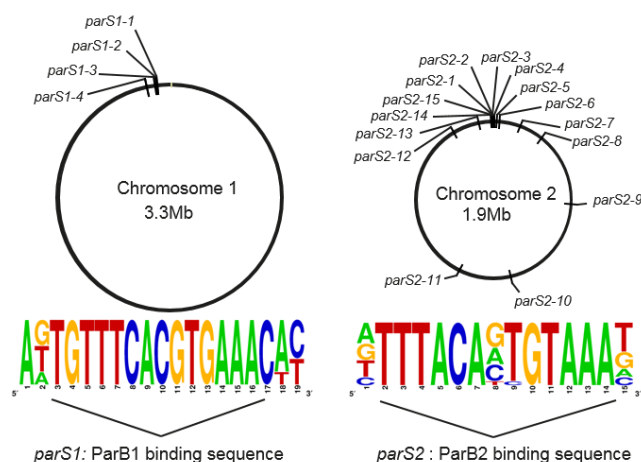


Figure 9: Schematic depicting the consensus sequence (sequence logo) of *parS1* and *parS2* centromere sites and their location on *V. parahaemolyticus* chromosome 1 and 2, respectively.

Similarly, *V. parahaemolyticus* encodes two ParABS chromosome partitioning systems, ParABS1 and ParABS2 for chromosome 1 and 2, respectively. Additionally, each chromosome encodes predicted *parS1* and *parS2* centromere sites near *ori1* and *ori2* (Figure 9) (Yamaichi et al., 2007a).

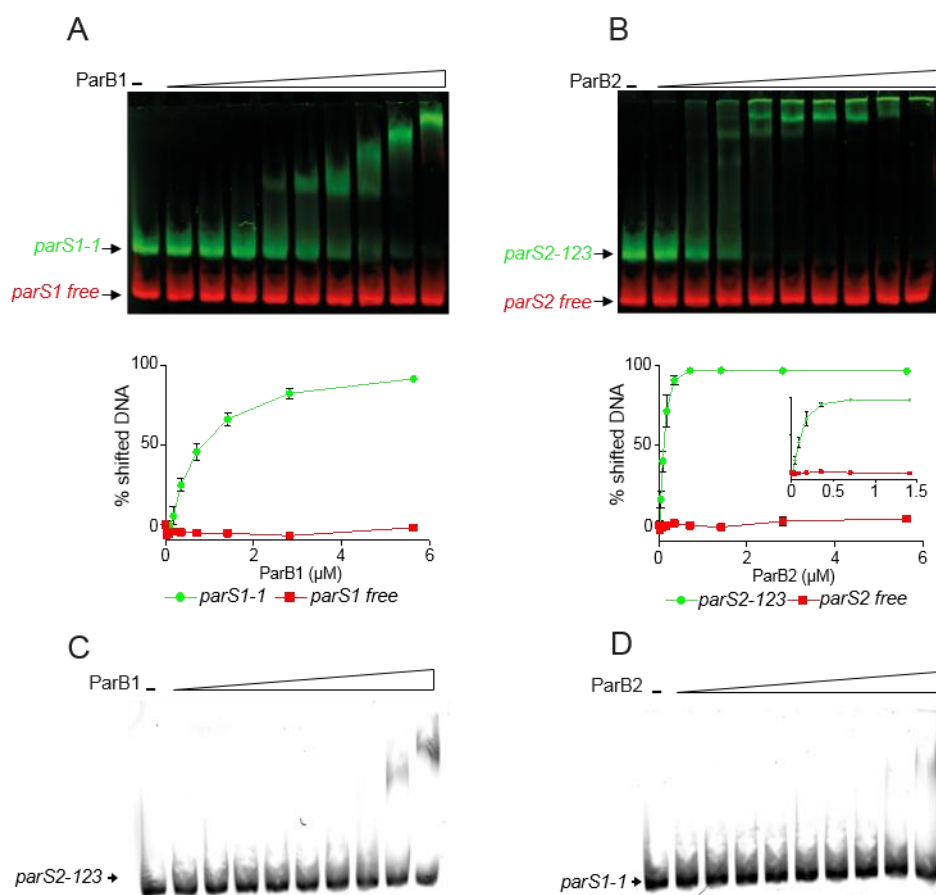


Figure 10: Specific DNA binding properties of ParB1 and ParB2. Gel-shift experiment with (A) ParB1 and (B) ParB2 testing for their ability to bind Cy5-labeled DNA (green) containing *parS1* and *parS2* sites, respectively. Cy3-labeled non-specific DNA (not containing either *parS1* or *parS2*) was added as a negative control (red). Graphs show the percentage of shifted DNA as a function of ParB1/ParB2 concentration. (C) EMSA experiment with ParB1 testing for its ability to bind Cy5-labeled *parS2*-DNA. (D) EMSA experiment with ParB2 testing for its ability to bind Cy5-labeled *parS1*-DNA. Error bars indicate SEM. ParB1 and ParB2 were added in the following concentrations: 0.022 μ M, 0.044 μ M, 0.088 μ M, 0.18 μ M, 0.35 μ M, 0.70 μ M, 1.40 μ M, 2.82 μ M and 5.63 μ M.

We investigated the localization pattern of the putative centromere binding protein ParB1 and ParB2 as a reporter of replication status and origin localization of chromosome I and chromosome II, respectively. We first confirmed the binding of ParB1 to *parS1* and ParB2 to *parS2* by electrophoretic mobility shift assays (EMSA), using purified C-terminally His₆-tagged ParB1 and ParB2 proteins. The EMSA showed that ParB1 and ParB2 specifically binds to DNA that includes the *parS1* and *parS2* sites, respectively (Figure 10A and B, in green). Neither proteins bound to non-specific DNA free of *parS1* and *parS2* sites (Figure

RESULTS

10A and B, in red). Importantly, ParB1 does not bind to *parS2* sites and ParB2 does not bind *parS1* sites (Figure 10C and D). Thus, by fluorescently labeling ParB1 and ParB2, we could specifically localize the position of the *parS1* and *parS2* sites within the cell – corresponding to the position of *ori1* and *ori2* respectively.

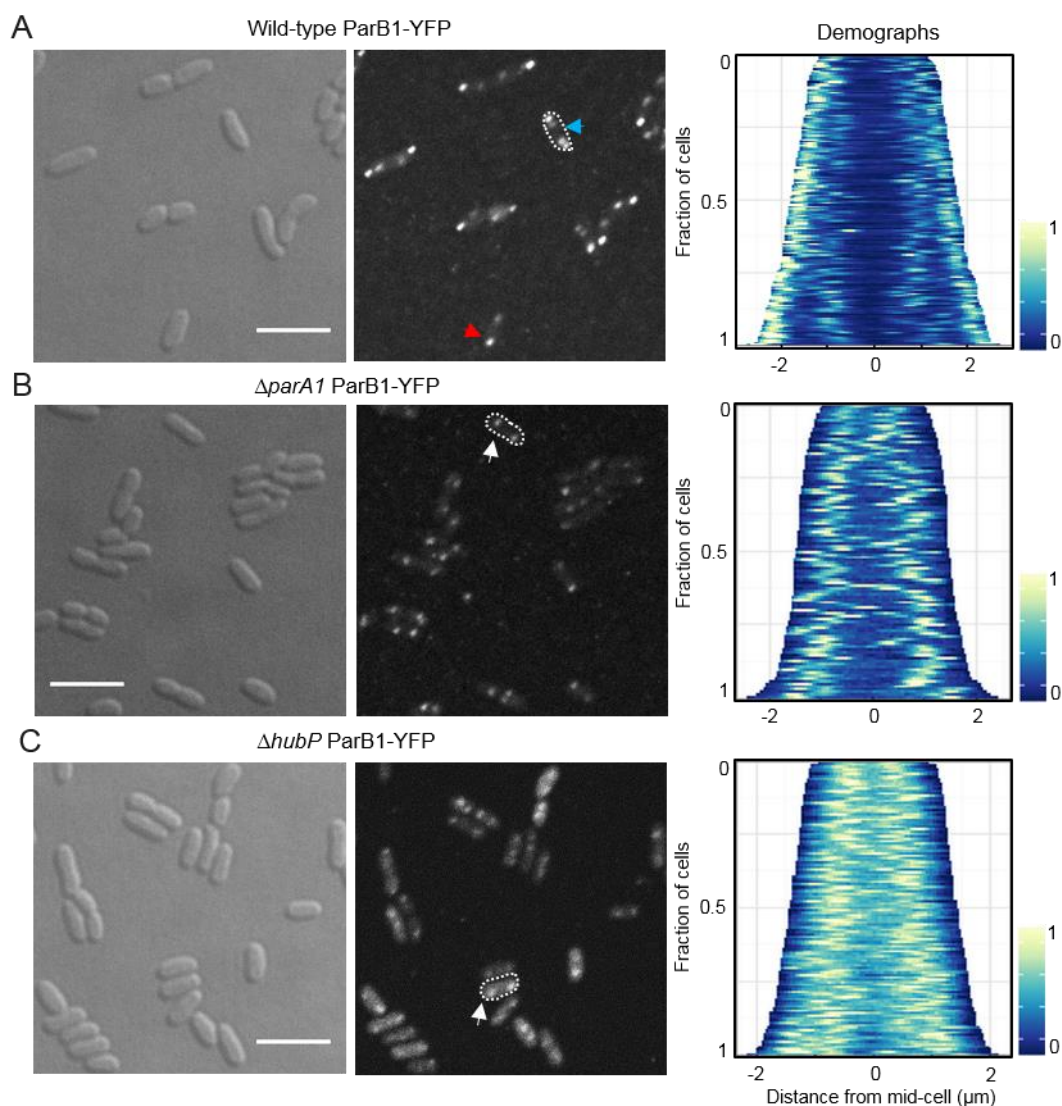


Figure 11: Proper ParB1 localization in *V. parahaemolyticus* swimmer cells is dependent on ParA1. (A) Fluorescence microscopy and demograph showing the intracellular localization of ParB1-YFP in wild-type *V. parahaemolyticus* swimmer cells. (B) Fluorescence microscopy and demograph showing the intracellular localization of ParB1-YFP in $\Delta parA1$ *V. parahaemolyticus* swimmer cells. (C) Fluorescence microscopy and demograph showing the intracellular localization of ParB1-YFP in $\Delta hubP$ *V. parahaemolyticus* swimmer cells. Scale in each image is 5 μm .

Afterwards, strains were generated in which the native *parB1* and *parB2* were replaced with *parB1-YFP* and *parB2-mCherry*, respectively. The resulting strain with tagged ParB1 strictly displayed at least two ParB1-YFP foci in the new born (short) cells (Figure 11A, red arrow) and three or four foci in the growing (long) cells (Figure 11A, blue arrow). This

strongly indicates that the new born cell inherits an already replicating Chromosome I as was already observed in *V. cholerae* grown in rich media (Stokke et al., 2011). Additionally, both the ParB1 foci localized to the two poles of the cell, suggesting an anchoring of the segregated origins of chromosome 1 to the opposite poles. HubP, which localizes bi-polarly in *Vibrios* (Galli et al., 2017; Yamaichi et al., 2012), could localize the origin bound ParB1 to the poles by directing ParA1 to the cell poles.

To verify this hypothesis, the localization pattern of ParB1 in the $\Delta parA1$ and the $\Delta hubP$ strain was compared to that of the wild-type. Both deletions resulted in a deviant positioning of ParB1. In the $\Delta parA1$ background, ParB1 still formed foci, but was no longer strictly tethered to the poles (Figure 11B, white arrow). Also, the number of foci in growing cells seemed to be fewer than in wild-type (Figure 11B). This could be because the segregation of the replicated origins from each other is affected in the absence of ParA1. This may influence the resolution of the chromosomes and thus the two foci could appear to be one. Additionally, the deletion of *hubP* also affected ParB1 localization in an almost similar way as that in the $\Delta parA1$ mutant. In the absence of *hubP* (that directs positioning of ParA1), ParB1-YFP was also not tethered to the poles and remained not well separated as in the $\Delta parA1$ mutant (Figure 11C, white arrow). Interestingly, ParB1 displayed an additional diffused signal in the cytosol in $\Delta hubP$ (Figure 11C).

Similar to ParB1-YFP, ParB2-mCherry also formed at least one focus in the new born cells and more foci as the cells grew. However, the ParB2 foci did not attach to the cell poles and instead localized between the quarter positions of the cell (Figure 12A). This suggests that either *ChrII* is not anchored to the cell poles, or that its anchoring point is not the origin, as was suggested for *V. cholerae* (Fiebig et al., 2006). Additionally, in a *parA1* deletion background, no significant change in the localization pattern of ParB2 was observed (Figure 12B). This suggests that the two chromosomes could be following different mechanisms of segregation.

The analysis of the static images suggested that the replication and origin segregation dynamics of the two chromosomes are distinct. A comparison of the scatter plots of ParB1 and ParB2 foci clearly shows more ParB1 foci at any point in the cell cycle, suggesting that *orII* initiates replication ahead of *orIII* (compare demographs of Figure 11A and Figure 12A) as was also observed earlier in *V. cholerae* (Fogel & Waldor, 2005).

RESULTS

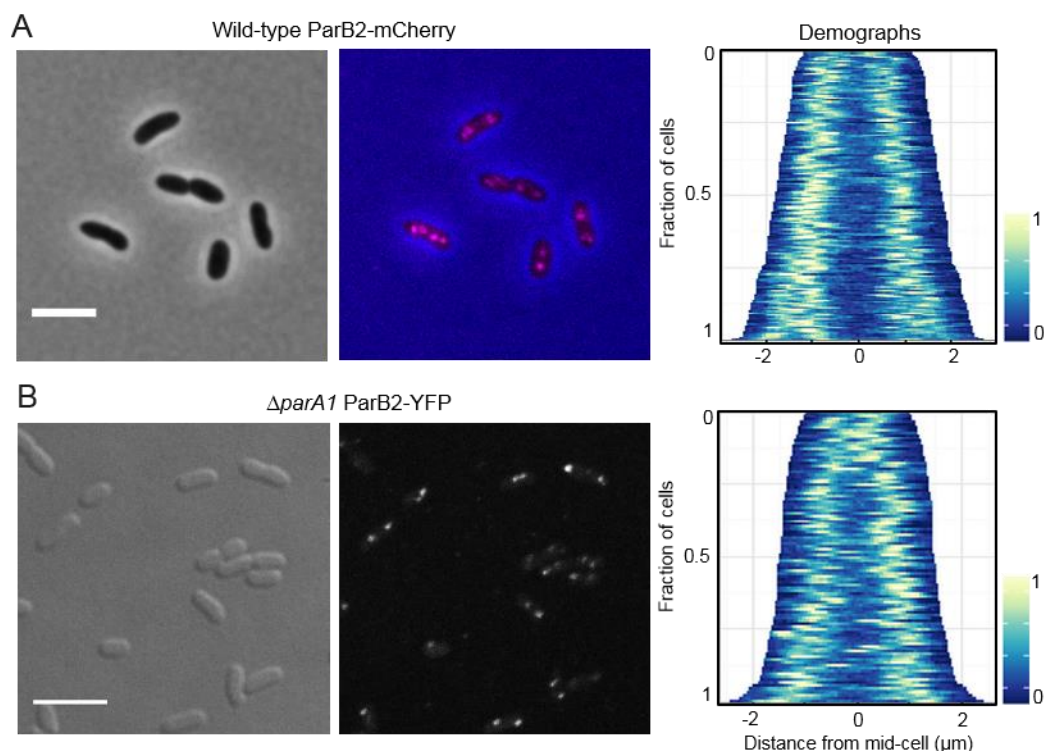


Figure 12: Segregation of chromosome II is not likely dependent on ParA1 in swimmer cells of *V. parahaemolyticus*. (A) Fluorescence microscopy and demograph showing the intracellular localization of ParB2-mCherry in wild-type *V. parahaemolyticus* swimmer cells. (B) Fluorescence microscopy and demograph showing the intracellular localization of ParB2-YFP in $\Delta parA1$ *V. parahaemolyticus* swimmer cells. Scale is 5 μ m.

Our data revealed that the mode of division of *V. parahaemolyticus* swimmer cells, as well as the localization of several cell division proteins, shares similarities with *V. cholerae*. However, unlike *V. cholerae*, *V. parahaemolyticus* follows a dimorphic lifestyle (Figure 6). The localization of the cell division proteins, division regulators, and their function in swarmer cells remain unaddressed until now. Therefore, we next addressed cell division and its regulation in swarmer cells.

2.1.4. A cell length-dependent switch from mid-cell to non-mid-cell placement of the Z-ring and the division site in *V. parahaemolyticus* swarmer cells

The flares extending outward from *V. parahaemolyticus* swarmer colonies consist of swarmer cells stacked in a few layers, thinning to a monolayer of swarmer cells at the very edge (Figure 13A), which enables single cell microscopy analysis (Heering et al., 2017; Heering & Ringgaard, 2016). The population of swarm flares is heterogeneous, comprising cells ranging from 2 μ m to >40 μ m in length (Figure 13B).

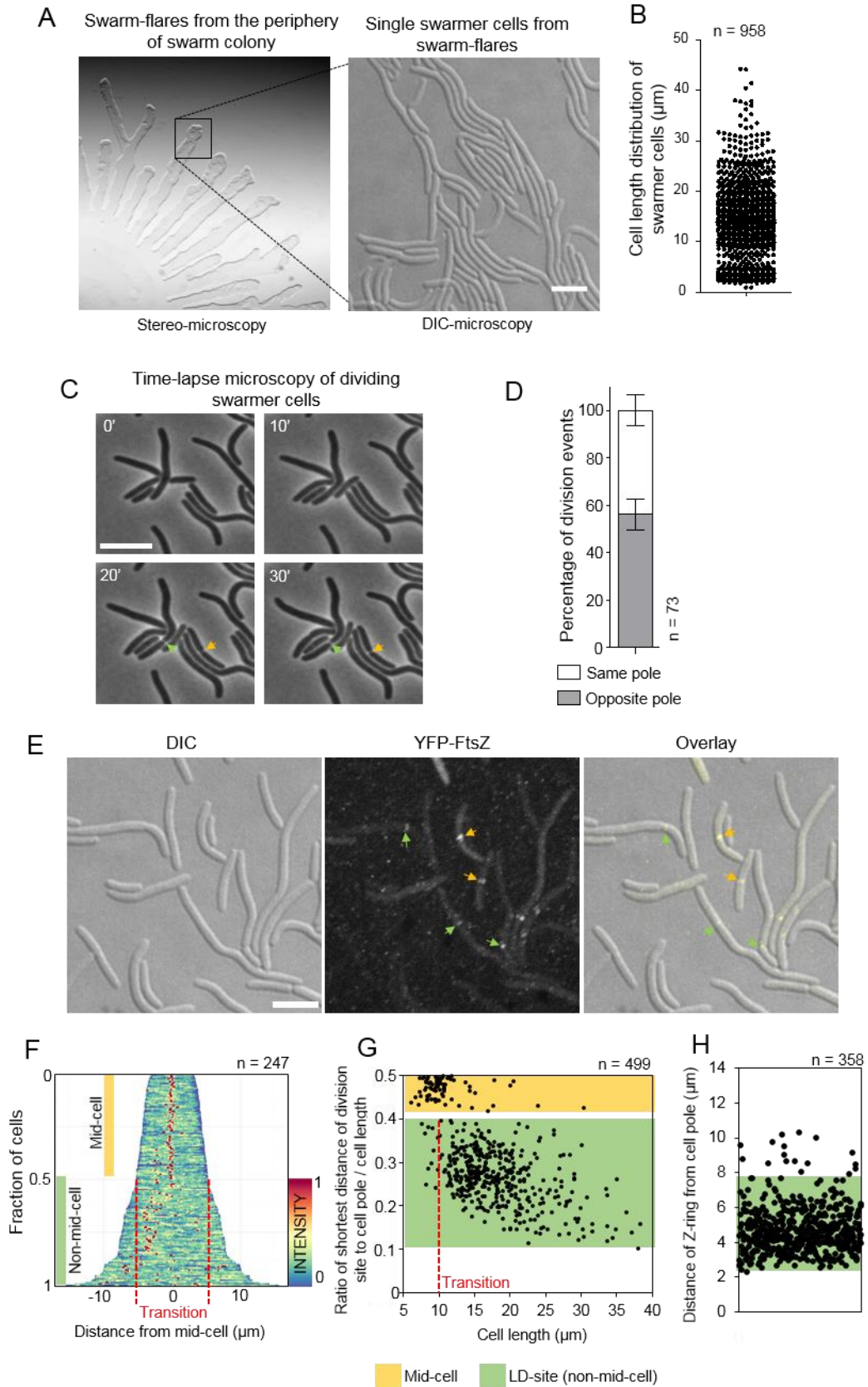


Figure 13: A cell length-dependent switch in the positioning of the Z-ring and division site in swarmer cells. (A) Stereo- and DIC microscopy of swarm-flares and individual swarmer cells from swarm-flares, respectively. (B) Scatter plot showing the cell length-distribution of wild-type swarmer cells from swarm-flares. (C) Phase contrast time-lapse microscopy of dividing *V. parahaemolyticus* swarmer cells.

RESULTS

Orange arrow indicates a mid-cell division. Green arrow indicates a non-mid-cell division. (D) Bar graph showing the percentage of division event occurring proximal to same or opposite pole in respect to the previous division events during non-mid-cell division of swarmer cells. Error bars indicate standard error of the mean. (E) Fluorescence microscopy showing the intracellular localization of YFP-FtsZ in wild-type *V. parahaemolyticus* swarmer cells. (F) Demographic analysis showing the fluorescence intensity of YFP-FtsZ along the cell length in a population of *V. parahaemolyticus* swarmer cells relative to cell length. In cells shorter than 10 μm FtsZ is symmetrically positioned at mid-cell. In cells longer than 10 μm FtsZ is positioned at a non-mid-cell position. Red lines indicate the cell length at which the transition from mid-cell to the non-mid-cell LD-site (Length Dependent-site) positioning of the Z-ring occurs. (G) Graph depicting the ratio of shortest distance of division site from cell pole as a function of cell length in swarmer cells. Placement of the division site falls within two groups; mid-cell (yellow) and the non-mid-cell LD-site (green) position. Red line indicates the cell length at which a transition from mid-cell to LD-site positioning of division occurs. (H) Scatter-plot of the distance of Z-ring from the cell pole in swarmer cells. Green lines indicates the region of 2.5-8 μm from the cell pole – the LD-site – where the cell division takes place during non-mid-cell division of swarmer cells. (A, F) Scale bar represents 5 μm .

Interestingly, we observed that swarmer cells divide but experienced different types of division events; a subset of cells divided at mid-cell (Figure 13C, orange arrow), while in others division occurred at a non-mid-cell position, resulting in progeny cells of different sizes (Figure 13C, green arrow) - suggesting that the heterogeneity in cell size could in part be a result of non-mid-cell division events. Time-lapse microscopy demonstrated that during non-mid-cell division, cells showed no preference for one cell pole in the placement of the division site, as non-mid-cell division occurred equally often towards the same pole or the opposite pole, with respect to the previous division event (Figure 13D).

In order to further characterize cell division in swarmer cells we localized YFP-FtsZ in the wild-type swarmer cells. Importantly, swarmer cells displayed marked differences in FtsZ positioning and placement of the division site, depending on their cell length: in short swarmer cells (< 10 μm), the Z-ring formed at mid-cell (Figure 13E, orange arrows, F). We then analyzed the position of division sites by measuring the distance of division invaginations to the cell pole and relative to the cell length (henceforth, these invaginations are referred to as division sites). Consistently, short swarmer cells divided at mid-cell (Figure 13G, orange group), resulting in daughter cells of equal sizes. However, when swarmer cells reached 8 - 10 μm in length, a transition from a mid-cell localization to a non-mid-cell placement of the Z-ring occurred (Figure 13E, green arrows, F). Non-mid-cell localization of the Z-ring in swarmer cells longer than 10 μm always (97 % of cells) occurred at distance of 2.5-8 μm from the cell pole (Figure 13H) – thus, we defined this region as the swarmer's LD-site (Length-Dependent division-site). Consistent with placement of the Z-ring at the LD-site, swarmer cells ultimately divided at this position (Figure 13G, green group), resulting in progenies of different cell lengths. Divisions were never observed within the first 0-2.5 μm , therefore polar regions of the cell are protected from division events (Figure 13G, H). Altogether, these data show that both long and short

swarmer cells can divide and that the placement of the division site is cell length-dependent.

2.1.5. The MinCDE system is required for proper cell division in swimmer cells and swarmer cells of *V. parahaemolyticus*.

Despite the clear differences in the spatio-temporal regulation of FtsZ positioning during the developmental stages of *V. parahaemolyticus* (Compare Figure 8B and Figure 13F), a subset of the swimmer and swarmer cell populations also share the common characteristic of Z-ring formation at mid-cell, suggesting a common mechanism regulating the positioning of the division machinery at mid-cell. As the MinCDE system regulates the positioning of the Z-ring to mid-cell in many rod-shaped bacteria, the effect of deleting the Min-system ($\Delta minCDE$) in swimmer and swarmer cells was analyzed. In swimmer cells, deletion of *minCDE* resulted in non-mid-cell divisions leading to the formation of both mini-cells (4.0 %) and elongated cells (4.6 %) (Figure 14A, C, D), a common phenotype of cells relying on MinCDE for the positioning of the Z-ring (Ortiz et al., 2015).

In swarmer cells, deleted of *minCDE* an even larger proportion (21.3 %) were mini-cells compared to 1.3 % the wild-type swarmer cells (Figure 14B, C, and G). Consistent with the formation of mini-cells, YFP-FtsZ localized to the cell pole (Figure 14E, F, and H) in 50.5 % of the swarmer cells lacking MinCDE, while only 7.2 % of wild-type swarmer cells showed polar localization of FtsZ (Figure 14H). Importantly in the swarmer cells deleted of the MinCDE system, polar localization of FtsZ and all polar division events occurred within 0-2 μm from the cell pole (Figure 14I). However, this region is always protected from division events in wild-type cells (Figure 14I). Thus, the Min system regulates cell division and protects the pole from aberrantly localized FtsZ and consequently from polar division events in both swimmer and swarmer cells.

RESULTS

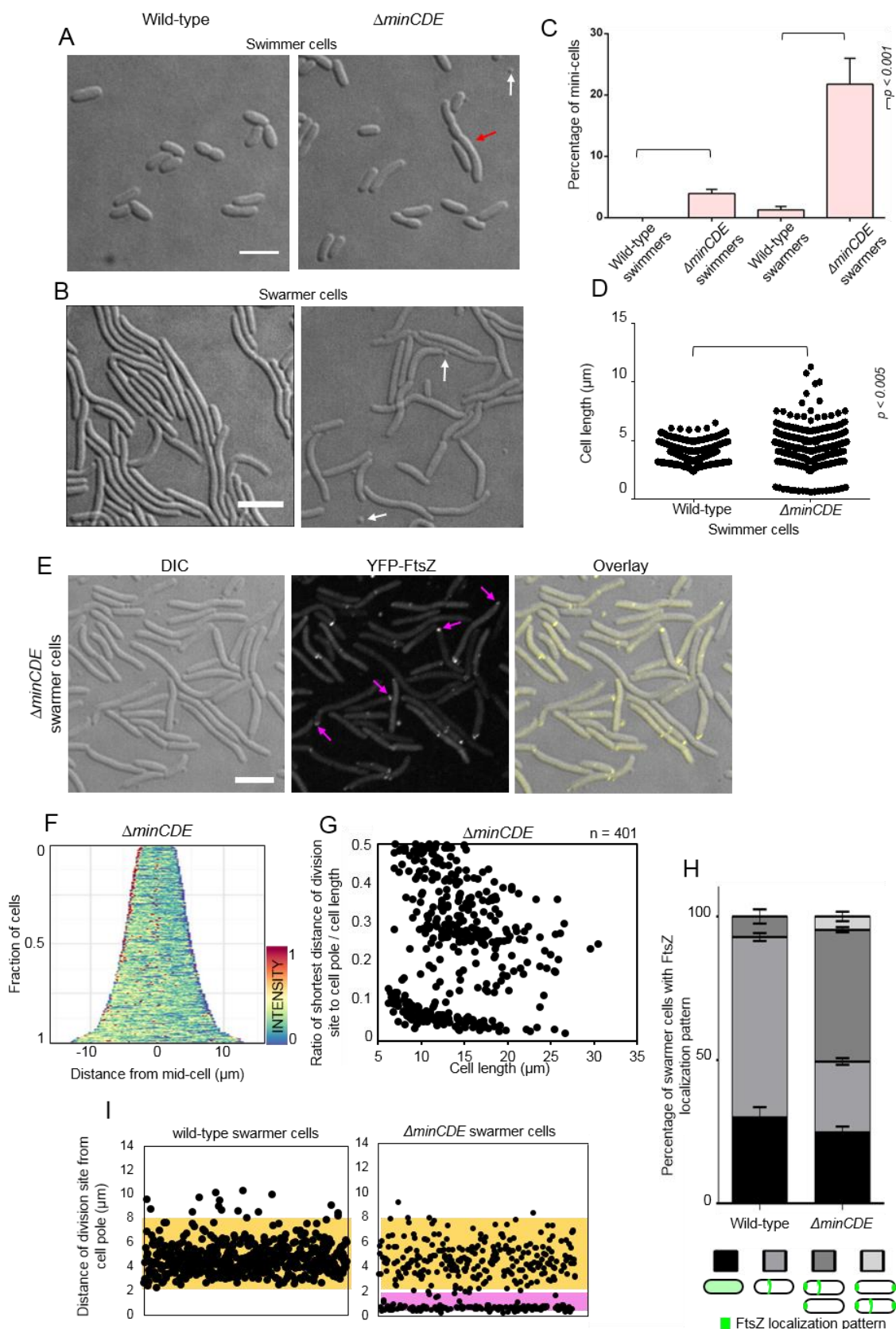


Figure 14: MinCDE system regulates cell division in both swimmer cells and swarmer cells of *V. parahaemolyticus*. (A) DIC microscopy images of wild-type and $\Delta minCDE$ swimmer cells. Red arrow indicates long cells and white arrow indicates mini-cells. (B) DIC microscopy images of wild-type and $\Delta minCDE$ swarmer cells. White arrow indicates mini-cells. (C) Bar graph showing the percentage of a

population that consists of mini-cells in wild-type and mutant *V. parahaemolyticus* swimmer and swarmer cells. (D) Box plot showing the cell length distribution in wild-type and $\Delta minCDE$ swimmer cells. (E) Fluorescence microscopy of YFP-FtsZ in different $\Delta minCDE$ *V. parahaemolyticus* swarmer cells. Magenta arrows indicate polarly localized FtsZ. (F) Demographic analysis showing the fluorescence intensity of YFP-FtsZ along the cell length in a population of $\Delta minCDE$ *V. parahaemolyticus* swarmer cells. (G) Scatter plots depicting the ratio of the shortest distance of the division site to cell pole as a function of cell length in $\Delta minCDE$ swarmer cells. (H) Stacked bar-graphs showing the percentage of a bacterial population with distinct localization patterns of YFP-FtsZ in wild-type and $\Delta minCDE$ *V. parahaemolyticus* swarmer cells. (I) Scatter-plot of the distance of division-site from the cell pole in wild-type and $\Delta minCDE$ swarmer cells. Scale bar represents 5 μm .

2.1.6. The MinCDE system ensures the correct positioning of the divisome at the LD-site in swarmer cells.

Importantly, in the absence of *minCDE*, the position of the Z-ring (Figure 15) and division site (Figure 14G-compare to wild-type in Figure 13G) were not confined to the mid-cell and LD-site positions, but instead on a population basis distributed along the entire cell length. This indicates that the Min-system is also important for the proper mid-cell and LD-site Z-ring positioning and subsequently for the division site-placement in short and long swarmer cells respectively.

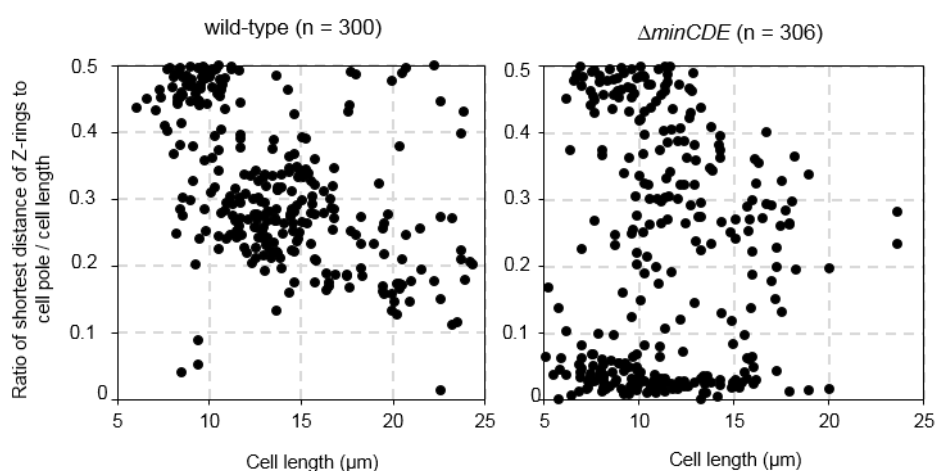


Figure 15: Min system regulates the LD site divisions. Scatter plots depicting the ratio of the shortest distance of the Z-ring to cell pole as a function of cell length in wild-type and $\Delta minCDE$ swarmer cells.

2.1.7. SlmA prevents the formation of division incompetent FtsZ clusters

Next we addressed the importance of the nucleoid occlusion factor SlmA on regulation of cell division. Cell division in swimmer and swarmer cells deleted for *minCDE* alone, *slmA* alone, and both systems simultaneously ($\Delta minCDE \Delta slmA$) were analyzed to determine the extent of the effect of each of the systems.

RESULTS

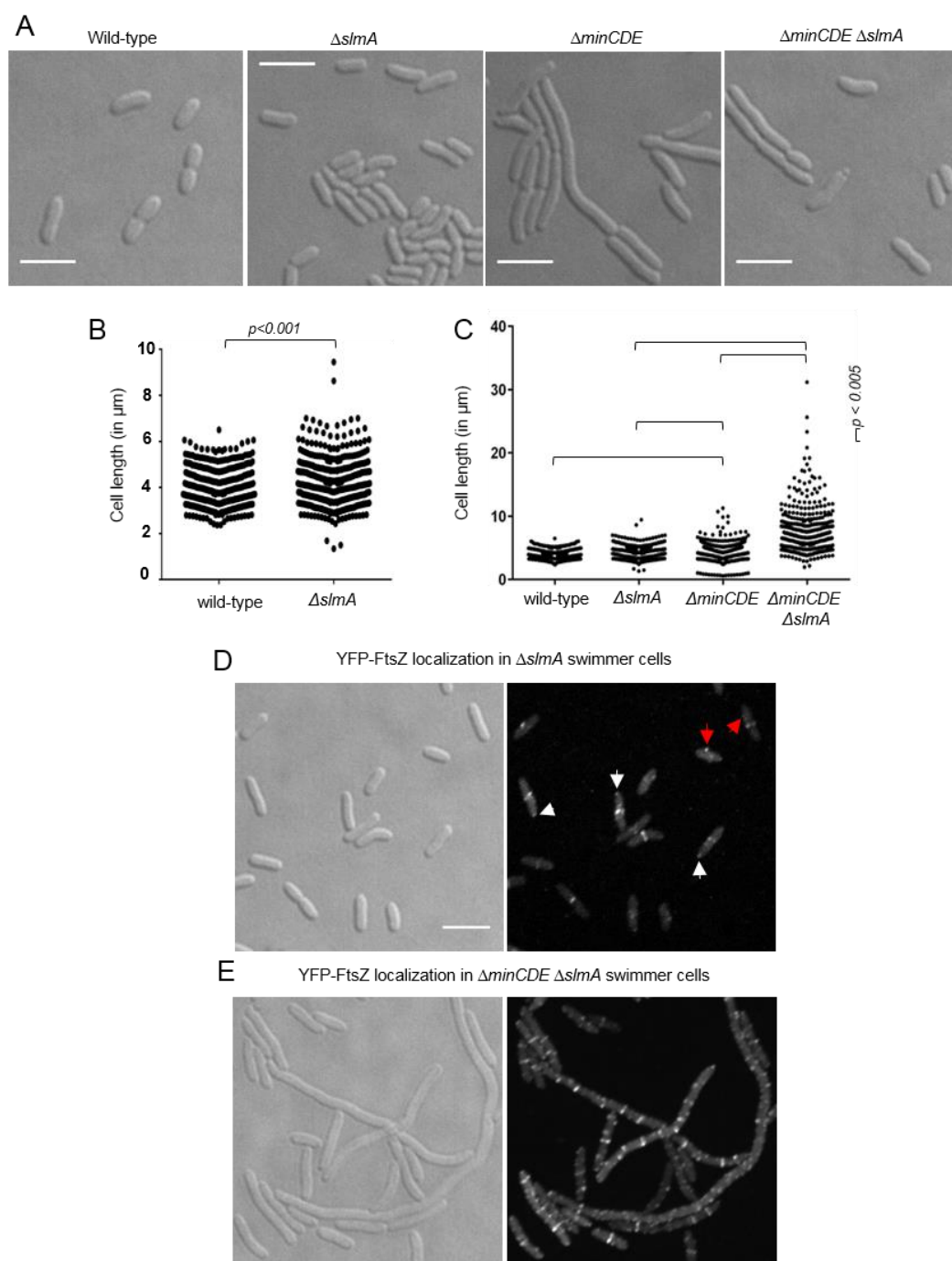


Figure 16: Absence of SlmA exerts significant elongation in swimmer cells when deleted alone and severe elongation on deletion together with Min system. (A-C) Deletion of *slmA* results in elongation of swimmer cells. Deletion of *slmA* together with *minCDE* deletion results in severe elongation of swimmer cells. (D) Fluorescence microscopy of YFP-FtsZ in swimmer cells of $\Delta slmA$ background (E) Fluorescence microscopy of YFP-FtsZ in swarmer cells of $\Delta minCDE \Delta slmA$ background. Multiple Z-rings are formed in the double deletion background. Scale bar represents 5 μm .

Swimmer cells

Deletion of *slmA* resulted in mild elongation of swimmer cells when deleted alone. The cells exhibited slight increase in cell length (Figure 16A and B). On deletion of *slmA* in a *minCDE* deletion background, the cells were hyper elongated, almost resembling the

swarmer cells (Figure 16A and C). The localization of FtsZ was distinctly different upon deletion of SlmA. Unlike the polar YFP-FtsZ that was only observed in short (new born) cells in wild-type, the longer (older) cells of the $\Delta slmA$ strain exhibited polar foci (Figure 16D, white arrow). In addition to the Z-rings formed in dividing cells, there were random clusters of YFP-FtsZ along the cell length (Figure 16D, red arrow). However, irrespective of polar FtsZ, there was no formation of mini-cells in the $\Delta slmA$ strain.

The hyper elongated cells with the $\Delta minCDE \Delta slmA$ background displayed numerous FtsZ clusters and patches along the entire cell length (Figure 16E). This probably is because the deletion of the exclusion mechanisms of FtsZ polymerization leads to non-functional FtsZ polymers that are incompetent of cell division. Thus, in the absence of the negative regulators of FtsZ polymerization proper cell division in the swimmer cells is impaired.

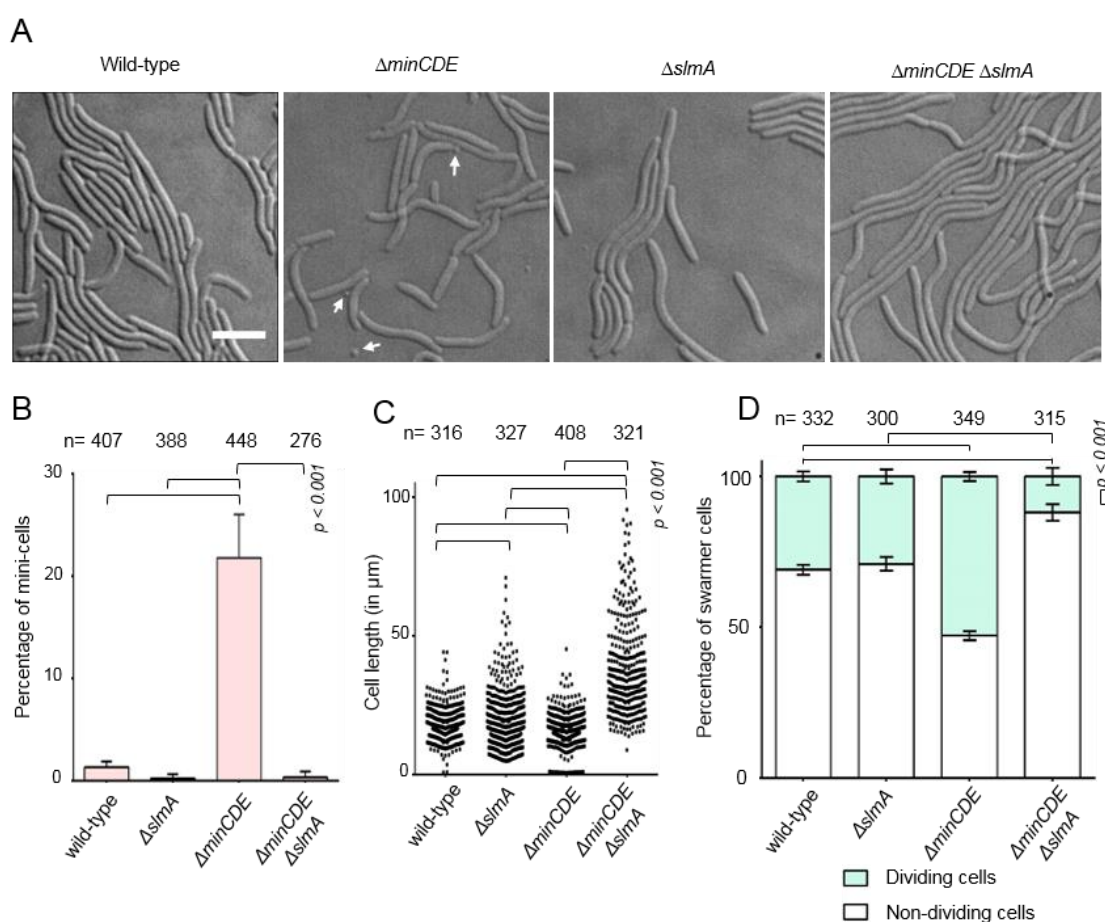


Figure 17: The Min-system regulates cell division and the proper transition from mid-cell to non-mid-cell LD-site division in swarmer cells. (A) DIC microscopy imaging of wild-type and mutants of *V. parahaemolyticus* swarmer cells. White arrows indicate mini-cells in $\Delta minCDE$ swarmer cells. Scale bar represents 5 μm . (B) Bar graph showing the percentage of a population that consists of mini-cells in wild-type and mutant *V. parahaemolyticus* swarmer cells. Error bars indicate standard error of the mean (SEM). (C) Box plot showing the cell length distribution in wild-type and mutants of *V. parahaemolyticus* swarmer cells. (D) Bar graph showing the percentage of swarmer cells undergoing division.

Swarmer cells

The absence of SlmA in the swarmer cells did not result in formation of mini-cells (Figure 17A-B), however, it resulted in an increase in cell length when compared to the wild-type and the $\Delta minCDE$ strain (Figure 17C). Cells lacking both systems ($\Delta minCDE \Delta slmA$) also did not form mini-cells (Figure 17A-B), but were highly elongated (Figure 17 C) and divided less frequently compared to wild-type, $\Delta minCDE$, and $\Delta slmA$ cells (Figure 17D).

Importantly, in the absence of SlmA, division sites were properly positioned at the mid-cell in short swarmer cells and at the LD-site in long swarmer cells, similar to wild-type cells (Figure 18B – compare to Figure 13G) and unlike the broad distribution in the $\Delta minCDE$ strain (Figure 18A). However, the absence of SlmA significantly influenced the intracellular localization of FtsZ, as YFP-FtsZ localized as clusters randomly positioned along the cell length (Figure 18C and D). Lateral clusters of YFP-FtsZ were present in ~95 % of the $\Delta slmA$ cells compared to 0 % in both the wild-type and the $\Delta minCDE$ strain (Figure 18D). Lateral clusters did not coincide with division sites and did not transverse the cytoplasm perpendicular to the long axis of the cell (Figure 18C, yellow arrows), as is observed when the Z-ring required for cell division is formed (Figure 18C, green arrow). Therefore, these lateral clusters most likely do not represent functional Z-rings. A Z-ring was present in ~50 % of $\Delta slmA$ cells compared to ~65 % of wild-type cells (Figure 18D).

Since wild-type and $\Delta slmA$ cells divided with equal frequencies (Figure 17D), it is likely that the Z-rings formed in $\Delta slmA$ cells are fully functional. Clusters of YFP-FtsZ were also observed at the cell poles in the absence of SlmA (Figure 18C, purple arrows, Figure 18D). However, since no polar divisions occurred in the $\Delta slmA$ strain (Figure 18B), these polar clusters likely do not represent functional Z-rings, but instead are similar to the lateral clusters of YFP-FtsZ formed in this background. Additionally, the levels of native FtsZ remained largely the same in all the mutant backgrounds as that in the wild-type, indicating that the observed phenotypes is not due to differences in FtsZ levels in the different mutant backgrounds (Figure 18E). Altogether, these data suggest that SlmA prevents the formation of division deficient FtsZ clusters along the cell length but does not regulate proper positioning of non-mid-cell division sites in long swarmer cells.

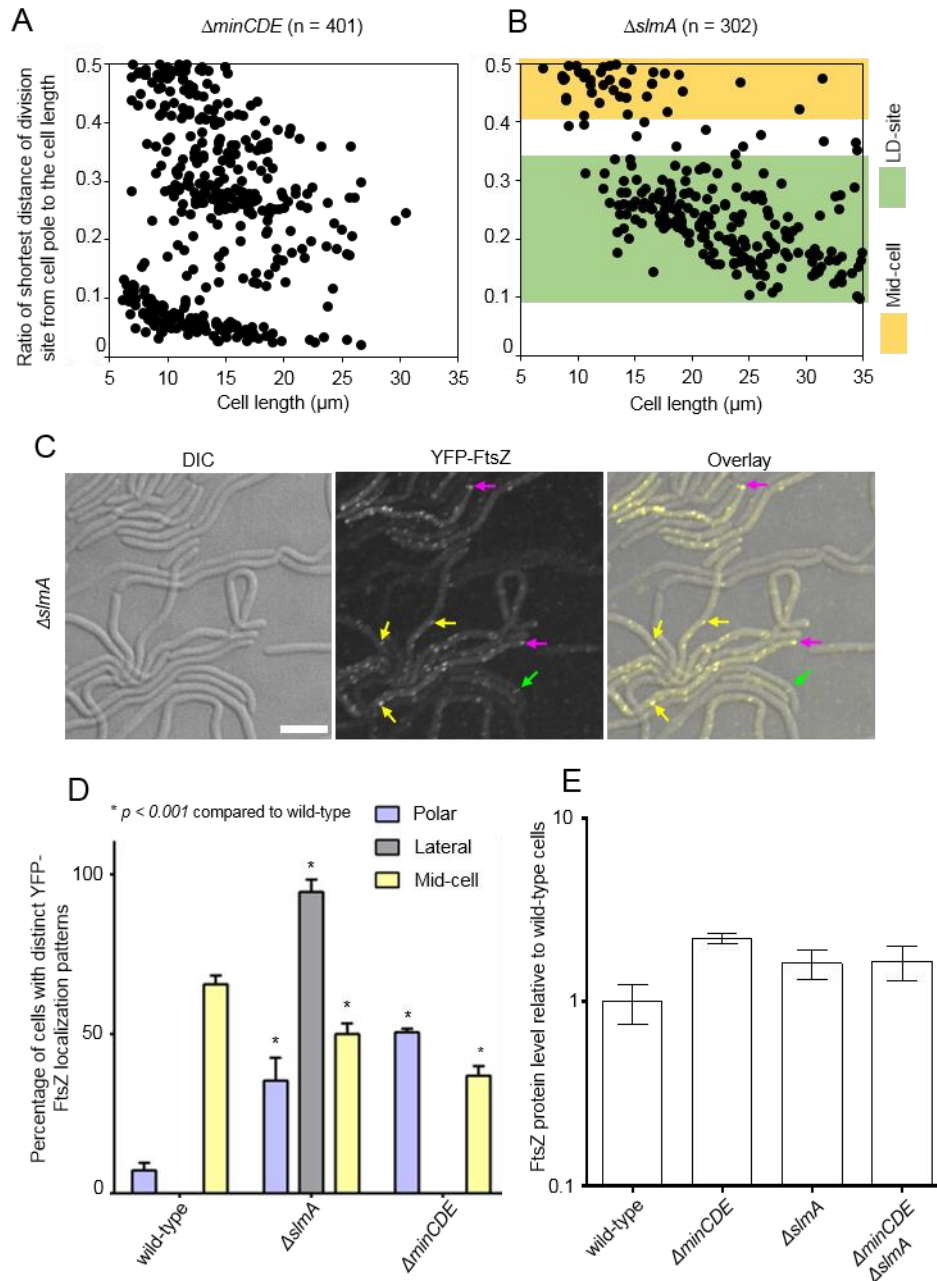


Figure 18: Effect of *minCDE* deletion and *slmA* deletion in FtsZ localization in swarmer cells. Graphs depicting the ratio of the shortest distance of the division site to the cell pole as a function of cell length in $\Delta minCDE$ (A) and $\Delta slmA$ (B) swarmer cells. (C) Fluorescence microscopy of YFP-FtsZ in $\Delta slmA$ backgrounds. Magenta arrows indicate polarly localized FtsZ. Yellow arrows indicate lateral FtsZ clusters. Green arrows indicate Z-rings, that at these sites lead to division. Scale bar represents 5 μm . (D) Bar graph showing the percentage of cells with distinct YFP-FtsZ localization patterns in different *V. parahaemolyticus* strain backgrounds. (E) Bar graph showing the FtsZ protein level of mutant *V. parahaemolyticus* cells relative to wild-type. Error bars indicate standard error mean.

2.1.8. MinD undergoes a pole-to-pole oscillation in swimmer cells

The *minCDE* operon in *V. parahaemolyticus* encodes for all three components of the Min-system (MinC, MinD, and MinE). In order to follow the dynamics of the Min system, an N-

RESULTS

terminal YFP fusion of MinD was expressed ectopically from an L-arabinose inducible promoter in addition to the native *minD* allele. The YFP-MinD signal extended from the cell poles to the middle of the cell in a gradient fashion irrespective of the cell size (Figure 19A, B). This was the first indication of the classical pole-to-pole oscillation of MinD as was previously described in *E. coli*. Furthermore, the cells were followed in a time-lapse experiments. YFP-MinD oscillated in a pole-to-pole manner with a time-averaged minimum developing at mid-cell (Figure 19C), where eventually the mother cell formed the septum and divided.

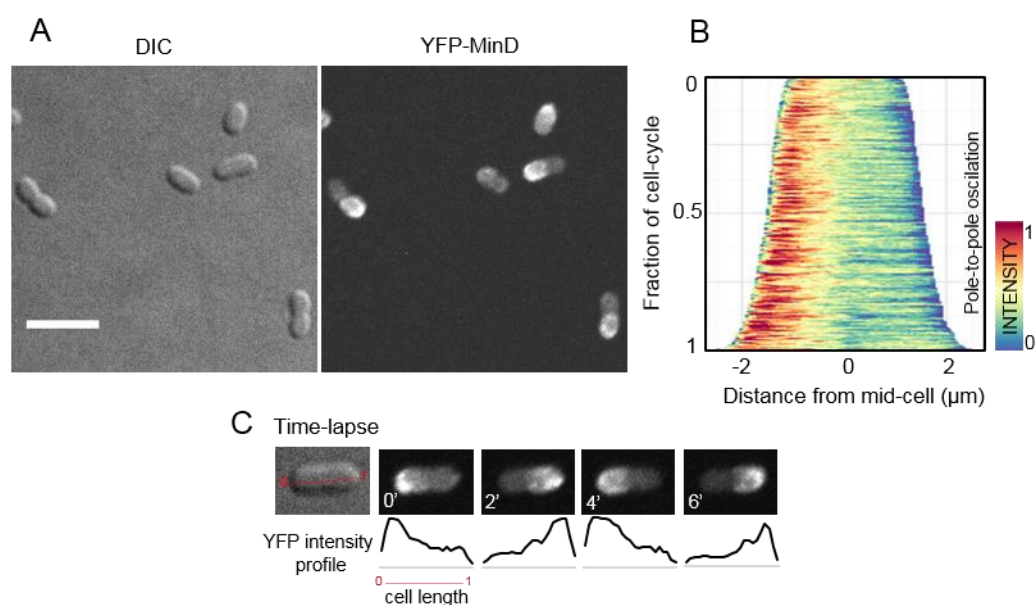


Figure 19: Pole-to-pole MinD oscillation in swimmer cells of *V. parahaemolyticus*. Microscopy images showing the intracellular localization of YFP-MinD in swimmer (A. Scale-bar represents 5 μm. (B) Demographic analysis showing the fluorescence intensity of YFP-MinD along the cell length in a population of *V. parahaemolyticus* relative to cell length in swimmer cells. (C) Time-lapse microscopy of YFP-MinD dynamics showing that MinD undergoes pole-to-pole oscillation in swimmer cells.

2.1.9. A cell length-dependent transition in MinD-dynamics

To understand how the Min-system promotes proper positioning of the Z-ring at mid-cell and the LD-site, the subcellular localization of MinD in swarmer cells was analyzed. In short swarmer cells (cells <10 μm), YFP-MinD formed a gradient extending from one cell pole towards mid-cell (Figure 20A-B). The time-lapse microscopy confirmed the YFP-MinD pole-to-pole oscillation (Figure 20C), resulting in a time-averaged lowest concentration of MinD at the mid-cell (Figure 20C, bottom panel). Interestingly, a change in MinD localization dynamics occurred in swarmer cells longer than ~10 μm, the same cell length at which the transition in positioning of the Z-ring from mid-cell to the LD-site in swarmer cells occurred. Demographic analysis indicated that in the long swarmer cells, MinD no longer localized as a gradient extending from the cell pole (Figure 20B).

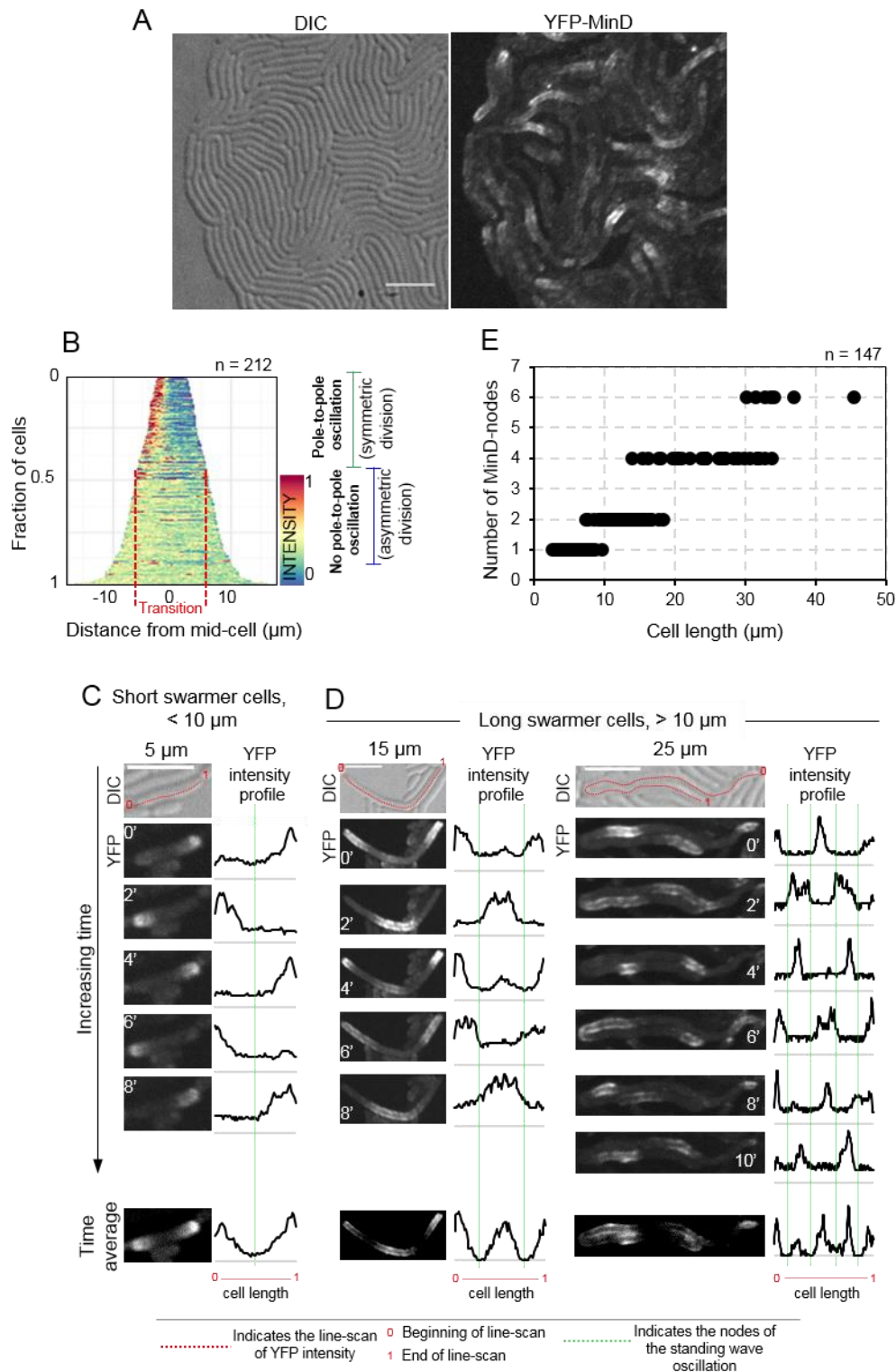


Figure 20: A cell length-dependent switch from pole-to-pole to multi-node standing-wave oscillation of MinD. (A) Microscopy images showing the intracellular localization of YFP-MinD in swarmer cells. Scale bar represents 5 μm . (B) Demographic analysis showing the fluorescence intensity of YFP-MinD along the cell length in a population of *V. parahaemolyticus* swarmer cells relative to cell length. (C) Time-lapse microscopy of YFP-MinD localization-dynamics in swarmer cells shorter than 10 μm in cell length (<math>< 10 \mu\text{m}</math>), showing that MinD undergoes pole-to-pole oscillation in short swarmer cells. (D) Time-lapse microscopy of YFP-MinD localization-dynamics in swarmer cells longer than 10 μm in cell length (>math>> 10 \mu\text{m}</math>), showing that dynamic localization of MinD change from a pole-to-pole oscillation to a multi-node standing wave oscillation in swarmer cells > 10 μm in cell length. The number of nodes increases with increasing cell length. (C, D) Numbers in white indicate time in minutes. Graphs next to the YFP-MinD images represent a line-scan of

RESULTS

the corresponding YFP-MinD intensity as indicated by the red dashed line in the DIC image. The nodes of YFP-MinD oscillations are indicated by green dashed lines. Scale bar represents 5 μm . (E) Graph showing the number of MinD nodes per cell as a function of cell length.

Instead, MinD localized in local minima and maxima along the cell length and moved from regions of local maxima to regions of previous local minima and back again (Figure 20D). This is consistent with a multi-node standing wave oscillation of MinD, where the point along the standing wave with minimum amplitude (the node), corresponds to the sites along the cell length experiencing the time-averaged minimum concentration of MinD (and consequently MinC) (Figure 20, bottom panel). The number of nodes correlated with cell length and as cells reached a length longer than $\sim 8\text{-}10\ \mu\text{m}$, the number of nodes increased from one to two. Thereafter, for every $\sim 8\text{-}10\ \mu\text{m}$, two additional MinD-nodes were added to the oscillation pattern (Figure 20E). Hence, indicating that the maximum length of a MinD-wave is $10\ \mu\text{m}$, which is consistent with the cell length at which the transition from pole-to-pole to multi-node standing wave oscillation occurred. Thus, the localization dynamics of MinD in swarmer cells is cell length-dependent and changes from a pole-to-pole oscillation in short swarmer cells ($<10\ \mu\text{m}$), to a multi-node standing wave oscillation with a maximum wavelength of approximately $10\ \mu\text{m}$ in long swarmer cells ($>10\ \mu\text{m}$).

A multi-node standing-wave oscillation of MinD was also observed in artificially elongated planktonic cells (Figure 21), further supporting that the switch in MinD localization dynamics is a consequence of cellular elongation.

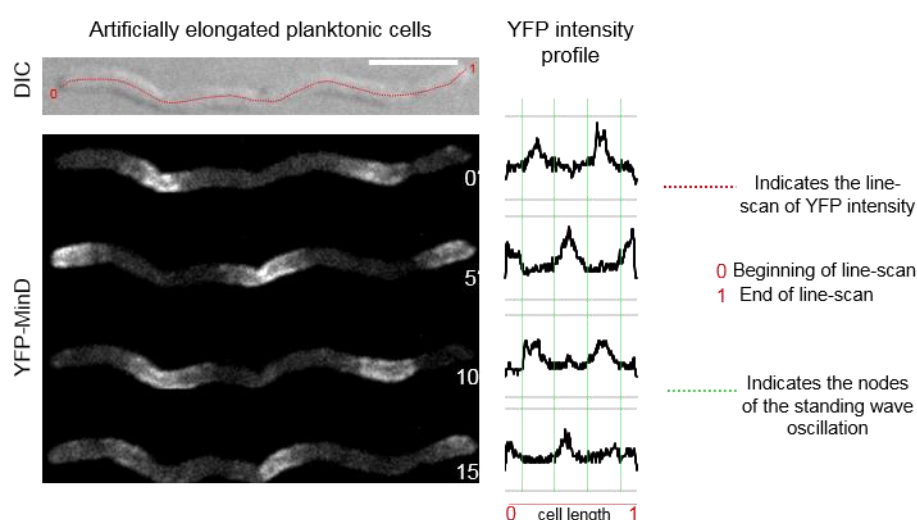


Figure 21: Localization dynamics of YFP-MinD in artificially elongated planktonic cells. Time-lapse microscopy of YFP-MinD localization-dynamics in aztreonam treated, artificially elongated wild-type planktonic cells, showing that MinD undergoes multi-node standing-wave oscillation in long planktonic cells. Numbers in white indicate time in minutes. Graphs next to YFP-MinD images represent a line-scan of the corresponding YFP-MinD intensity as indicated by the red dashed line in the DIC image. The nodes of YFP-MinD oscillations are indicated by green dashed lines. Scale bar represents $5\ \mu\text{m}$.

2.1.10. The LD-site at which division occurs in long swarmer cells is at the utmost pole proximal MinD node

After understanding the central role of the Min system in positioning the division site exactly at the LD-sites, a close look at the oscillation pattern of the waves was attempted in an effort to correlate the precise scaling of divisions in elongated cells.

The LD-site was positioned at 2.5-8 μm from the cell pole (Figure 13H), indicating that the Z-ring primarily forms at one specific MinD-node, even in very long cells with four or six nodes. To further address this, the position of the division site from the cell pole relative to cell length was measured. Cells were then grouped into four categories based on their length: group (1), < 10 μm ; (2), 10 – 20 μm ; (3), 20 – 30 μm ; and (4), 30 – 40 μm , which based on data from Figure 20E primarily will have 1, 2, 4, and 6 MinD-nodes, respectively.

Strikingly, there was a clear shift in the primary placement of the division site towards a closer proximity to the cell pole relative to mid-cell. The more MinD-nodes (the longer the cell is) the closer the division site was positioned to the cell pole relative to mid-cell (Figure 22A). A similar shift is expected for the placement of the most pole-proximal MinD-node with increasing cell length (Figure 22B). Thus the question arose if the division site corresponds to the first MinD-node from the cell pole. Indeed, analysis of YFP-MinD localization in long swarmer cells, in comparison with positioning of the division site, showed that the placement of the LD-site of long swarmer cells precisely corresponded to the position of the most pole-proximal MinD-node during the multi-node standing wave oscillation (Figure 22C). Altogether, this further supports the result that the Min-system contributes to the positioning of the Z-ring at this site and shows that the LD-division site primarily forms at the utmost pole proximal MinD-node independent of the cell length.

Furthermore, the utmost pole-proximal MinD-maximum occupied the initial 0-2 μm from the cell pole (Figure 22C), which exactly corresponds to the region protected from Z-ring formation and cell division in wild-type cells (Figure 13F-H). This explains how the Min-system can simultaneously protect the cell poles from aberrantly positioned division sites and regulate proper divisions at mid-cell and the LD-site. A similar correlation between MinD-localization and placement of the division site was observed in the absence of the SlmA-system (Figure 22D), further supporting that primarily MinCDE and not SlmA regulates the positioning of the division machinery.

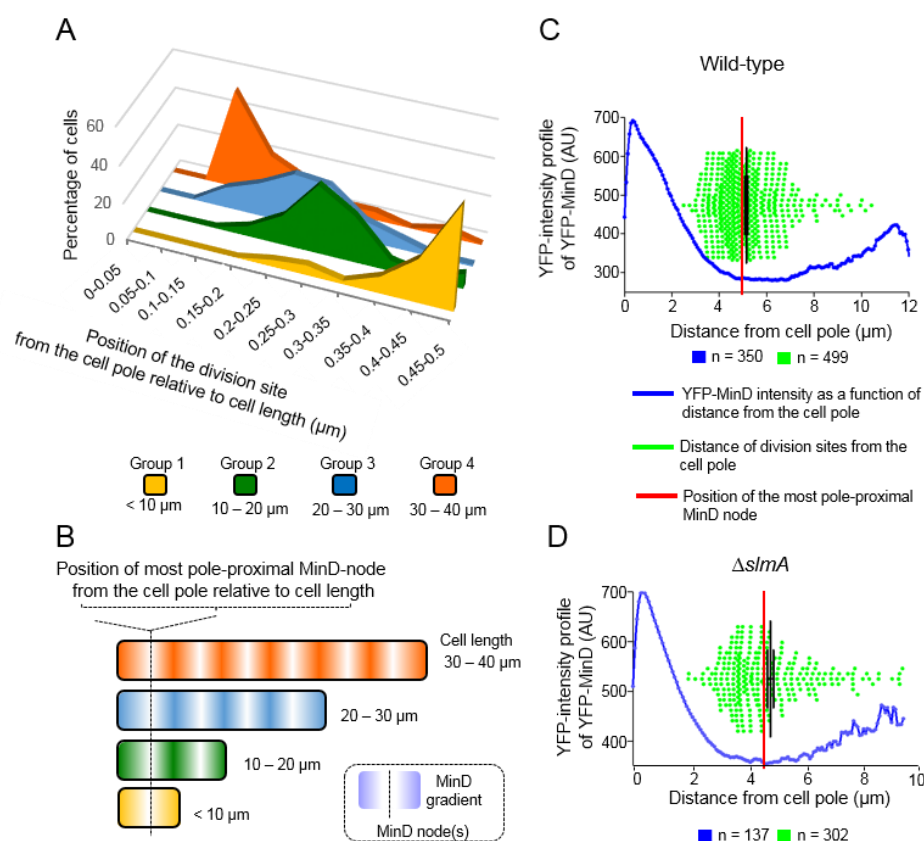


Figure 22: The LD-division site is positioned at the utmost pole-proximal MinD-node. (A) Graph showing the percentage of cells as a function of the position of the division site from the cell pole relative to cell length. Cells were divided into four groups based on their cell length. (B) Schematic showing the position of the most pole-proximal MinD-node from the cell pole relative to cell length and the number of nodes in the cell. (C,D) The LD-site is positioned at the utmost pole-proximal MinD-node. Combined graphs showing the fluorescence intensity of MinD as a function of the distance from the cell pole (blue graph) and scatter plot showing the position of the division site in individual cells as a function of the distance from the cell pole (green) in wild-type (C) and (D) ΔslmA *V. parahaemolyticus* cells. For the scatter plot, error bars indicate SEM. The red line indicates the position of the utmost pole proximal MinD-node.

2.1.11. Positive linear correlation between cell length and *ori* count in polyploid swarmer cells

For a bacterium like *V. parahaemolyticus* that can switch between two cell types, varying approximately 20-fold in cell length, organization of the chromosome for proper inheritance of genetic material is of prime importance. To investigate the effect of non-mid-cell divisions on the inheritance of genetic material, the position and organization of both the chromosomes, with respect to cell length and cell division in swarmer cells, were studied. By fluorescently labeling ParB1 and ParB2, we could specifically localize the position of the *parS1* and *parS2* sites within the cell – corresponding to the position of *ori1* and *ori2*, respectively.

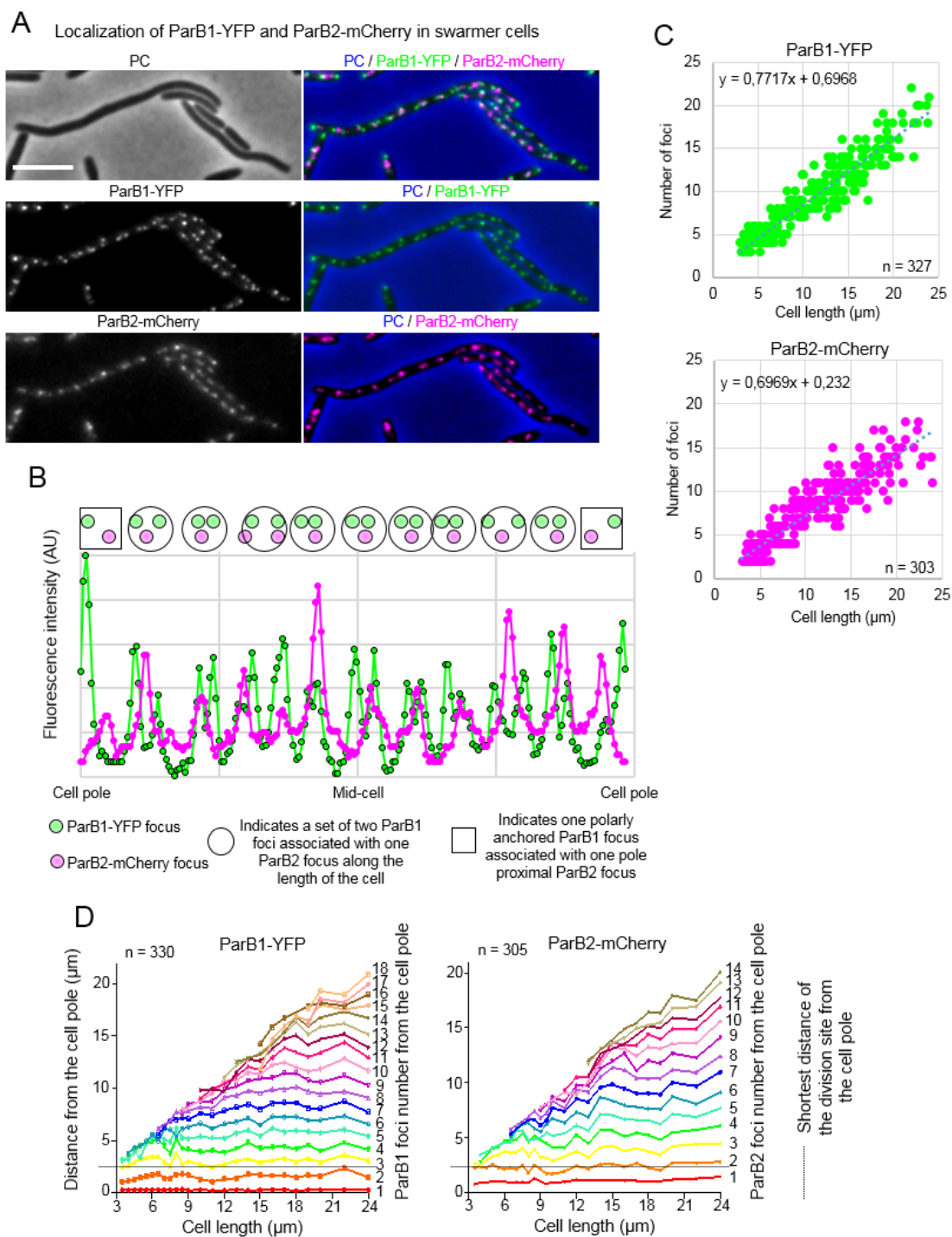


Figure 23: Equidistant segregation of the chromosomal origins in polyploid swarmer cells. (A) Fluorescence microscopy showing the intracellular localization of ParB1-YFP (green) and ParB2-mCherry (magenta) in wild-type *V. parahaemolyticus* swarmer cells. (B) Graph showing the fluorescence intensity as a function of cell length from a line-scan of the cell indicated by a red dashed line in "D". Green and magenta circles indicate the position of ParB1 and ParB2 foci (peaks of the line scan) along the cell. In general two ParB1 foci are associated with one ParB2 focus as highlighted by the large circle. One ParB1 focus is tethered at each cell pole and has an associated pole-proximal ParB2 focus, as highlighted by a rectangle. (C) Graphs showing the number of ParB1-YFP and ParB2-mCherry foci as a function of swarmer cell length. Dashed line shows the trend line. Trend line equation is shown. (D) The average distance of ParB1-YFP and ParB2-mCherry foci from the cell pole as a function of swarmer cell length. Numbers next to each colored graph indicate the focus number from the cell pole. Black line indicates the shortest distance of the division site from the cell pole.

RESULTS

ParB1-YFP and ParB2-mCherry localized as distinct foci that were distributed along the long axis of the cell (Figure 23A-B), with a ratio between ParB1 and ParB2 foci of 1.4:1, with a positive linear correlation between cell length and the number of both ParB1-YFP and ParB2-mCherry foci, indicating an increasing copy number of each chromosome with increasing cell length (Figure 23C).

2.1.12. Equidistant positioning of ParB1/*ori1* and ParB2/*ori2* in swarmer cells is independent of cell length

Analysis of the distribution of ParB1-YFP and ParB2-mCherry foci along the cell length, revealed that independent of the number of origins and cell length, both *ori1* and *ori2* were on average equidistantly positioned along the cell (Figure 23B and D). Importantly, a ParB1/*ori1* focus was always positioned at each cell pole accompanied by a pole proximal ParB2/*ori2* focus. The pole proximal ParB2/*ori2* focus was always positioned closer to the cell pole than the division site (shortest distance of the division site from the pole- 2.5 μm , Figure 13H) (Figure 23D, black dashed line). This suggests that each daughter cell will inherit at least one copy of each chromosome after cell division, independently of cell length and placement of the division site.

2.1.13. A cell length-dependent switch from mid-cell to LD-site placement of complete chromosome segregation correlates with the position of the division site

Interestingly, nucleoid staining of swarmer cells with DAPI, revealed that despite the ordered segregation of the *ori* regions, the entire cell was occupied by chromosomal DNA with no clear segregation of nucleoids (Figure 24A, white arrows, B), indicating that complete chromosome segregation had not occurred in the majority of swarmer cells. However, a subpopulation of cells did show a single clear nucleoid free region along the cell (Figure 24C, white arrows). Line-scan analysis of the DAPI signal revealed that the DNA free region was positioned at mid-cell in short swarmer cells (< 10 μm) and at non-mid-cell in cells longer than 10 μm (Figure 24E). This revealed a cell length-dependent positioning of the nucleoid free region similar to that observed for the placement of the Z-ring and division site (Fig. 8C-E). Indeed, double labeling of YFP-FtsZ and the late cell division protein YFP-FtsK with DAPI showed that localization of both the Z-ring (Figure 24C, green arrows) and FtsK (Figure 24F, green arrows) coincided with the position of the nucleoid free region. Thus, indicating that there is a correlation between the position of the division site and the region of complete chromosome segregation.

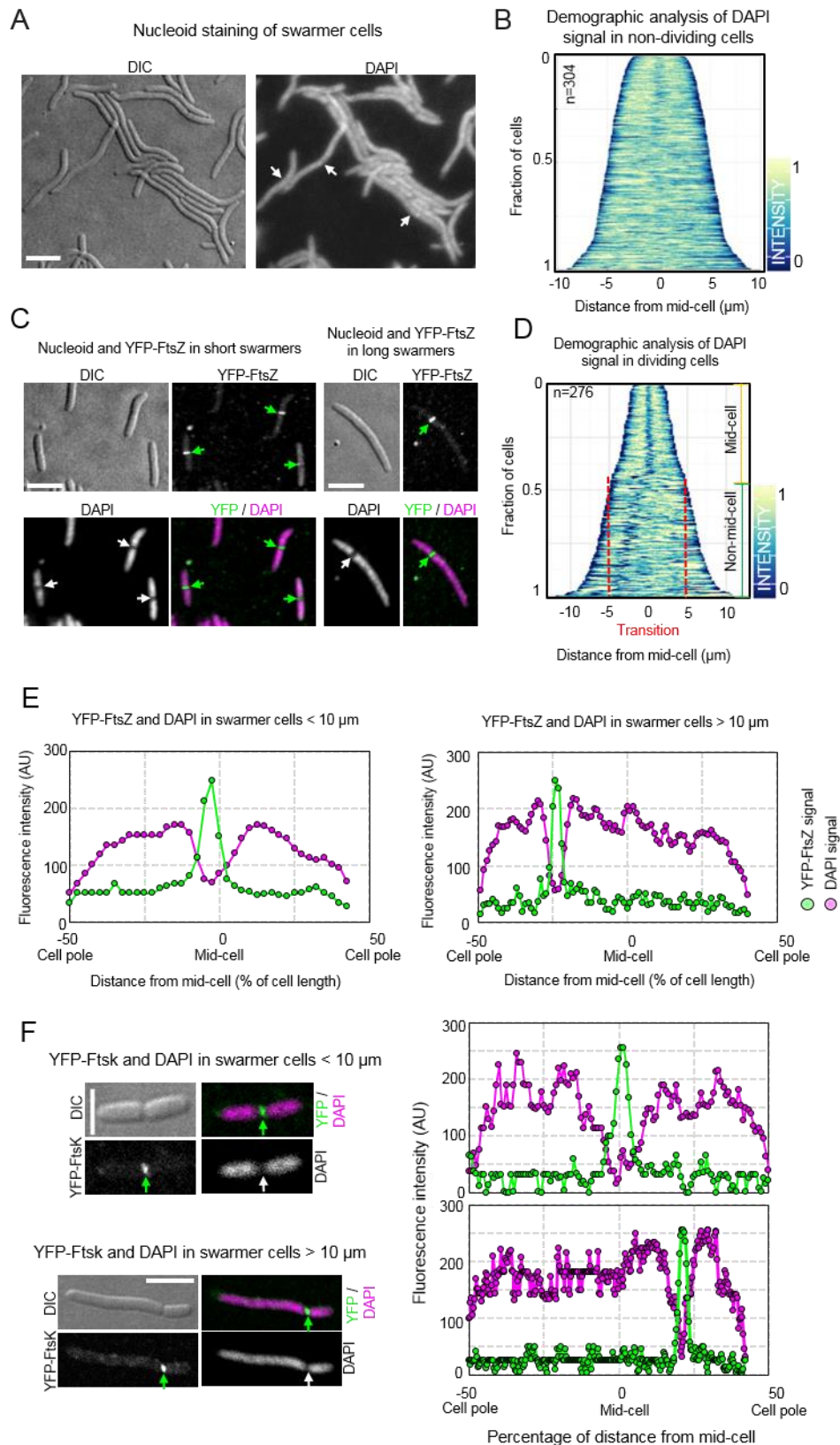


Figure 24: Cell length-dependent switch in the site of complete chromosome segregation correlates with the position of the division site. (A) Fluorescence microscopy of swarmer cells treated with the nucleoid stain DAPI. White arrows indicate cells where the nucleoid fills the entire cell and no nucleoid free region (no DAPI signal) is observed. (B) Demograph of DAPI signal in non-dividing swarmer cells. (C) Double labeling fluorescence microscopy of YFP-FtsZ and DAPI stained nucleoid DNA in swarmer cells shorter and longer than 10 μm in length. Green arrows indicate localization of YFP-FtsZ. White arrows

RESULTS

indicate the position of complete chromosome segregation. (D) Demographic analysis showing the fluorescence intensity of DAPI along the cell length in a population of *V. parahaemolyticus* swarmer cells with a clear DAPI free region relative to cell length. In cells shorter than 10 μm the DAPI free region is symmetrically positioned at mid-cell. In cells longer than 10 μm the DAPI free region is positioned at a non-mid-cell position. Dashed red lines indicate the cell length at which the transition from mid-cell to non-mid-cell positioning of the Z-ring occurs. (E) Graphs showing the fluorescence intensity YFP-FtsZ and DAPI along the cell length in a short (< 10 μm) and a long (> 10 μm) double labeled swarmer cell. The cells from which the line scan originates are highlighted with a red dashed line in panel C. (F) Double labeling fluorescence microscopy of YFP-FtsK and DAPI stained nucleoid DNA in cells shorter and longer than 10 μm in length. Graphs show the fluorescence intensity along the cell length. Green arrows indicate localization of YFP-FtsK. White arrows indicate the position of complete chromosome segregation.

Interestingly, and in contrast to long swarmer cells, multiple Z-rings were positioned regularly along the cell in artificially elongated planktonic swimmer cells (Figure 25A green arrows, B), with the number of Z-rings increasing with increasing cell length (Figure 25B). Furthermore, DAPI staining showed multiple sites of nucleoid free regions positioned regularly along the cell length (Figure 25A white arrows, C), which coincided precisely with the localization of the Z-rings (Figure 25A, graph and B-C) and YFP-FtsK (Figure 25D-F). These data further demonstrate the correlation between the localization of the division apparatus and the site of complete chromosome segregation and suggests that formation of the Z-ring directs the site at which complete chromosome segregation occurs.

2.1.1. Regulation of FtsZ levels ensures only one Z-ring is formed in swarmer cells

In order to understand how swarmer cells ensure that primarily only one Z-ring forms independent of cell length, while artificially elongated planktonic cells are able to form multiple Z-rings, FtsZ protein levels in planktonic cells, swarmer cells, and artificially elongated planktonic cells were analyzed by liquid chromatography-mass spectrometry (LC-MS) (Figure 26 A-C). Interestingly, FtsZ levels were identical in planktonic and swarmer cells (Figure 26A), while in comparison, artificially elongated planktonic cells showed a significantly higher level of FtsZ (Figure 26B). Likewise, the level of FtsA was identical in planktonic cells and swarmer cells (Figure 26C), while artificially elongated planktonic cells showed a significantly higher level of FtsA (Figure 26D). The level of LafA -the lateral flagellin subunit, which is specifically expressed in swarmer cells (Gode-Potratz et al., 2011) was measured as a control. Indeed, the level of LafA was much higher in swarmer cells compared to planktonic cells (Figure 26E), and thus did not follow the same pattern in protein level as FtsZ and FtsA. This suggests that the FtsZ expression level is regulated in swarmer cells to match that of planktonic cells. This could ensure that only enough FtsZ is present in swarmer cells for the formation of a single Z-ring, effectively restricting the number of Z-rings to one, independent of cell length in swarmer cells.

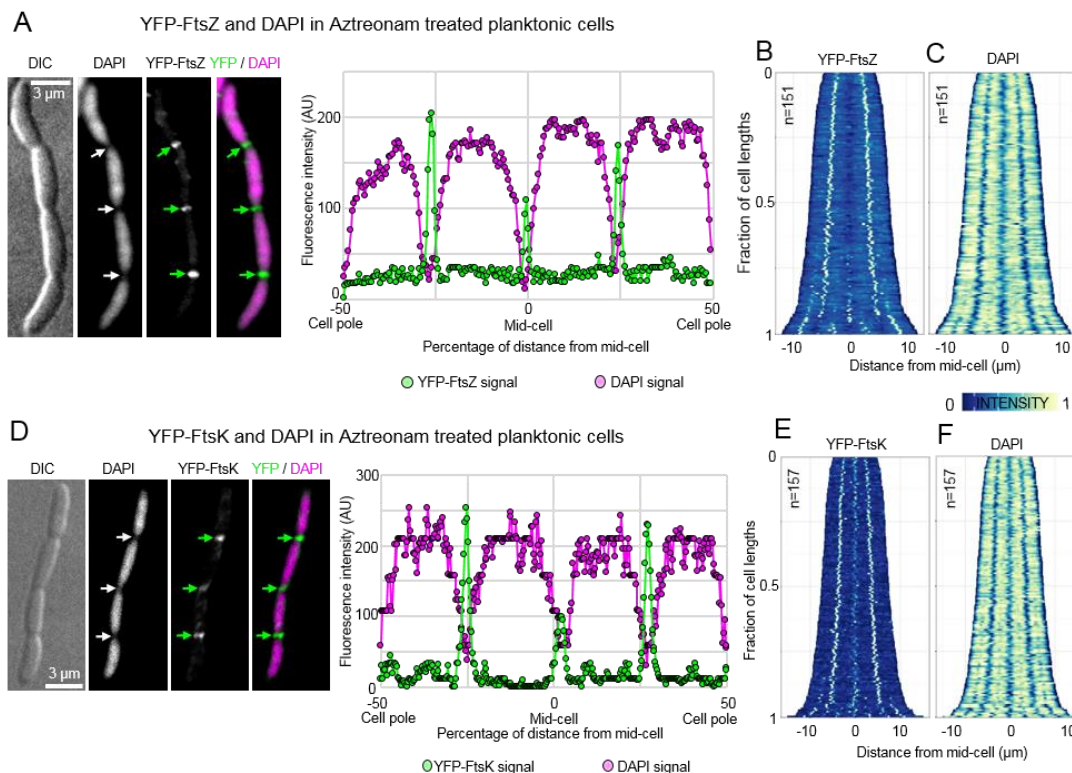


Figure 25: Formation of multiple division sites in artificially elongated planktonic cells correlates with positions of complete chromosome segregation. (A) Double labeling fluorescence microscopy of YFP-FtsZ and DAPI stained nucleoid DNA in Aztreonam treated, artificially elongated planktonic cells. Graph shows the fluorescence intensity along the cell length of the single cell in panel “A”. Green arrows indicate localization of YFP-FtsZ rings. White arrows indicate the position of complete chromosome segregation. (B, C) Demographs showing the fluorescence intensity of (B) YFP-FtsZ and (C) DAPI along the cell length in a population of Aztreonam treated, artificially elongated wild-type planktonic cells relative to cell length. (D) Double labeling fluorescence microscopy of YFP-FtsK and DAPI stained nucleoid DNA in Aztreonam treated, artificially elongated planktonic cells. Graph shows the fluorescence intensity along the cell length. (E, F) Demographs show the fluorescence intensity of (E) YFP-FtsK and (F) DAPI along the cell length in a population of double labeled *V. parahaemolyticus* swarmer cells relative to cell length.

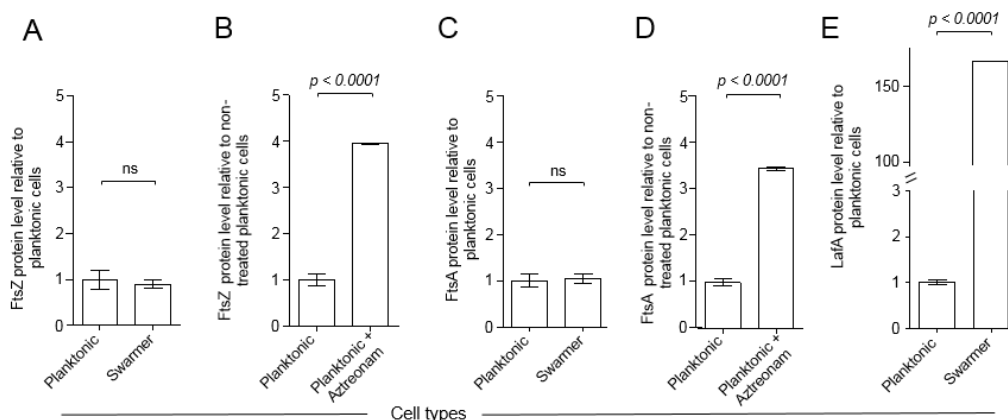


Figure 26: The FtsZ protein level of swarmer cells is similar to that of planktonic cells. (A) FtsZ protein level in planktonic and swarmer cells relative to planktonic cells. (B) FtsZ protein level in planktonic cells and Aztreonam-treated, artificially elongated wild-type planktonic cells relative to planktonic cells. (C) FtsA protein level in planktonic and swarmer cells relative to planktonic cells. (D) FtsA protein level in planktonic cells and Aztreonam-treated, artificially elongated planktonic cells relative to planktonic cells. (E) LafA protein level in planktonic and swarmer cells relative to planktonic cells. (A-E) FtsZ/FtsA/LafA levels are presented as the mean level with error bars indicating standard deviation.

RESULTS

Indeed, upon overproduction of YFP-FtsZ from an IPTG inducible promoter in swarmer cells, multiple Z-rings were observed along the cell length of long swarmer cells (Figure 27A). Furthermore, there was a significant decrease in swarmer cell length with increasing concentration of the inducer IPTG (Figure 27B), consistent with multiple divisions per swarmer cell and the formation of shorter cells.

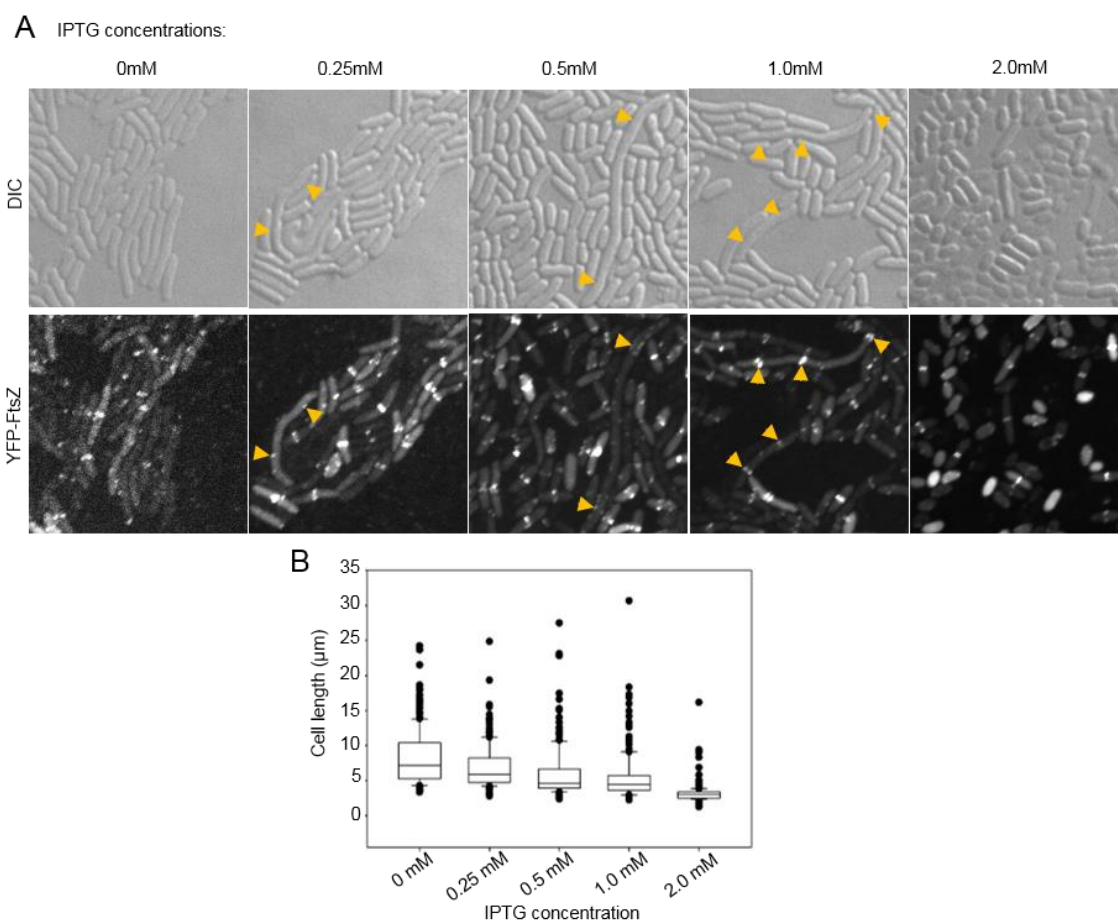


Figure 27. Overexpression of FtsZ results in the formation of multiple Z-rings in swarmer cells, reduced swarmer cell length and swarming behavior. (A) Fluorescence microscopy of YFP-FtsZ ectopically expressed from the IPTG inducible Plac, in wild-type swarmer cells from swarm plates with different amounts of IPTG. (B) Cell length distribution of swarmer cells imaged in “A”. Swarmer cell length decreases with increasing amount of FtsZ expression.

Altogether, these data indicate that the concentration of FtsZ in swarmer cells are regulated to match that of planktonic cells, so that only the formation of a single Z-ring is allowed, regardless of the length of the swarmer cells – thus, effectively restricting the number of division events per cell to one, independent of their cell length.

2.1.2. All cells from swarm flares have initiated the swarm program

Next we analyzed if all cells from swarm flares have initiated the swarm program independent of cell length. For this purpose we used the promoter of *lafA*, encoding the

lateral flagellin subunit, LafA, as a maker for cells that have initiated the swarm program (Gode-Potratz et al., 2011).

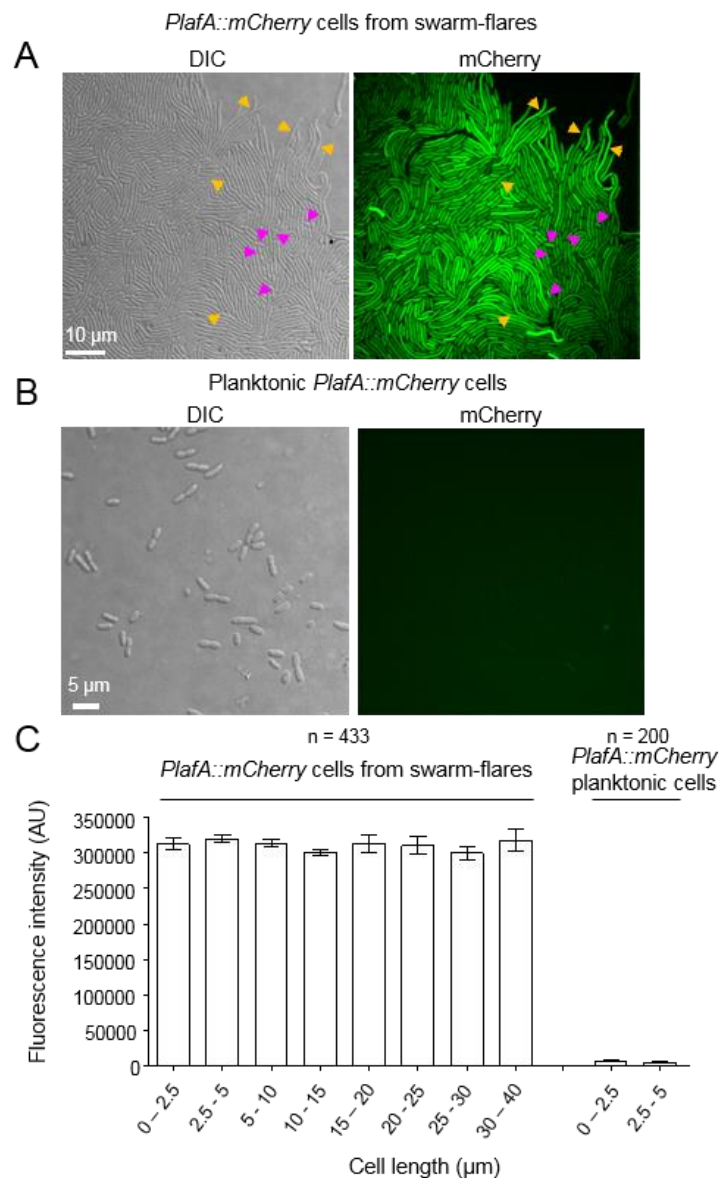


Figure 28: All cells from swarm flares have initiated the swarm-program independent of their length. (A-B) Fluorescence microscopy of wild-type *V. parahaemolyticus* cells, encoding the PlafA::mCherry reporter for swarm-program induction, from swarm-flares (A) or as planktonic cells from a liquid culture (B). (C) Fluorescence intensity of mCherry expressed from the PlafA::mCherry reporter in swarmer cells and planktonic cells relative to cell length.

The promoter of *lafA* (PlafA) was fused to the gene encoding mCherry (PlafA::mCherry) and integrated in the chromosome of wild-type *V. parahaemolyticus*. Indeed, 100 % (n = 500) of cells from swarm flares expressed mCherry from the *lafA* promoter (Figure 28A–C). Importantly, both short (Figure 28A magenta arrows, C) and long cells (Figure 28A yellow arrows, C) from swarm colonies expressed mCherry. This was in contrast to

planktonic cells from liquid cultures where no fluorescent cells were seen (0 %, n = 350) (Figure 28B and C). Independent of their length, cells from swarm-flares expressed equal amounts of mCherry (Figure 28C), indicating that all cells independent of their length have initiated the swarm-program to the same degree. This suggests that both progenies of non-mid-cell LD-site division continues the swarm program subsequent to completion of cell division.

2.1.3. Asymmetric division results in progeny cells with different swimming abilities and the formation of a heterogeneous population

Swarming behavior primarily takes place in the periphery of the swarm-colonies, where swarmer cells assemble into flares that extend outward from the colony (Figure 13A) (Heering et al., 2017; Heering & Ringgaard, 2016). We hypothesized that the purpose of asymmetric division of long swarmer cells might be to create progeny cells with distinctive capacities and thus have a sub-population of cells prepared for potentially changing environmental conditions. We therefore collected cells from the swarm flares and analyzed their swimming proficiency as a function of cell length, since the natural habitat for *V. parahaemolyticus* is the marine environment. Indeed, there was a clear correlation between swimming speed and cell length (Figure 29A), with short cells swimming at much higher speeds than long cells.

Importantly, we also observed a clear correlation between cell length and cellular displacement (Figure 29B-C), where short cells had a significantly higher displacement than long cells. Thus, short cells from the swarm flares not only swim at much higher speeds but also travel much further from their starting point than long cells. Almost no swimming or cellular displacement was observed for cell longer than 10 μm of cell length. These results show that positioning of the LD-site within 2-8 μm from the cell pole (Figure 13H) will result in at least one daughter cell with a high swimming and displacement proficiency. Thus, asymmetric division leads to the formation of a heterogeneous population; specifically, in the formation of cells with distinct swimming capabilities – fast swimming short cells and swimming deficient long cells.

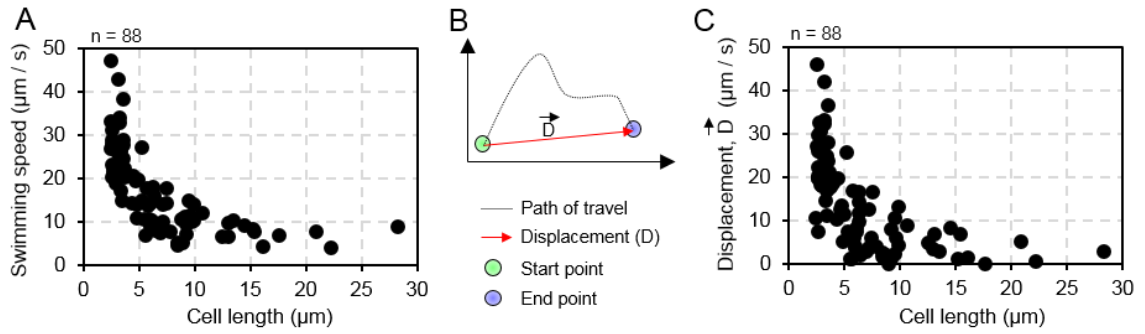


Figure 29: Asymmetric division results in the formation of progeny cells with distinct swimming capabilities and drives population heterogeneity. (A) Graph showing the swimming speed of single cells as a function of their cell length. (B) Schematic depicting the definition of swimming displacement. (C) Graph showing the displacement of single cells as a function of their cell length.

2.2. Part II-Cell type specific regulation of cell division by ParC in *Vibrio parahaemolyticus*

2.2.1. Specific developmental regulation of cell division by ParC

To identify additional regulators of cell division in swarmer cells, we performed a visual assay screening for *V. parahaemolyticus* mutants with cell division defects during the swarmer cell cycle. Interestingly, we observed the appearance of mini-cells in a strain lacking the cell pole determinant ParC. (Figure 30A, C and F). In the absence of *parC*, 18.6% of the swarmer population consisted of mini-cells, a comparable fraction to that observed in $\Delta minCDE$ (21.8%), but completely opposed to the wild-type strain, where mini-cells accounted for only 1.3% of the population (Figure 30C). Time-lapse microscopy revealed that mini-cell formation in swarmer cells upon deletion of *parC* was a result of division events occurring in the sub-polar region of the cells (Figure 30D). These observations indicate ParC is a regulator of cell division and is required to prevent cell division occurring at the cell pole and subsequent formation of mini-cells.

As the Min system also is required for preventing cell divisions close to the cell pole, we tested the effect on cell division on a strain lacking both ParC and MinCDE. Interestingly, in the strain deleted for both *parC* and *minCDE*, a higher percentage of the population consisted of mini-cells compared to the single deletion mutants (Figure 30C). This indicates that each system functions independently in preventing polar divisions and that the lack of both the systems has an additive adverse effect on the placement of the division site.

Strikingly, we noted that the absence of ParC did not lead to any cell division defect or mini-cell formation in swimmer cells of *V. parahaemolyticus* (Figure 30B, C), while deletion of *minCDE* resulted in mini-cells (Figure 30B, white arrow) and elongated cells (Figure 30B, red arrow) in swimmer population. A double deletion of *parC* and *minCDE* in swarmer cells resulted in an increased occurrence of mini-cells and we tested if the same was true for swimmer cells. Importantly, no increase in mini-cell formation (Figure 30C) or of swimmer cells of aberrant sizes (Figure 30E) was observed when deletion of *minCDE* was combined with deletion of *parC*. Thus, indicating that the function of ParC in preventing polar division depends on the differentiated state of the bacterium and is specific to the swarmer cells.

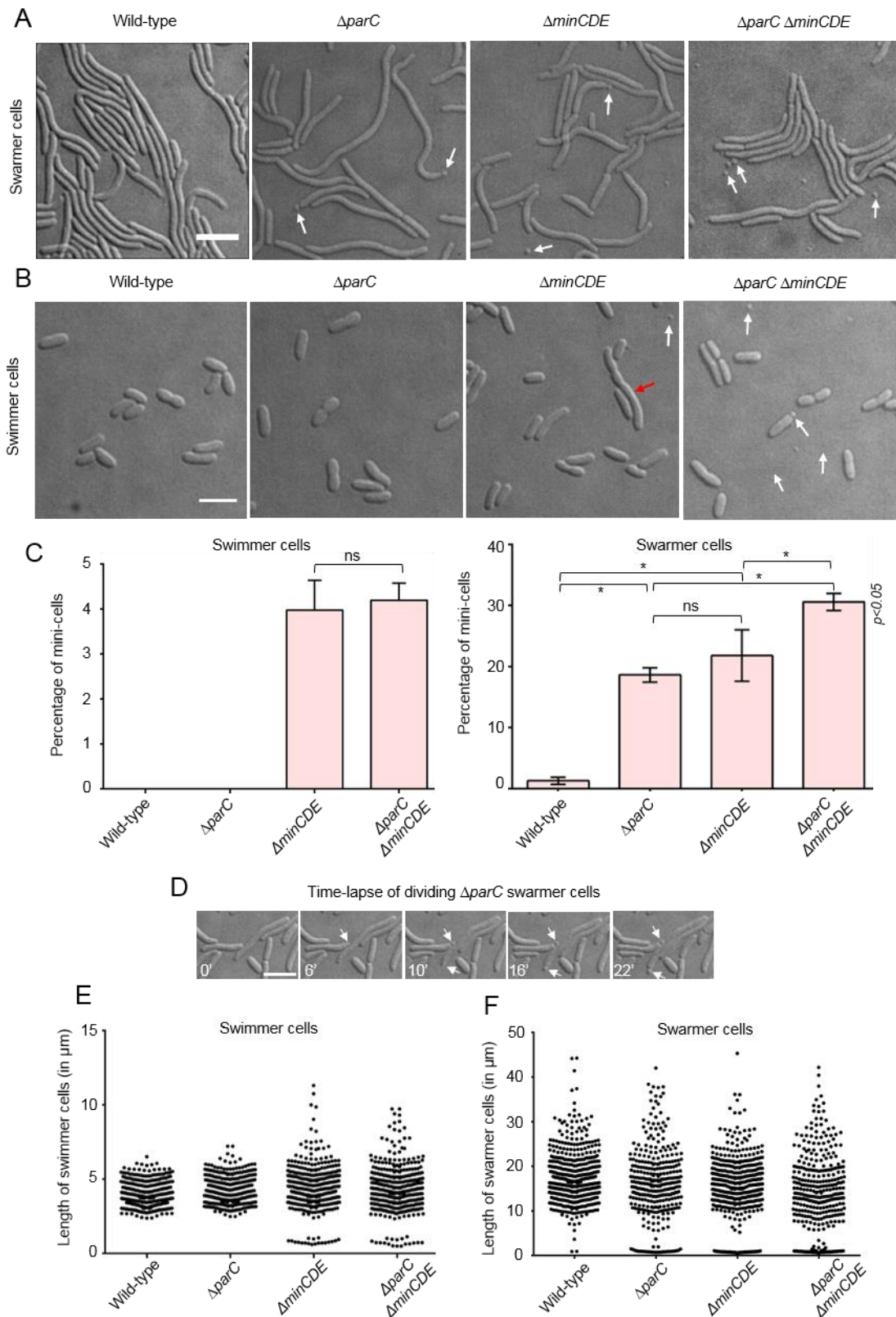


Figure 30: ParC exerts specific developmental regulation of cell division. (A-B) DIC microscopy imaging of wild-type and mutant *V. parahaemolyticus* swimmer (A) and swammer cells (B). White arrows indicate mini-cells. Red arrows indicate elongated swimmer cells. Scale-bar represents 5 μm . (C) Bar graph showing the percentage of a population that consists of mini-cells in wild-type and mutant *V. parahaemolyticus* swammer cells. Error bars indicate standard error of the mean (SEM). (D) Time-lapse imaging of dividing *V. parahaemolyticus* $\Delta parC$ swammer cells showing that mini-cells originate from polar

RESULTS

division events in swarmer cells deleted for *parC*. (E-F) Box plot showing the cell length distribution in wild-type and mutants of *V. parahaemolyticus* swimmer (E) and swarmer cells (F).

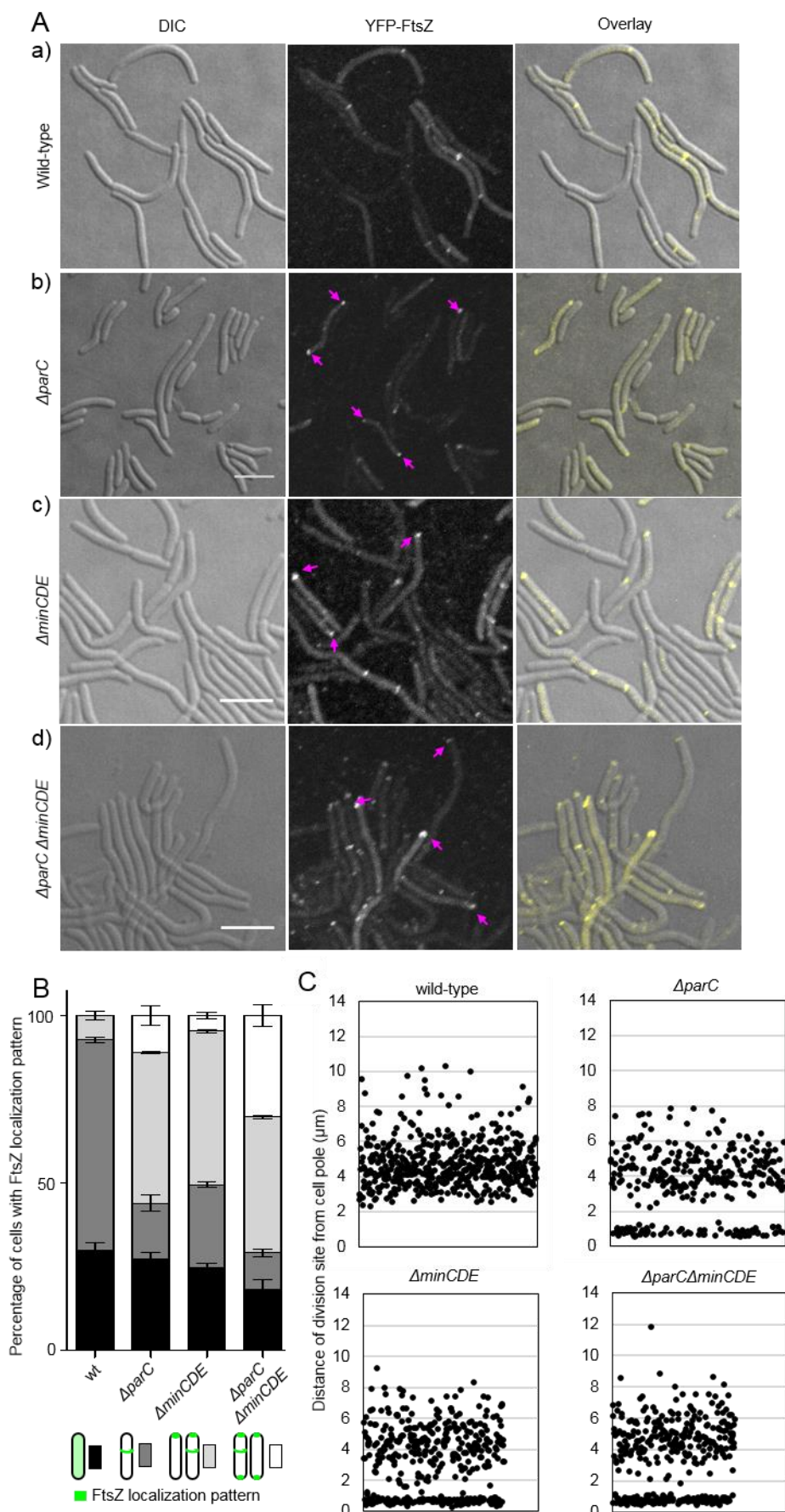
2.2.2. ParC prevents polar localization of FtsZ in swarmer cells

To understand how ParC prevents polar division events, we analyzed the intracellular localization of FtsZ in swarmer cells deleted for *parC*. YFP-FtsZ localized to the cell poles in a uni- and/or bi-polar manner in the absence of ParC (Figure 31A (b) purple arrows) in 56.0% of swarmer cells (Figure 31B), which was only very rarely observed in wild-type background (Figure 31A (a) and Figure 31B).

Importantly, in the absence of ParC, polar localization of YFP-FtsZ, and consequently polar division events, occurred in the pole-proximal region of the cell. These pole-proximal regions are otherwise devoid of YFP-FtsZ localization and division events in wild-type cells (Figure 31C). These data suggest that ParC has an additional role in regulating cell division by preventing aberrant positioning of FtsZ to the cell poles in *V. parahaemolyticus* swarmer cells. However, polar accumulation of FtsZ did not seem to affect the mid-cell and LD-site divisions in swarmer cells (Figure 31C).

Due to the similarity of $\Delta parC$ phenotype in swarmer cells to that observed in $\Delta minCDE$ swarmer cells, we compared the effects in the single deletions to that in the strain lacking both systems. An absence of both systems resulted in an increased fraction of cells with uni-polar and bi-polar positioning of YFP-FtsZ (Figure 31B), which is consistent with the increase in formation of mini-cells in the absence of both systems (Figure 30C). Notably, there was a significant increase in the percentage of $\Delta minCDE \Delta parC$ cells with bi-polarly localized YFP-FtsZ (30.2%) compared to the single mutants ($\Delta parC$, 11.1%; $\Delta minCDE$, 4.7%). Additionally, the cells in the single deletion backgrounds that did not exhibit a wild-type like FtsZ localization majorly displayed uni-polar FtsZ localization (Figure 31B). These results indicate that ParC and MinCDE function independently in preventing polar divisions and that the two systems have an additive effect on the protection of the polar regions (0-2 μm from the cell pole) from aberrantly positioned FtsZ.

Figure 31: ParC prevents polar localization of FtsZ in swarmer cells. (A-a to d) Fluorescence microscopy of YFP-FtsZ in swarmer cells of different *V. parahaemolyticus* strain backgrounds. (B) Stacked bar-graphs showing the percentage of a bacterial population with distinct localization patterns of YFP-FtsZ in wild-type and mutants of *V. parahaemolyticus* swarmer cells. Black: diffuse cytosolic YFP-FtsZ localization; dark gray: Z-ring either at mid-cell or pole proximal position; light gray: distinct uni-polar localization of FtsZ either in the absence or presence of a Z-ring positioned either at mid-cell or at the pole proximal position; white: distinct bi-polar localization of FtsZ either in the absence or presence of a Z-ring positioned either at mid-cell or at the pole proximal position. Error bars indicate standard error of the mean (SEM). (C) Scatter-plots of the distance of Z-ring from the cell pole in swarmer cells of wild-type and mutant backgrounds.



RESULTS

By studying the phenotypic changes, we suggested in the previous section that the deletion of *parC* did not alter cell division in swimmer cells. We further investigated the localization of YFP-FtsZ in $\Delta parC$. As expected, there was no observable deviations in FtsZ localization in swimmer cells of $\Delta parC$ strain. Short cells harboured a uni-polar FtsZ focus and the long cells showed a mid-cell FtsZ localization (Figure 32A), comparable to that observed in the wild-type (Figure 8A).

Deletion of *parC* did not alter the precise mid-cell divisions of swimmer cells. The mid-cell localization of FtsZ in growing cells of $\Delta parC$ strain (Figure 32A, B) was further supported by quantification of position of division sites in $\Delta parC$ swimmer cells (Figure 32C). Thus, supporting that the function of ParC in preventing polar localization of FtsZ is specific to the swarmer cell stage. Therefore, ParC is a dual functional protein that in addition to ensuring polar recruitment of chemotaxis signaling arrays in swimmer and swarmer cells (Heering & Ringgaard, 2016; Ringgaard et al., 2011) cells, can prevent polar divisions in swarmer cells.

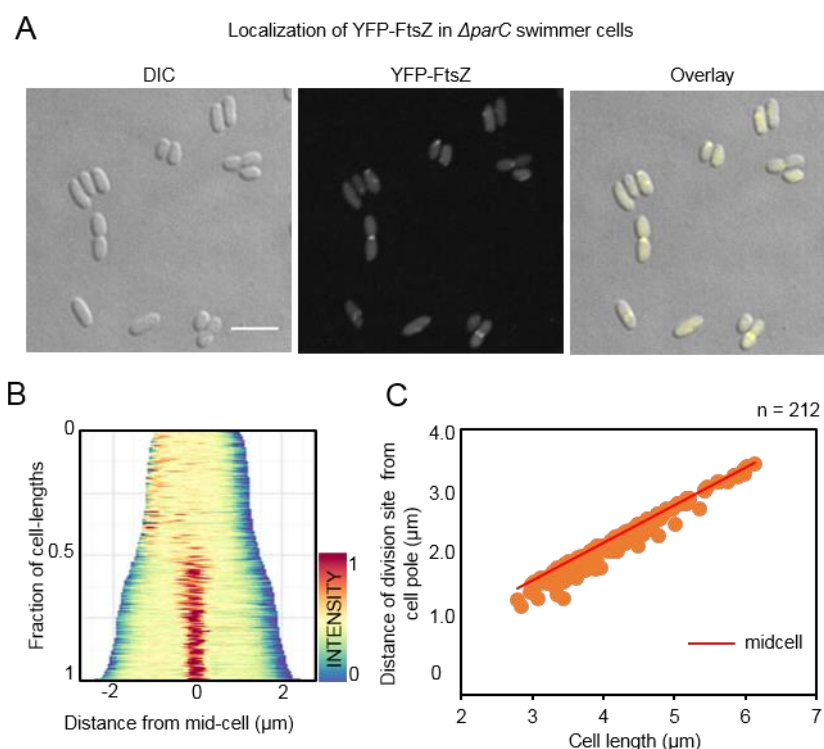


Figure 32: Deletion of *parC* does not affect cell division in swimmer cells. (A) Fluorescence microscopy showing the intracellular localization of YFP-FtsZ in $\Delta parC$ swimmer cells. Scale bar is 5 μm (B) Demographic analysis showing the fluorescence intensity of YFP-FtsZ along the cell length in a population of *V. parahaemolyticus* swimmer cells relative to cell length. (C) Graph depicting the distance of division sites from the cell pole as a function of cell length.

2.2.3. ParC cycles between the cell poles and cytoplasm

As ParC was now established to also function in preventing polar cell division in swarmer cells, we next analyzed the intracellular localization of ParC in this cell type by ectopically expressing a functional YFP-ParC fusion (Ringgaard et al., 2014). Fluorescence microscopy of YFP-ParC showed bi-polar localization pattern throughout the entire swarmer cell-cycle (Figure 33A-B). The bi-polar localization of ParC is consistent with its proposed function where the polar ParC prevents accumulation of FtsZ at the poles.

To further understand how the polarly localized ParC can protect the sub-polar region from aberrantly positioned divisome, we performed a detailed characterization of ParC dynamics using time lapse microscopy. FRAP (fluorescent recovery after photobleaching) experiments showed that there is an exchange between polar and cytoplasmic ParC. When polar YFP-ParC foci were photobleached, a recovery of polar YFP-ParC fluorescence was observed (Figure 33C-D, red arrowheads). Within 3 minutes of bleaching of the polar ParC focus, 35-40% of the signal had recovered and reached a steady-state level (Figure 33C-D). This shows a continuous recruitment of new ParC from the cytosol to the cell pole.

In order to analyze if ParC is likewise released from the cell pole into the cytoplasm, we performed photoactivation experiments. Photoactivation of PAmCherry-ParC at the cell pole generated polar ParC foci (Figure 33E, red arrowhead). A follow-up time-lapse microscopy showed that the activated PAmCherry-ParC focus at the cell pole decreased in intensity over time and in co-occurrence of PAmCherry-ParC fluorescence was detected in the cytoplasm (Figure 33E-F). This indicated that, over time, a portion of PAmCherry-ParC is released from the cell pole into the cytoplasm. Furthermore, photoactivation of PAmCherry-ParC along the cell length (excluding the cell poles), generated a diffusely localized PAmCherry-ParC signal in the cytosol (Figure 33G). Subsequent time-lapse microscopy revealed that activated cytosolic PAmCherry-ParC was recruited to the cell poles where it localized as distinct foci (Figure 33G, red arrowheads). This confirmed the results from FRAP microscopy of YFP-ParC, i.e. there is a continuous recruitment of cytosolic ParC to the cell pole.

Altogether, these data show that there is a continuous release of ParC molecules from the pole to the cytoplasm and recruitment of new ParC from the cytoplasm to the cell pole (Figure 33H). This cycle of ParC possibly extends the reach of ParC's action beyond the extreme cell pole. Thus, explaining how ParC is able to regulate FtsZ localization in a sub-polar region of almost 2 μm from the cell poles.

RESULTS

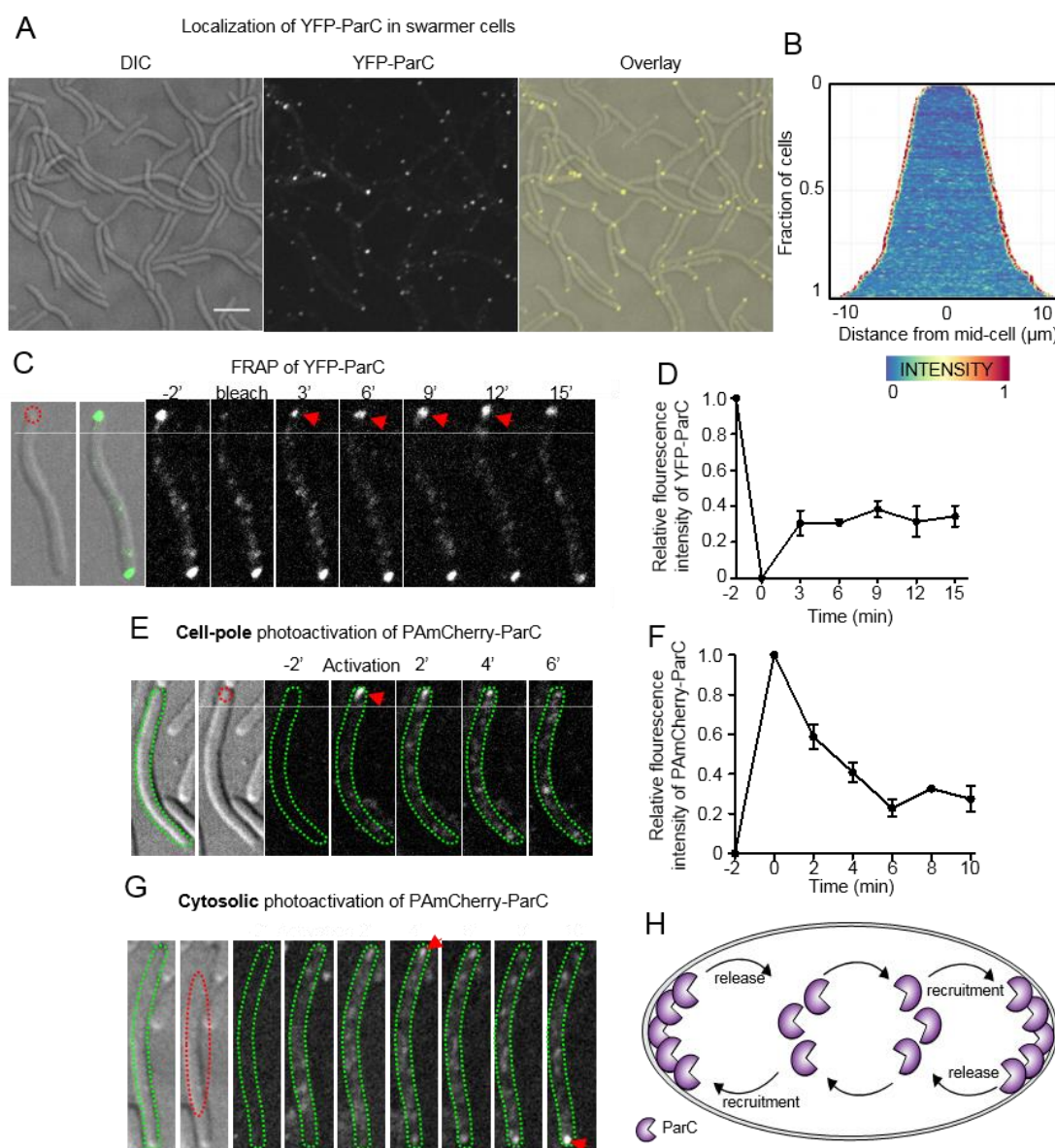


Figure 33: An ATP-driven ParC cycle is required for its regulation of FtsZ localization. (A-B) Intracellular localization of YFP-ParC in *V. parahaemolyticus* swarmer cells. (A) Fluorescence microscopy imaging showing the intracellular localization of YFP-ParC in $\Delta parC$ swarmer cells of *V. parahaemolyticus*. Scale-bar represents 5 μm . (B) Demographic analysis showing the fluorescence intensity of YFP-ParC along the cell length in a population of *V. parahaemolyticus* swarmer cells relative to cell length. (C) Fluorescence-recovery-after-photobleaching (FRAP) experiment of YFP-ParC localized at the cell poles in swarmer cells showing that bleached regions of YFP-ParC at the cell pole recover post-bleaching. Numbers indicate minutes pre- and post-bleach. The red dashed circle shows the bleached region, and red arrowheads indicate areas of Yfp-ParC recovery post-bleaching. (D) Graph depicting the fluorescence intensity of YFP-ParC pre- and post-bleach at the bleached cell pole relative to the initial intensity at the pole pre-bleach during time-lapse series. The average recovery is shown along with the standard error mean. (E) Photoactivation of PAmCherry-ParC localized to the cell pole in wild-type *V. parahaemolyticus* swarmer cells. Numbers indicate minutes pre- and post-activation. The red dashed circle shows the activated region, the red arrow indicates the signal from PAmCherry-ParC localized to the old pole after activation. The outline of the cell is highlighted by a green dashed line. (F) Graph depicting the fluorescence intensity of PAmCherry-ParC pre- and post-activation at the activated cell pole relative to the initial intensity at the pole pre-activation during time-lapse series. The average intensity is shown along with the standard error mean. (G) Photoactivation of PAmCherry-ParC localized in the cytoplasm in wild-type *V. parahaemolyticus* swarmer cells. Numbers indicate minutes pre- and post-activation. The red dashed circle shows the activated region, the red arrows indicate the signal from PAmCherry-ParC that has been recruited from the cytoplasm to the cell poles after activation in the cytoplasm. The cell body is highlighted by a green dashed line. (H) Schematic showing the cycle of ParC between the cell pole and the cytoplasm. There is a continuous release of ParC molecules from the pole to the cytoplasm and recruitment of new

ParC from the cytoplasm to the cell pole resulting in a continuous cycle of ParC between the pole and the cytoplasm.

2.2.4. ParC's intracellular localization is regulated by its ATPase cycle and DNA binding

The ATPase activity of ParC is found in an earlier study to be important for its function of cell pole maturation when facilitating proper recruitment of the chemotaxis proteins (Ringgaard et al., 2011). Based on previous works, we constructed ParC variants that carried amino acid substitutions, which were predicted to i) prevent ATP binding and lock ParC in its apo-monomeric form (ParCK15Q), ii) prevent DNA binding and ATP hydrolysis and lock ParC in its monomeric ATP-bound form (ParCG11V) and iii) prevent non-specific DNA binding of ParC (ParCR191E). Unpublished results by Alvarado et al., (Ringgaard lab) showed that ParC non-specifically associates with DNA and that DNA binding by ParC was required for its function in recruitment of chemotaxis proteins to the cell pole. Particularly, they have shown that the ParCR191E variant is unable to bind DNA.

We studied the intracellular localization of these mutants in swarmer cells to address how ParC's DNA binding and ATPase cycle influence its localization dynamics in this cell type. The three variants, ParCK15Q, ParCG11V and ParCR191E were individually expressed in *V. parahaemolyticus* $\Delta parC$ swarmer cells. The microscopy analysis showed that YFP-ParCK15Q did not localize to the poles but remained largely in the cytosol forming random foci or patches along the cell length (Figure 34A). In contrast, YFP-ParCG11V localized to the cell poles and formed bi-polar foci (Figure 34B). In addition to the foci formation at the cell poles, demographic analysis revealed that a larger proportion of YFP-ParCG11V was retained diffused in the cytosol when compared to wild-type YFP-ParC (Figure 33A-B). Furthermore, YFP-ParCR191E strictly localized to the poles in a bi-polar manner and almost no cytosolic signal was observed (Figure 34C).

These data suggest that the ATP-bound form of ParC is recruited to the poles, while the Apo-monomeric form is excluded from the pole. Thus, suggesting that ATP binding of ParC is required its polar localization. The variation in polar and cytosolic signal intensity of the ParC variants suggests significance of the ATPase cycle and DNA binding state in the protein's localization. In conclusion, this suggests that ParC's ATPase activity and DNA binding ability drive the cycling of ParC between the cell pole and the cytoplasm.

RESULTS

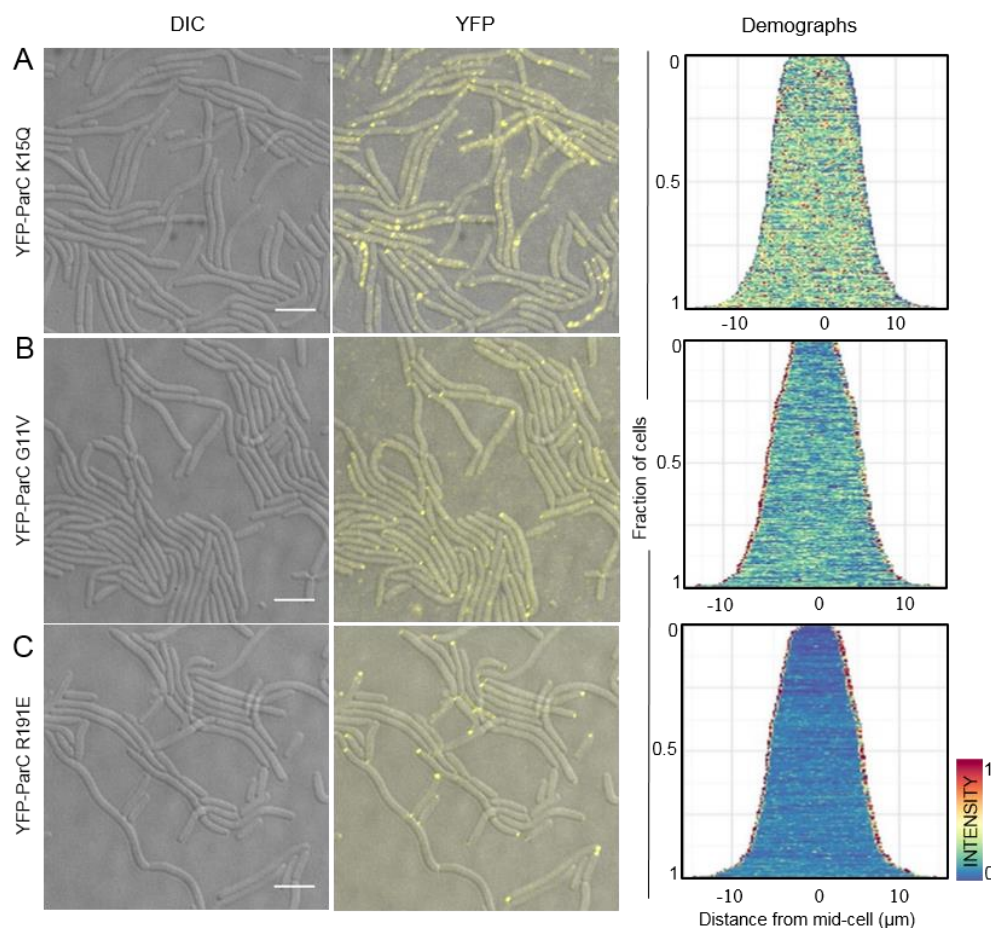


Figure 34: Intracellular localization of ParC is regulated by its ATPase cycle and DNA binding. Fluorescence microscopy imaging and demographic analysis showing the intracellular localization of (A) ParCK15Q, (B) ParCG11V and (C) ParCR191E along the cell length in a population of *V. parahaemolyticus* $\Delta parC$ swarmer cells.

2.2.5. ParC's ATPase cycle and DNA binding determines its effect on polar FtsZ

Since the ATPase activity of ParC is important for its function in polar recruitment of chemotaxis proteins (Ringgaard et al., 2014) and its polar localization in swarmer cells, we speculated that its ATPase activity might also be important for ParC's function in cell division by preventing polar accumulation of FtsZ. Thus, we investigated the localization of YFP-FtsZ in *V. parahaemolyticus* strains where the native *parC* locus was replaced individually by *parCK15Q*, *parCG11V* and *parCR191E*, which encode the protein variants ParCK15Q, ParCG11V and ParCR191E, respectively.

Interestingly, in all the three backgrounds we observed polar localization of FtsZ to a degree similar to that of a strain lacking ParC. In the *parCK15Q* background YFP-FtsZ localized at the cell poles (Figure 35A-C, purple arrows, D).

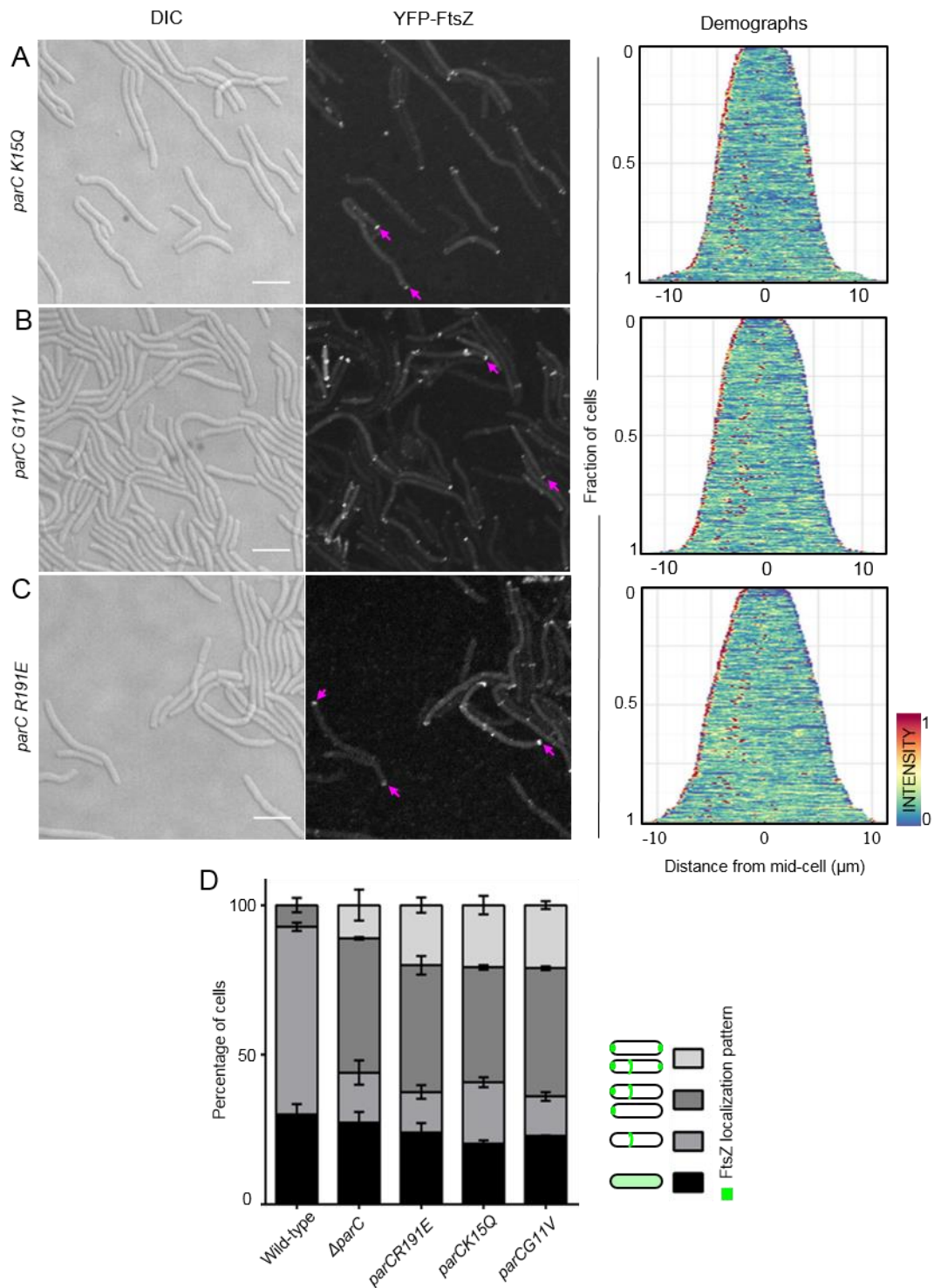


Figure 35: ParC's ATPase cycle and DNA binding determines its effects on polar FtsZ. (A)(B)(C) Fluorescence microscopy imaging showing the intracellular localization of YFP-FtsZ in *V. parahaemolyticus* strains encoding *parCK15Q*, *parCG11V* and *parCR191E* respectively. Demographs show the fluorescence intensity of YFP-FtsZ along the cell length in a population of *V. parahaemolyticus* swarmer cells relative to cell length. Scale-bar represents 5 μm . (D) Stacked bar-graph showing the percentage of a bacterial population with distinct localization patterns of YFP-FtsZ in wild-type and mutant *V. parahaemolyticus* swarmer cells. Black: diffuse cytosolic YFP-FtsZ localization; dark gray: Z-ring either at mid-cell or pole proximal position; light gray: distinct uni-polar localization of FtsZ either in the absence or presence of a Z-ring positioned either at mid-cell or at the pole proximal position; white: distinct bi-polar localization of FtsZ either in the absence or presence of a Z-ring positioned either at mid-cell or at the pole proximal position. Error bars indicate standard error of the mean (SEM).

RESULTS

Additionally, like $\Delta parC$ strain, proper FtsZ localization at its swarmer specific division sites were formed in these strain backgrounds, further confirming that ParC acts to prevent polar localization of FtsZ but not regulate its position in the swarmer specific LD-sites (compare Figure 35A-C, demograph and Figure 13B). It was particularly interesting that ParCG11V and ParCR191E were non-functional in regulating FtsZ localization as both these protein variants localize to the cell pole.

These data suggests that polar localization of ParC itself is not sufficient for ParC function but ATP hydrolysis and DNA binding are also both required for ParC function in preventing polar localization of FtsZ and formation of mini-cells.

2.2.6. ParC actively prevents polar division events through a possible direct interaction with FtsZ

To analyze if ParC regulates cell division through its direct interaction with FtsZ, we performed a yeast-two-hybrid experiment to test for protein-protein interactions. These experiments suggested that FtsZ self-interacts, and importantly that ParC and FtsZ interact directly (Figure 36A).

To further analyze if ParC directly interacts with FtsZ as suggested by the yeast-two-hybrid experiment, we performed a co-immunoprecipitation experiment using α -YFP antibodies on cells expressing only YFP, YFP-FtsZ and YFP-ParC and tested for co-immunoprecipitation of FtsZ using α -FtsZ antibodies. No FtsZ was pulled down in cells expressing only YFP (negative control) (Figure 36B, lane 1). Native FtsZ was clearly pulled down from cells expressing YFP-FtsZ (Figure 36B, lane 2), hence confirming that FtsZ self-interacts and that the YFP-FtsZ fusion is functional for self-interaction. Importantly, we could detect the presence of FtsZ when using YFP-ParC as bait (Figure 36B, lane 3), showing that immunoprecipitation of YFP-ParC is able to co-purify native FtsZ. Thus, indicating that ParC and FtsZ interact directly and confirming the results of the yeast-two-hybrid assay. Altogether, this indicates that ParC actively prevents polar localization of FtsZ and mini-cell formation by direct protein interaction with FtsZ.

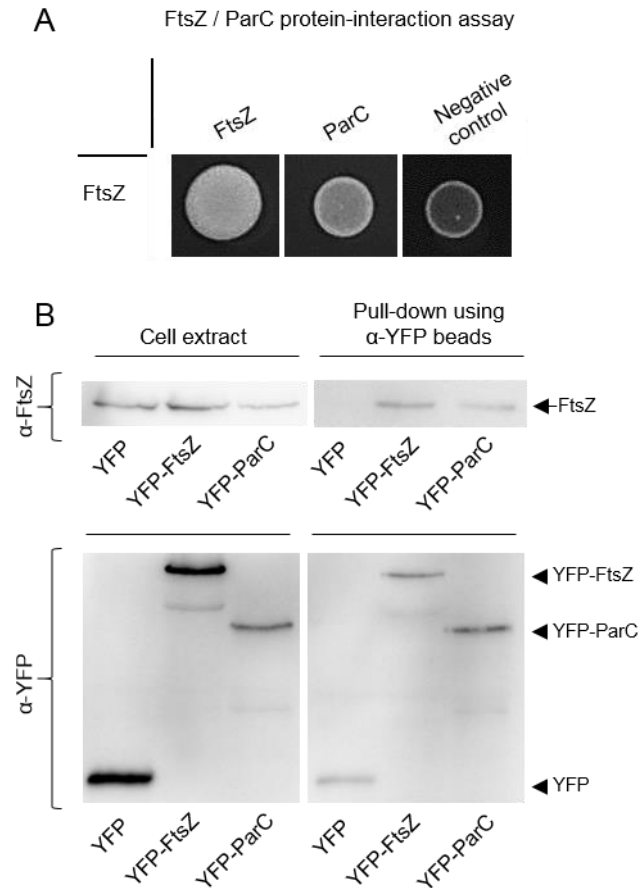


Figure 36: ParC actively prevents polar division events through direct interaction with FtsZ. (A) Yeast-two-hybrid experiment assaying for protein interactions between ParC and FtsZ. Growth of yeast colonies suggests a protein interaction occurs. (B) Co-immunoprecipitation experiment using α -YFP antibodies on wild-type *V. parahaemolyticus* cells expressing YFP (negative control), YFP-FtsZ, and YFP-ParC respectively. Samples were analyzed by Western blot using α -FtsZ antibodies to test for the co-purification of FtsZ protein.

CHAPTER III

DISCUSSION

3.1. FtsZ forms distinct localization patterns in the swimmer cells

In this study we address the cell division of the two cell types of *Vibrio parahaemolyticus*. The 2.5-4 μm long swimmer cells of *V. parahaemolyticus* propagate by a binary division resembling that of *V. cholerae*. *V. parahaemolyticus* encodes in its genome the central division protein, FtsZ, which localizes in a distinct pattern in the swimmer cells. It also encodes some of the most widely studied cell division regulators, MinCDE - an FtsZ positioning system, SlmA - the nucleoid occlusion factor and ParABS-the chromosome partitioning system. The polar localization of FtsZ at the new pole following division, although momentary, is distinct as has not been widely reported. Polar FtsZ was first reported in chromosome segregation study in *V. cholerae* (Srivastava et al., 2006), and further confirmed in the cell division studies of the same bacterium (Galli et al., 2016a). Galli *et al.*, by timing cell division using cell length distribution, suggest that FtsZ relocates to the mid-cell from the new pole in *V. cholerae* for the Z-ring formation at a much later stage of the cell cycle compared to that in *E. coli*. Interestingly, polar localization of FtsZ was also reported in short cells of *Helicobacter pylori* (Specht et al., 2013). They describe that this polar focus at the new pole relocates to the mid-cell forming spiral intermediates. Thus *H. pylori* is yet another example of a bacterium displaying polar FtsZ despite harboring Min system in its genome.

Masking of function of the oscillating Min system by the chromosome arrangement factors was proposed as the reason for the occurrence polar FtsZ localization in *V. cholerae* (Galli et al., 2016a). This could be verified in *V. parahaemolyticus* by studying the effect of MinCDE deletion together with the deletion of the chromosome arrangement proteins (HubP, ParAB1 and MatP). However, we have not probed into this yet. Together with evidences from other organisms, our research points out that, unlike the popular belief, a bacterial cell with a functional oscillating Min system can still exhibit deviations in divisome protein dynamics.

3.2. Daughter cells of the swimmer cell cycle inherit replicating chromosomes

The characterization of genome organization and replication has been widely studied in bacteria with a single chromosome. Only in the last decade, several studies have begun to unravel the differences in chromosome organization, replication and segregation in multi-chromosomal species with *V. cholerae* as the popular model. Although *V. parahaemolyticus* is also a two-chromosomal bacterium like *V. cholerae*, it is not certain

DISCUSSION

to what extent the processes in the latter can be extrapolated to the former. *V. parahaemolyticus* are fast dividing bacteria with replication time of 12-14 minutes at 37°C in LB (Dryselius et al., 2008). Localizing the origin associated proteins of the two chromosomes, ParB1 and ParB2, allowed us to track the positions of the origins during cell cycle. The cells were born with one *oriI* at each cell pole while *oriII* largely localized at the mid-cell. The single ParB2 foci seen in the new born cell suggest either a non-replicated origin of chromosome II or a replicated but unresolved origin. The chromosomes appear to be symmetrically placed in the cell and appear to follow a symmetric segregation pattern. This is different compared to the well-studied chromosome organization and segregation in *V. cholerae* primarily in chromosome I. In the new born cells of *V. cholerae*, *oriI* is located near the pole. During segregation, one of the replicated *oriI* moves to the opposite pole while the other stays at the initial pole, thereby following an asymmetric segregation (Fogel & Waldor, 2005). However, in *V. parahaemolyticus* the ParB1 focus at each of the poles suggests replicated origins tethered to the poles, indicating an already segregating chromosome I. This allows replication to span more than a single generation facilitating a shorter generation time than the chromosome replication time, which have been described for fast growing bacteria (Skarstad et al., 1985).

In *V. cholerae* HubP was discovered to be the landmark protein that anchors several proteins and thus playing an essential role in pole maturation. HubP was shown to localize ParB1 to the poles via directing the localization of ParA1 (Yamaichi et al., 2012). In a later study, HubP was shown to localize only to the old-pole in new born cells and to form a bi-polar pattern as the cell elongates, explaining how HubP could orchestrate the segregation of *oriII*/ParB1 sister copies (Galli et al., 2017). Therefore, anchoring of origins to the poles observed in our study could also be facilitated by the interaction of HubP to ParA1 which is known to directly interact with ParB1. The failure to tether the ParB1 foci to the poles in a *parA1* deletion background supports this hypothesis. Polar HubP could sequester the replicated *oriII*/ParB1 to the poles, ensuring proper inheritance of chromosome in the rapidly dividing swimmer cells. Thus, the presence of bi-polar HubP in the new born cells explains the tethering of sister *oriII*/ParB1 in new born *V. parahaemolyticus* swimmer cells to either poles. Although the exact localizations of ParB1 in $\Delta parA1$ and $\Delta hubP$ strains vary, both deletions result in mislocalization of ParB1. Thus, suggesting that HubP is involved in chromosome segregation of *V. parahaemolyticus* by tethering origins through ParA1.

Additionally, the untethered ParB1 foci observed occasionally in wild-type cells might be due to a momentary release of the origins from the polar anchor during the replication of this region. Following the release of ParB1 anchoring and subsequent replication of the

oril site, one sister *oril* re-attaches to the pole and the other possibly gets segregated directed by ParA1.

3.3. Min, NO and their role in division of swimmer cells

The polar positioning of FtsZ could cause an uncertainty in the functionality of the Min system. The localization of YFP tagged MinD confirmed an oscillatory Min. On quantifying the effect of a Min deletion by estimating the percentage of mini-cell formation, it turned out to pose the same extend of effect as that in *V. cholerae*. The Min system in *V. cholerae* is active in regulating division but this function is masked by the regulators of chromosome segregation and chromosome arrangement (Galli et al., 2016a). Albeit, the scenario of polar FtsZ in an environment of oscillating Min in *V. parahaemolyticus* displays a stark similarity to the observations in *V. cholerae*, the chromosome segregation state and hence chromosome positioning are very different. The origins of the replicating chromosomes in a new born *V. parahaemolyticus* swimmer cell are already segregated and positioned at the opposite poles. This is unlike that of ChrI in *V. cholerae* where its origin is positioned at the old pole. Hence, the arrangement of chromosome cannot be the driving force behind polar FtsZ or the factor masking the effect of Min deletion in *V. parahaemolyticus*. Further research needs to be carried out to investigate this interesting FtsZ dynamics.

In spite of the differences in localization patterns of the key cell division proteins and deviation in functions of the conserved regulator proteins compared to previously studied organisms, *V. parahaemolyticus* swimmer cells continue to divide at precise mid-cell positions.

Absence of any observable phenotype in a $\Delta slmA$ background was not surprising because the discovery of the function of SlmA itself was in a Min deletion background (Bernhardt & De Boer, 2005). $\Delta slmA$ cells of *E. coli* were also reported to appear wild-type like, although no quantification of cell length was shown. The slight elongation effect in a $\Delta slmA$ *V. parahaemolyticus* swimmer cells became evident on quantification. The hyper elongation of swimmer cells in the double deletion background $\Delta minCDE \Delta slmA$ indicates that oscillating Min system is essential in a nucleoid occlusion deficient environment to regulate cell division.

Studies in *E. coli* have shown multiple Z-ring clusters in Min and partition double mutants (Yu & Margolin, 1999). According to the model 'targeting and activation of division sites are activated by the position of nucleoids', all positions along a cell length are equally competent for cell division. But these divisions are prevented in regions of the nucleoid by the nucleoid occlusion factors. Therefore, this inhibition should get lifted as soon as the

chromosome segregates or in the absence of occlusion factors. This explains what we see in *V. parahaemolyticus* cells. When *SlmA* is deleted, misplaced nucleation of FtsZ polymers are observed in the cell. Nucleation of FtsZ polymerization at non-mid-cell sites, also reduces the availability of FtsZ molecules for Z-ring formation at the proper division sites, which might be the cause for slight elongation phenotype. However, we do not observe several divisions at these random sites probably because of the still oscillating Min system that exerts a significant force on FtsZ ring placement. Absence of extreme cell division defects could be because of the strong regulation by the Min system and also by other unknown division regulators. In the observations associated with the discovery of nucleoid occlusion function of *Noc* in *B. subtilis*, deletion of *Noc* on its own also did not produce any apparent growth defect, chromosome segregation defect or other division phenotypes (Wu & Errington, 2004). Although it was mentioned that cell lengths were normal and FtsZ localized as bands at the expected future division sites, the data is not shown. Hence the possibility of slight elongation phenotypes cannot be ignored.

Effect of Min deletion is largely the formation of mini-cells and mildly elongated daughter cells. The concentration of FtsZ in a cell supports only a single functional Z-ring. Therefore, a misplaced polar division occurs at the cost of a mid-cell division ring. This being the cause of the observed mildly long progenies (Bernhardt & De Boer, 2004). Strikingly, the average site of division of a Min deletion, in spite of mini-cells and elongated cells, is biased to the mid-cell, suggesting the presence of other factors or mechanisms that place divisions to the mid-cell. In the observations associated with discovery of the *Noc* in *B. subtilis*, Wu et al reports the observation of multiple non-productive accumulations of division proteins and hence block in cell division (Wu & Errington, 2004). This also explains our observation of accumulation of non-functional FtsZ clusters along the cell length in a $\Delta minCDE \Delta slmA$ double deletion background. The scattered spots and weak tilted or incomplete bands of FtsZ in this background results from the availability of new regions for potential FtsZ clustering in the absence of the above mentioned 'FtsZ-targetting and activation' systems.

3.4. Cell division in swarmer cells

During differentiation of *V. parahaemolyticus* swimmer cells in viscous environment, an inhibition of cell division results in the formation of highly elongated cells, the swarmer cells, a morphological change that is important for swarming behavior (Böttcher et al., 2016; McCarter, 2010). For a swarmer colony to expand, it is crucial for the population to combine the seemingly contradictory requirements of cell division and maintenance of the characteristic long cells that are ideally equipped for swarming behavior. However, it was

not known how the highly elongated *V. parahaemolyticus* cells are able to divide without diminishing the population of long cells required for swarming. Here we show that *V. parahaemolyticus* has developed a mechanism to achieve this by switching from a mid-cell to a non-mid-cell division when a total cell length of approximately 10 μm is attained. This simultaneously allows for the maintenance and growth of the long cell and for proliferation, hereby presenting an elegant solution for this problem (Figure 37A). The Min-system is required for proper positioning of the division site, both at mid-cell and the non-mid-cell LD-site. Our data indicate that the proper switch to non-mid-cell division at the LD-site is mediated by a cell length-dependent transition in the localization-dynamics of MinD from a pole-to-pole oscillation in short swimmers to a multi-node standing-wave oscillation in long swimmers.

The swarmer cells divide in a pattern that has not been previously described. Although this is not the first study directed towards understanding the pattern of cell division in supersized bacteria, it is for the first time that an asymmetry in division site placement is being reported in such organisms. A prominent study reported by Pende et al. shows symmetric divisions in the *Gammaproteobacteria* attached to the nematodes *Eubostrichus fertilis* and *Eubostrichus dianeae*, where those on *E. dianeae* are the longest cells in which symmetric divisions has ever been observed. They rule out size as a trigger for division (Pende et al., 2014). On the contrary, *V. parahaemolyticus* swarmer cells that also attain great lengths of 55-60 μm , exhibit a cell length dependent positioning of division site. In this surface growing cell type of *V. parahaemolyticus*, short cells divide symmetrically and the long cells switch to a pole-proximal division pattern. The lengths of these cells evidently seem to play an important role in deciding the placement of division site. The swarmer cells of this bacterium switch from symmetric to asymmetric placement of division site at precise cell lengths. Furthermore, with steady increments in cell lengths, the division sites move to precise locations that are increasingly closer to the cell poles relative to total cell length (Figure 22B).

Proliferating cells have to ensure a safe and reliable cell division without putting the genomic integrity and overall cellular fitness in jeopardy. Swarmer cells are polyploid and there is a positive linear correlation between chromosome count and cell length. The *ori* regions of both chromosomes are equidistantly segregated along the long axis of the cell, however, our results indicate that independent of the cell length, complete chromosome segregation only occurs at one site and once per cell cycle. The site of complete chromosome segregation is correlated with the position of the division machinery and follows a similar cell length-dependent transition from a mid-cell position in short swarmer cells to a non-mid-cell position at the LD-site in long swarmer cells.

In the earliest studies of MinCDE system in *E. coli* cells, standing wave oscillations were observed in FtsZ⁻ cells (Raskin & de Boer, 1999c). In the same strain background several MinE rings were also described (Raskin & De Boer, 1997). This was the first time standing wave pattern formation of MinD was observed in cells. The cell divisions in such artificially elongated cells were not followed up after the study by W.D. Donachie and K.J. Begg. Donachie and Begg proposed a model of cell growth that suggested an increase in potential division sites with an increase in cell length (Donachie & Begg, 1970). In our study, we report a correlation of increased cell lengths to its corresponding MinD wave pattern and location of division sites. A parallel study to ours, followed divisions in elongated *E. coli*, almost five decades after the study by Donachie and Begg (Wehrens et al., 2018). They observed characteristic divisions at specific lengths from the poles in spite of multiple Z-rings. The findings by Wehrens and colleagues support our conclusions on positioning division sites in long cells by a multi-node standing wave oscillation of MinD. Studies on Min oscillation in long rods (Raskin & de Boer, 1999c) and aberrantly shaped cells (Varma et al., 2008) has pointed out that the oscillation periods remain same in normal and as well as atypically shaped cells. This is because fast diffusion of proteins in a cell ensures that the oscillation period is dependent on the accumulated protein concentrations and not the length or structure of the cells. However, the resultant patterns formed will depend on the dimensions of the cell or vesicle. Our study thereby confirms that the geometry detection mechanism of Min oscillatory system, that has been proposed (Varma et al., 2008), can in fact be utilized by naturally occurring differently shaped bacteria as a scale to position divisions at the desired sites.

3.5. Role of Min and NO in division of swarmer cells

The Min-system is required for proper positioning of the division site, both at the mid-cell and the length dependent division site (LD-site). Our data indicate that the switch to non-mid-cell division is mediated by a cell length-dependent transition in the localization-dynamics of MinD from a pole-to-pole oscillation in short swarmers to a multi-node standing-wave oscillation in long swarmers.

Multi-node standing wave oscillation of MinD has been reported in artificially elongated *E. coli* cells that are unable to divide due to an artificial block in cell division. When these artificially elongated cells reach a length of ~10 μm or more, the number of wavelengths of MinD oscillations present in the cell increases and the MinD dynamics change to a multi-node standing wave oscillation (Fu et al., 2001; Huang et al., 2003; Meinhardt & de Boer, 2001; Raskin & de Boer, 1999b). Thus, the wavelength of the MinD wave, and consequently the cell length at which a transition in MinD dynamics occur, are very similar

between the Min systems of *E. coli* and *V. parahaemolyticus*. Hence, suggesting that the number of MinD nodes and the MinD localization dynamics will remain cell length-dependent. This is further supported by *in vitro* reconstitution experiments of Min dynamics in fabricated microchambers, where Min dynamics has been observed to switch from a pole-to-pole oscillation to symmetric double oscillations or traveling waves and is correlated with chamber length for a constant protein concentration (Caspi & Dekker, 2016; Schweizer et al., 2012; Zieske & Schwille, 2013, 2014). In this study, we show for the first time that multi-node standing wave MinD-oscillations happen in naturally occurring cells, and that the oscillation pattern ensures the proper positioning of the Z-ring and division site in naturally occurring filamentous swarmer cells. Additionally, providing probable explanation for the cell growth model that was proposed five decades ago suggesting an increase in potential division sites with increase in cell length. The number of MinD nodes per cell increased with increasing cell length. However, Z-ring formation, and in consequence cell division, almost always occurred at the most cell pole-proximal MinD-node (the LD-site) (Figure 22A-C), preferring this node over the others in swarmer cells with more than two nodes. Formation of a single Z-ring in *V. parahaemolyticus* swarmer cells, at the pole-proximal MinD node, is unlike what has been described in the artificially elongated *E. coli* cells. *E. coli* formed multiple Z-rings positioned in an almost equidistant manner along the cell length. However, only one site underwent division at a time. Additionally, the positions of the Z-rings remained dynamic with the increasing cell length and also with subsequent divisions. Artificially elongated swimmer cells of *V. parahaemolyticus* also has been observed to form multiple Z-rings. What leads to the robust increase in FtsZ levels on artificial elongation, which in turn results in multiple Z-rings, remain unknown. Nevertheless, in both naturally occurring and artificially elongated cells, only one division occurs at a time and the most probable division site is the pole-proximal site.

Our finding that MinCDE system is in fact responsible for specific division rules agreed with the finding of Wehrens et al. The probability of divisions occurring at the cell length specific sites reduced drastically in $\Delta minCDE$ swarmer cells and the same was observed in artificially elongated *E. coli*. The consistent mid-cell divisions even in the absence of Min system implies the presence of additional regulators. It is possible that epigenetic information based on previous division events, as has been reported in *Staphylococci* (Turner et al., 2010), or perhaps unknown cell pole factors or birth scar proteins similar to *C. crescentus* (Huitema et al., 2006; Lam et al., 2006), helps to direct Z-ring formation towards the region proximal to the pole. Furthermore, here we show that the chromosomal origins are equidistantly placed along the swarmer cell, however, the positioning of termini

remains to be elucidated. One possibility is that they are differently positioned at the poles, and this may assist in pole-proximal positioning of FtsZ via a positive regulation for FtsZ through an FtsZ-ZapB-MatP-*matS* mechanism (Castillo et al., 2016; Demarre et al., 2014; Espeli et al., 2012; Espinosa et al., 2017; Mercier et al., 2008) – however, more research is needed to understand this question.

Our results suggest that SlmA does not direct positioning of the division site, but instead prevents the accumulation of FtsZ into division-deficient clusters along the cell length. The prospective outcome is that free FtsZ molecules exist in a concentration sufficient for Z-ring formation at mid-cell and LD-sites when directed to these locations by the Min-system. In *E. coli* (Bernhardt & De Boer, 2005; Cho et al., 2011b; Nam K. Tonthat, Sara L. Milam, Nagababu Chinnam, Travis Whitfill, William Margolin, 2013) and *V. cholerae* (Galli et al., 2016b), SlmA prevents Z-ring formation when bound to specific DNA sequences. It is likely that SlmA similarly in *V. parahaemolyticus* needs to be DNA bound in order to perform its role in preventing formation of division-deficient FtsZ clusters. As our results suggest that FtsZ is present at a level that sustains only the formation of a single Z-ring, complete chromosome segregation at multiple localizations along the cell, too, would have the potential to deplete FtsZ and interfere with cell division, as incomplete Z-rings likely would form at each nucleoid free site. Thus, our results suggest that by segregating the chromosomal origins regularly along the cell length, but only allowing complete chromosome segregation at one specific site, swarmer cells ensure that SlmA is able to act along the entire length of the cell.

3.6. Ensuring the preservation of long swarmer cells

The significant extension of the cell body that occurs during differentiation of swimmer cells to swarmer cells suggest an inhibition or regulation of cell division once differentiation is initiated. The mechanism responsible for this process remains an open question. We show that neither of the cell division regulators MinCDE and SlmA are essential for such a regulation. However, our results suggest that regulation of FtsZ levels contributes to the preservation of long cells within the swarmer population. If long swarmer cells were able to divide at multiple sites, the population of long cells would quickly get diminished. Thus, by regulating FtsZ levels to only sustain one division event per cell, *V. parahaemolyticus* ensures that long swarmer cells are allowed to divide, while simultaneously maintaining their their population.

DAPI staining experiments indicate that, in contrast to swarmer cells, the chromosomes of artificially elongated planktonic cells are completely segregated at multiple sites along the

cell length. However, similar to swarmer cells, each site of complete chromosome segregation correlates with the position of the division machinery. Furthermore, we show that the concentration of FtsZ is identical in planktonic and swarmer cells, while artificially elongated planktonic cells have significantly higher concentration of FtsZ than both wild-type planktonic cells and swarmer cells. It suggests that formation of a Z-ring at each MinD-node in artificially elongated planktonic cells simply is a consequence of the higher FtsZ concentration in these cells – i.e. FtsZ is abundant enough to sustain formation of multiple Z-rings, one at each MinD-node. Thus, the regulation of the FtsZ concentration level in swarmer cells to match that of planktonic cells, likely ensures that only enough FtsZ is present in swarmer cells to sustain the formation of a single Z-ring. Thus, effectively restricting the number of Z-rings formed to one, independent of swarmer cell length and the number of MinD-nodes. Furthermore, as the position of each Z-ring in artificially elongated planktonic cells correlates with the site of complete chromosome segregation, and as our data suggest that the formation of multiple Z-rings in artificially elongated planktonic cells is a consequence of higher FtsZ level, it probably suggests that the division machinery assists in determining the site at which complete chromosome segregation takes place.

Furthermore, a non-mid-cell position of the division site in long swarmers, ensures a continuous population of long cells, as non-mid-cell division results in a short and a long daughter cell. Consequently, by limiting the number of cell division events to one per cell at a non-mid-cell position in long swarmer cells, *V. parahaemolyticus* promotes the preservation of long cells within a multiplying population of swarmer cells. Therefore, this mechanism of cell division regulation allows swarmer cells to divide without the need for dedifferentiation.

3.7. A model summarizing the processes leading to an asymmetric cell division in swarmer cells

Our data support a model, where swarmer cells are polyploid with a positive linear increase in chromosome count with increasing cell length. The origins of both chromosomes are distributed evenly along the cell length, but complete chromosome segregation does not occur at this stage. SlmA prevents the formation of division deficient FtsZ clusters over the nucleoid. The even distribution of chromosomal origins along the cell length ensures that SlmA can act along the entire cell length. Pole-to-pole oscillation of MinD in short swarmer cells and multi-node standing-wave oscillation in long swarmer cells promote the positioning of the Z-ring to mid-cell and the non-mid-cell LD-site, respectively (Figure 37B, #1).

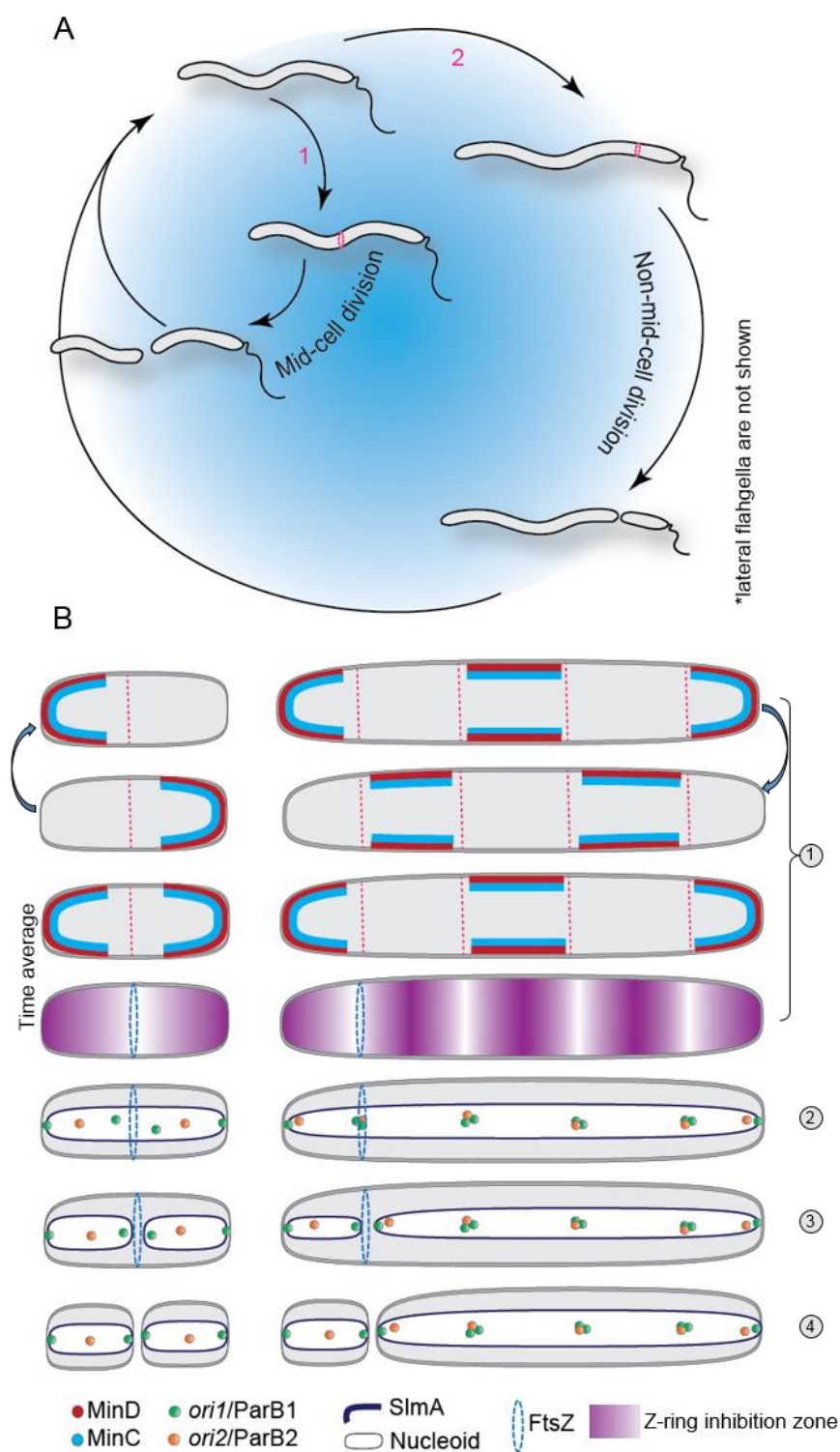


Figure 37: Cell division in swarmer cells of *V. parahaemolyticus*. (A) Model figure showing the cell cycle and cell division characteristics of *V. parahaemolyticus*. Depending on their cell length, swarmer cells undergo two distinct types of cell division: short swarmer cells position the Z-ring at mid-cell, resulting in swarmer progenies of equal sizes (#1); in long swarmer cells the Z-ring is positioned at the non-mid-cell LD-site, resulting in daughter cell of different sizes – a long and a short cell (#2). Division occurs with equal frequency towards either of the cell poles. (B) Schematic summarizing the spatio-temporal localization-dynamics of MinD and chromosome segregation in short and long swarmer cells. The model is described in detail in the main text.

The level of FtsZ protein allows for the formation of only one Z-ring at one MinD-node independent of cell length. The site of Z-ring formation in turn directs the site at which complete chromosome segregation takes place (Figure 37B, #2 → #3). Ultimately the cell divides at either mid-cell or the LD-site, resulting in daughter cells of equal sizes or in one short and one long daughter cell, respectively (Figure 37B, #4). In this way the combined actions of cell length-dependent MinD-dynamics, origin segregation, nucleoid occlusion by SlmA and regulation of FtsZ levels ensure that formation of the Z-ring and complete chromosome segregation only occurs once per cell at a cell length dependent location.

3.8. Cell type specific regulation of cell division by ParC in swarmer cells.

How cell division occurs and is regulated in swarming bacteria has so far been unknown and uncharacterized. In addition to the function of the MinCDE system in protecting the cell poles from aberrant divisions and ensuring proper position of the Z-ring in a cell length dependent manner, here we show that the placement of the division site is differentially regulated by distinct mechanisms, depending on the developmental stage. Particularly, we show that ParC, previously shown to function as a cell pole determinant (Ringgaard et al., 2011, 2014), is a bi-functional protein with an additional important role as regulator of cell division, specifically during swarmer cell development. ParC inhibits polar division events in swarmer cells by directly interacting with and actively preventing polar localization of FtsZ, and therefore division at that site. As ParC does not appear to fulfil the same function in swimmer cells, it is possible that another so far uncharacterized development-specific cue, which is only present in swarmer cells mediates or regulates ParC's action on FtsZ. Importantly, ParC functions in cooperation with the Min-system, which regulates cell division in both swimmer and swarmer cells. Occurrence of polar divisions in cells solely lacking ParC suggests that the Min-system is not able to absolutely protect the cell poles during the swarmer cell stage. Indeed, ParC is an important regulator of cell division in swarmer cells because absence of ParC results in aberrant polar divisions to an extent comparable to that of a *ΔminCDE* strain. Our results indicate that the ParC and Min-system function independently in swarmer cells, as deletion of both systems leads to an increased polar FtsZ localization and mini-cell formation compared to the single deletions. The precise reason for the requirement of an additional regulator of cell division (ParC) during swarmer development is interesting, but not clearly understood. Why an additional regulator of cell division (ParC) is required during swarmer development is interesting. In swarmer cells undergoing morphological differentiation there is a continuous elongation of the cell body, which our data clearly shows influences MinD-dynamics. The

effect of cell elongation on MinD-dynamics would be particularly prominent when the transition to an oscillation pattern with a higher degree of nodes occurs and could potentially disrupt Min-function for a period of time as the system adjusts to the new oscillation pattern. It is possible that during such transitions the Min-system is compromised and no longer be able to protect the cell poles from aberrantly positioned FtsZ as efficiently. In consequence, a factor preventing Z-ring formation, like ParC, that is always present as the cell poles is essential for protecting this region of the cell from aberrantly positioned division site.

Consistent with its role in preventing polar division events, ParC itself is bi-polarly localized during the swarmer cell cycle. Importantly, FRAP and photoactivation experiments showed a continuous exchange of ParC molecules between the cell pole and the cytoplasm. Localization of the ParC variants ParCK15Q and ParCG11V suggested that recruitment of ParC to the cell pole requires ATP binding and that the exchange of ParC between the pole and the cytoplasm is an active process driven by ParC's ATP-hydrolysis, similar to what has been reported for ParC in *V. cholerae* and swimmer cells of *V. parahaemolyticus* (Ringgaard et al. 2011, 2014). This cycle of release and recruitment from the cell pole could explain how ParC's function is sequestered to the cell pole region but enables ParC to extend its effect on FtsZ localization to a distance of 2 μm from the cell pole. This mode of action could be similar to that of MipZ in *C. crescentus*, another ParA-like ATPase, which protects the cell poles and restricts Z-ring formation to mid-cell. MipZ is a direct inhibitor of Z-ring formation and forms a steady-state gradient extending from the cell poles towards mid-cell.

MipZ is a ParA-like ATPase that restricts Z-ring formation to mid-cell and protects the cell poles by forming a gradient distribution extending from cell poles to the mid-cell with a concentration maximum at the cell poles (Thanbichler & Shapiro, 2006). MipZ's ATP binding and hydrolysis is important for its function and MipZ's gradient localization indicates the distribution of its dimers over the nucleoid (Kiekebusch et al., 2012). The ParB-*parS* complex recruits MipZ monomers to the poles and stimulates its dimerization. These MipZ dimers are then released from ParB and bind nonspecifically to the chromosome. The chromosomal binding results in MipZ's reduced diffusion rate. This leads to a higher retention of MipZ dimers to the regions close to the cell pole. As solely the dimeric form of MipZ interacts with FtsZ and inhibits Z- ring formation, division sites are correctly positioned at the region of minimum MipZ concentration in the gradient. Spontaneous ATP hydrolysis results in the dissociation of MipZ dimers to monomers, which then undergoes nucleotide exchange and gets recaptured by the ParB-*parS* complex. Mutations in MipZ that locks the protein in its monomeric or dimeric state results

in an increase or decrease in MipZ's diffusion rate, respectively, abolishing the gradient formation. Therefore, the polar source of MipZ dimers and its reduction in mobility are important for the establishment of cellular MipZ gradient (Kiekebusch et al., 2012). Although the exact mechanism behind the formation of such protein gradients are incompletely understood, data suggests that variations in diffusion rates of the different nucleotide dependent conformations of proteins (like MipZ) contribute to their gradient distribution.

A parallel study in our lab addresses the detailed intracellular localization of ParC and its variants in swimmer cells in *V. parahaemolyticus* using confocal fluorescence microscopy and single particle tracking super resolution microscopy (Alvarado et al, unpublished). This study indeed shows that ParC in swimmer cells forms a gradient that extends from the cell pole towards mid-cell with a concentration maximum at the cell pole. Indeed, this study shows that ParC's gradient formation is regulated by its ability to bind and hydrolyze ATP and associate with the nucleoid. Particularly, differential diffusion rates of ParC's distinct protein states drive gradient formation. Thus, similar to MipZ, ParC would be able to exert its function on regulating FtsZ localization beyond the immediate cell pole. However, the molecular mechanism by which ParC prevents polar localization of FtsZ and how ATP-binding and hydrolysis affect its interaction with FtsZ remains to be elucidated.

Interestingly, ParC is required for polar localization of chemotaxis arrays during both the developmental stages of *V. parahaemolyticus* (Ringgaard et al. 2011, 2014; Heering and Ringgaard 2016). Previously it has been shown that ParC acts with its cognate partner protein ParP in the recruitment of chemotaxis proteins to the cell pole. ParC primarily governs chemotaxis signaling array localization by mediating the polar localization of ParP, whereas ParP serves both to sequester arrays at the cell pole and stabilize arrays by preventing the release of chemotaxis proteins (Ringgaard et al. 2014). It is likely that ParP also influences ParC's function in regulation of cell division, since ParP regulates the polar localization of ParC in swimmer cells and likely influences the ParC cycle between the cell pole and the cytoplasm (Ringgaard et al. 2014). However, a potential role for ParP in regulation of cell division still is unknown and is an interesting question to be addressed in the future.

Our data show that ParC is a ParA-like ATPase with dual function that is essential for proper development of the cell pole. Particularly, ParC i) promotes cell pole maturation by facilitating polar localization of chemotaxis proteins in accordance with the cell cycle and ii) protects the cell pole from aberrant placement of the division machinery during swarmer cell development. Our results suggest that ParC's two functions in promoting localization

of signaling arrays and regulating cell division are interconnected, since disruption of ParC's ATP-cycle and polar localization influence both processes. Thus, our data indicate that the multiple functions of ParC connect the spatio-temporal regulation of diverse processes such as bacterial chemotaxis, cell pole development and regulation of cell division.

3.9. Conclusions and outlook

Here we have shown that several mechanisms regulate cell division in *V. parahaemolyticus* swimmer and swarmer cells. Particularly, swarmer cells undergo a novel and so far uncharacterized type of cell division regulated by ParC, MinCDE, SlmA as well as FtsZ protein levels. While the result of multi-node standing wave oscillation of MinD in swarmer cells, an asymmetric cell division, is similar to the first step of endospore formation in *B. subtilis* (Hutchison et al., 2014), the underlying mechanisms and purposes are very different. We show that, all cells from swarm-flares independent of their cell length, have initiated the swarm-program, and thus the swarmer-population is very heterogeneous in terms of cell length (Figure 28). Furthermore, our results indicate that the cell length-dependent asymmetric division of swarmer cells is a major regulator of this heterogeneity, as the consequence of an asymmetric division in *V. parahaemolyticus* swarmer cells is progeny cells of different cell lengths. However, the swarmer population is not only heterogeneous in cell length, but also in swimming capabilities, where short swarmer cells are swimming proficient and long swarmer cells are swimming deficient when released into a liquid environment (Figure 29). Thus, our results indicate that asymmetric division drives the separation of *V. parahaemolyticus* into two distinct population within the swarm colony. Particularly, both the progeny cells of an asymmetric division have initiated the swarm program but possess distinct capabilities- a swimming proficient short cell and a swimming deficient long cell. The sub-population of swimming proficient short swarmer cells has the potential to explore new surroundings by swimming if released into a liquid environment. We define cells belonging to this group as a population of "explorer" cells (Figure 38, explorers). This suggests that asymmetric division of long swarmer cells allows for swarming across surfaces while maintaining a sub-population of explorer cells that are ready to be released into liquid environments and immediately capable of exploring new surroundings (Figure 38). This result is in agreement with the finding that chemotaxis arrays always are positioned bi-polarly in swarmer cells (Heering & Ringgaard, 2016). Since only one division occurs in swarmer cells, a bi-polar positioning of signaling arrays will ensure that each daughter cell inherits an array upon cell division and thus the explorer cells will be able to immediately respond to changes in

their external milieu when released from the swarm-colony into their liquid surroundings. However, when not released, the fate of short cells within swarm colonies remains unknown – though, since they have initiated the swarm-program, it is likely that they are able to continue the swarmer life-style within the swarming population (Figure 38).

V. parahaemolyticus is a significant human pathogen and the cause of gastroenteritis worldwide – particularly due to consumption of undercooked seafood (Letchumanan et al., 2014). It is commonly found free swimming, attached to underwater surfaces, or associated with various species of shellfish (McCarter, 1999). Thus, the formation and release of explorer cells might also contribute to the spread of *V. parahaemolyticus* cells amongst shellfish and its dissemination in the environment (Figure 38). Importantly, *V. parahaemolyticus* cells that grow on a surface have increased cytotoxicity and likely an elevated virulence potential (Gode-Potratz et al., 2011). Consequently, the release of explorer cells from swarmer colonies has the potential to spread hyper infectious bacteria and thus increase the likelihood of human infections.

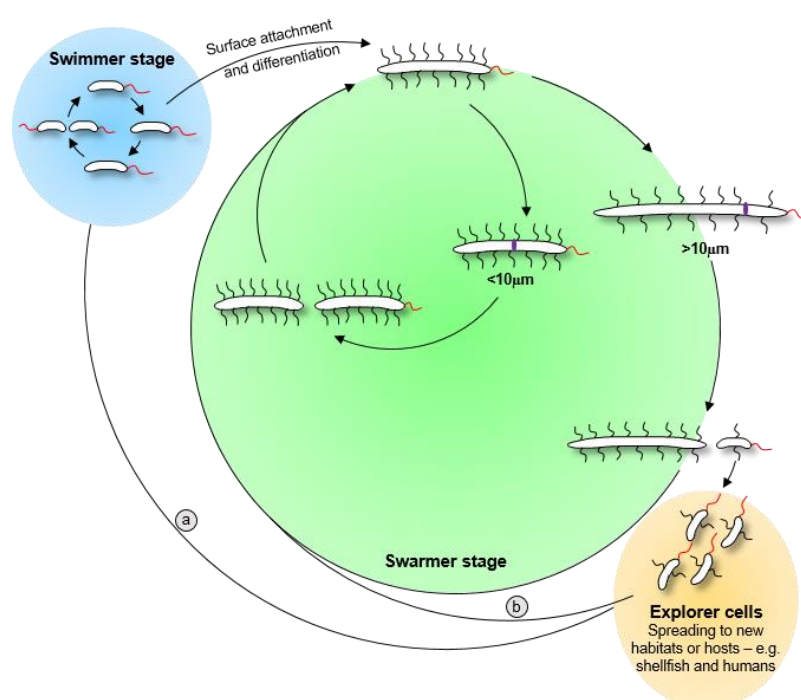


Figure 38: Development cycle of *Vibrio parahaemolyticus*.

Altogether, this work shows that *V. parahaemolyticus* swarmer cells exploit the dynamic nature of the Min-system to regulate an asymmetric cell division in consequence to swarmer cell elongation. This results in the formation of two distinct sub-populations of swarmer cells and explorer cells within the swarming colony. It is clear that swarm colonies are complex structures that consists of distinct sub-populations of cells. Future work is

DISCUSSION

needed to further characterize the coordination between chromosome segregation and cell division in swarmer cells and how the utmost pole-proximal MinD node is almost always chosen as division site. Furthermore, the architecture of the swarm colony needs to be characterized in order to understand how individual cells of the different sub-populations behave within the overall structure of the colony.

We hope this work will act as a base to initiate more cell division studies that shed insight into division mechanisms in naturally occurring bacteria with deviant cell shapes or that display dimorphism, unlike the popularly investigated cell division model organisms.

CHAPTER IV

MATERIALS AND METHODS

4.1. Chemicals, equipment and software

Reagents used (Table 1), kits (Table 2), software (Table 3) and equipments (Table 4) are listed below along their supplier and/or manufacturer. When available an identifier number is also provided.

Table 1: Reagents

Reagents	Supplier	Identifier
Genetic reagents		
Restriction enzymes	New England Biolabs (NEB) (Frankfurt a.M.)	
2-Log DNA Ladder (0.1-10.0KB)	New England Biolabs (NEB) (Frankfurt a.M.)	NEB Cat#: N3200S
Color Pre-stained Protein Standard Broad Range (11-245 KDA)	New England Biolabs (NEB) (Frankfurt a.M.)	NEB Cat#: P7712S
T4 Ligase	New England Biolabs (NEB) (Frankfurt a.M.)	NEB Cat#: M0202L
10X Buffer for T4 DNA Ligase with 10mM ATP	New England Biolabs (NEB) (Frankfurt a.M.)	NEB Cat#: B0202S
Q5 Hot Start High Fidelity DNA Polymerase	New England Biolabs (NEB) (Frankfurt a.M.)	NEB Cat#: M0493S
Q5 High GC Enhancer	New England Biolabs (NEB) (Frankfurt a.M.)	NEB Cat#: B9028A
Q5 Reaction buffer	New England Biolabs (NEB) (Frankfurt a.M.)	NEB Cat#: B9027S
Desoxyribonucleotide (dNTP) Solution Mix	New England Biolabs (NEB) (Frankfurt a.M.)	NEB Cat#: N04475
Alkaline Phosphatase Calf Intestinal (CIP)	New England Biolabs (NEB) (Frankfurt a.M.)	NEB Cat#: M0290L
Antibody		
Living Colors A.v. Monoclonal Antibody (JL-8) (Mouse monoclonal anti-GFP)	Clontech Laboratories, Inc. (USA)	Cat#: 632381
Chemical compound, drug		
Antibiotics: Chloramphenicol; Ampicillin sodium salt;	Carl Roth GmbH + Co KG (Karlsruhe)	Art.-Nr: 3886.3; k029.3; 0236.2
Kanamycin sulfate		
Isopropyl β -D-1 thiogalactopyranoside (IPTG)	Peqlab (Erlangen)	Nr.: 35-2030
Difco Agar, Granulated LB-Medium (Luria/Miller)	BD Carl Roth GmbH + Co KG (Karlsruhe)	Ref#: 214510 Art.-Nr: X968,3
L(+)-Arabinose	Carl Roth GmbH + Co KG (Karlsruhe)	Art.-Nr: 5118.3
peqGOLD Universal Agarose	Peqlab (Erlangen)	Nr.: 35-1020
Agarose NEEP Ultra-Quality	Carl Roth GmbH + Co KG (Karlsruhe)	Art.-Nr: 2267.3

MATERIALS AND METHODS

D(+) Saccharose	Carl Roth GmbH + Co KG (Karlsruhe)	Art.-Nr: 4621.1
Bacto Yeast Extract	BD	Ref#: 212750
Tryptone	Carl Roth GmbH + Co KG (Karlsruhe)	Carl Roth GmbH + Co KG (Karlsruhe)
Instant Blue	Expedeon (United Kingdom)	
EZ rich defined liquid medium	EZRDM, VWR, Germany	
Gel loading dye purple 6X	New England Biolabs (NEB) (Frankfurt a.M.)	#B7025S
5-Bromo-4-Chloro-3-Indolyl- β-D-Galactopyranoside (X- Gal)	Carl Roth GmbH + Co KG (Karlsruhe)	Art.-Nr: 2315.4
Materials		
96-well plates	Greiner Bio-One GmbH, Frickenhausen	
Microscopy slides	Carl Roth GmbH + Co KG (Karlsruhe)	Art.-Nr: 0656
Cover slips	Carl Roth GmbH + Co KG (Karlsruhe)	Art.-Nr: H875
Petri dish 92x16mm	Sarstedt	Cat#: 82.1472.001

Table 2: Commercial kits and assays

Name	Manufacturer	Identifier
NucleoSpin Gel and PCR Clean-up kit	Macherey-Nagel (Düren)	Ref.: 740609.250
NucleoSpin Plasmid Kit	Macherey-Nagel (Düren)	Ref.: 740588.250

Table 3: Software and on-line resources

Name	Source/Reference	Additional information
MetaMorph v7.5	Molecular Devices (Union City, CA)	
SeqBuilder v12.3.1	DNASTAR Software for Life Scientists (Madison, WI)	
SeqMan Pro v12.3.1	DNASTAR Software for Life Scientists (Madison, WI)	
ImageJ-Fiji	(Schindelin et al., 2012)	http://rsbweb.nih.gov/ij
R studio version 3.0.1		http://www.rstudio.com/
GraphPad Prism version 6.07	GraphPad Software (La Jolla CA)	https://www.graphpad.com/
Customized script for cell sorting	(Cameron et al., 2014b)	http://github.com/ta-cameron/Cell- Profiles

ggplot2 version 0.9.3.1	Hadley Wickham, Department of Statistics, Rice University	http://ggplot2.org
NIS-Elements Software AR 4.60.00 (Nikon)	NIS-Elements Software AR 4.60.00 (Nikon)	
STRING-known and predicted protein- protein interactions	(Jensen et al., 2009)	http://string-db.org/
Oligo Calc: Oligonucleotide Properties Calculator	(Kibbe, 2007)	http://biotools.nubic.northwestern.edu/OligoCalc.html
SMART: EMBL- Heidelberg	(Letunic & Bork, 2018)	http://smart.embl-heidelberg.de/

Table 4: Essential equipment

Application	Device	Manufacturer
Electroporation	MicroPulser electroporator	Bio-rad (München)
PCR	Mastercycler nexus PCR System	Eppendorf (Hamburg)
Centrifugation	Centrifuge 5424 and 5424R.	Eppendorf (Hamburg)
	Multifuge 1 S-R, Biofuge Pico17, multifuge X1R	Heraeus/Thermo Scientific (Dreieich)
Thermomixing	Thermomixer compact	Eppendorf (Hamburg)
DNA illumination and documentation	E-BOX VX2 imaging system	PeqLab (Eberhardzell)
DNA illumination	UVT_20 LE	Herolab (Wiesloch)
Protein electrophoresis	Mini-PROTEAN 3 cell	Bio-rad (München)
Western blotting	Transfer system from PeqLab	PeqLab (Eberhardzell)
Chemical-luminescence detection	Luminescent image analyzer LAS-4000	Fujifilm (Düsseldorf)
Microscopy	Ziess Axio Imager M1 fluorescence microscope, Zeiss Axioplan 2 fluorescence microscope, Nikon eclipse Ti inverted microscope	

4.2. Media, buffers and solutions

All media were sterilized by autoclaving at 121 °C for 20 min. Antibiotics and carbohydrates were filter-sterilized (pore size 0.2 µm or 0.45 µm; Sarstedt, Germany) and added to medium (at ~60 °C) at concentrations mentioned in Table 6. Standard buffers and solutions were prepared as described by Ausubel and Sambrook (Ausubel et al., 2002; Green & Sambrook D.W., 2012). Buffers and solutions used in specific experiments were described in the respective protocols. If needed, buffers and solutions were sterilized by

filtration (pore size 0.2 μm or 0.45 μm ; Sarstedt, Germany) or by autoclaving at 121°C for 20 min.

Table 5: Media, buffers and solutions

Media	Components	
LB (lysogeny broth) medium	1.0% (w/v)	Tryptone
	0.5% (w/v)	Yeast extract
	1.0% (w/v)	NaCl
YPAD	2.0% (w/v)	BactoPeptone
	1.0% (w/v)	Yeast extract
	2.0% (v/v)	Glucose
	0.003% (v/v)	Adeninehemisulphate
SD	2.0% (w/v)	Agar (for plates only)
	0.67% (w/v)	Yeast nitrogen base without amino acids
	2.0%	Agar (for plates only) Dropout supplement

Table 6: Concentrations of antibiotics used

Antibiotics	Final concentrations			
	<i>E. coli</i>		<i>V. parahaemolyticus</i>	
	liquid media	solid media	liquid media	solid media
Ampicillin	100 $\mu\text{g}/\mu\text{L}$	100 $\mu\text{g}/\mu\text{L}$	100 $\mu\text{g}/\mu\text{L}$	100 $\mu\text{g}/\mu\text{L}$
Kanamycin	50 $\mu\text{g}/\mu\text{L}$	50 $\mu\text{g}/\mu\text{L}$	50 $\mu\text{g}/\mu\text{L}$	50 $\mu\text{g}/\mu\text{L}$
Chloramphenicol	20 $\mu\text{g}/\mu\text{L}$	20 $\mu\text{g}/\mu\text{L}$	5 $\mu\text{g}/\mu\text{L}$	5 $\mu\text{g}/\mu\text{L}$

4.3. Microbiological Methods

4.3.1. Bacterial growth conditions

V. parahaemolyticus was grown at 37°C in LB broth with shaking at 220 rpm, or on LB agar plates. Antibiotics were added when necessary (Table 6). All *V. parahaemolyticus* strains used in this work were derived from the wild-type strain *V. parahaemolyticus* RIMD 2210633. Expression of genes under the control of arabinose promoter was induced with L-arabinose at 0.02% (w/v) concentration. *E. coli* was grown at 37 °C in LB with shaking at 220 rpm or on LB-agar plates. Antibiotics were supplemented to the final concentrations listed in Table 2. *E. coli* TOP10 (Invitrogen) or DH5 α pir chemically competent cells were used for general cloning purposes.

4.3.2. Strain storage

Densely grown bacterial cultures were stored supplemented with 16% (v/v) DMSO (dimethylsulfoxide) at -80 °C.

4.3.3. Growth curves

V. parahaemolyticus strains were grown in LB to OD >2.0, and then diluted with LB media to 1:200. Growth was then monitored by measuring the OD600 at different time points for 18 hours with three replicates per strain.

4.3.4. Swarming motility assay of *V. parahaemolyticus*

V. parahaemolyticus cells were inoculated in 5mL LB from a freshly streaked plate and grown to an OD600 of approximately 1.0. 1 μ L of this culture was spotted on swarm agar (40 g/L Difco Heart Infusion Agar (BD) supplemented with 4mM CaCl₂ and 50mM 2, 2'-bipyridyl (Sigma Aldrich)) Plates were then subsequently sealed and incubated overnight at 24°C.

4.3.5. Yeast Two-Hybrid assay

GAL4-based yeast two-hybrid system from Clontech was used as described by the manufacturers to analyze protein-protein interactions of the candidate genes. In GAL4 based systems, a native or synthetic GAL UAS (upstream activating sequence) consensus sequence provides the binding site for the GAL4 DNA-BD (Binding Domain) thereby conferring regulated expression of reporter genes. The HIS3 reporter of AH109 (yeast strain) is tightly regulated by GAL1 promoter. The plasmids encoding fusions of gene of interest to the GAL4 activation domain and DNA binding domain were transformed to GAL4 Yeast reporter strain AH109 in which the entire HIS3 promoter is replaced by GAL1 promoter (to ensure tight regulation of HIS3 reporter). The GAL4 DNA BD will be brought in interaction with the activation domain only when the two proteins fused to them interact. This interaction results in activation of the HIS3 reporter, enabling the strain to grow on histidine deficient media. Thus growth of AH109 yeast strain on HIS⁻ media is utilized as read out for positive protein-protein interaction (Egea-Cortines et al., 1999).

4.4. Molecular cloning

4.4.1. Isolation of chromosomal DNA

V. parahaemolyticus strains grown on LB plates overnight were re-suspended in distilled water and boiled at 98°C for 10 minutes. The samples were then centrifuged at 10,000rpm

for 5 minutes and the supernatant (which is the genomic DNA) were transferred to fresh eppendorfs for downstream usage.

4.4.2. Isolation of plasmid DNA

Plasmid DNA was isolated using NucleoSpin Plasmid kit (Macherey-Nagel).according to the instruction provided by the manufacturer. The concentration of DNA was determined using Nanodrop

4.4.3. Polymerase chain reaction (PCR)

The specific amplification of DNA fragments was conducted using Taq DNA Polymerase (homemade) or Q5 (NewEngland BioLabs). The reaction mixtures and programs are listed in Table 7. Amplification was verified by agarose gel electrophoresis. The reaction products were purified using NucleoSpin Gel and PCR Clean-up kit (Macherey-Nagel)

Table 7: Standard PCR reaction

Reagents	Concentrations
dNTPs	0.2mM
Buffer 1	1×
Buffer 2	1×
Template	50-200ng
Primer 1	0.5μM
Primer 2	0.5μM
Polymerase	0.5μL
ddH ₂ O	To make up to 50 μL

Colony PCR was performed using BioMix™ Red (Bioline, Germany). For colony PCR with *E. coli*, instead of DNA template the colony of interest was suspended in the PCR reaction mixture. For *V. parahaemolyticus*, genomic DNA was obtained by the method described earlier and was used a template in the reaction. Amplification was verified by agarose gel electrophoresis.

4.4.4. Restriction digestion

DNA digestion was performed by incubating 1-5 μg of DNA with selected restriction endonucleases (NEB, Germany; Fermentas, Canada) for 1-1.5 hours at 37 °C. 0.1 mg/ml bovine serum albumin (BSA; NEB, Germany) was supplemented if necessary. Similar procedure was also used to generate digested vector backbones. Digested products were further purified using NucleoSpin Gel and PCR Clean-up kit (Macherey-Nagel)

4.4.5. Ligation

DNA ligation was performed using T4 DNA ligase (New England BioLabs). In general, a mixture of digested insert DNA and recipient vector was incubated in 1:5 ratio with T4 DNA ligase and 10X Buffer for T4 DNA Ligase with 10mM ATP (New England BioLabs) at room temperature or 16°C for 1-2 hours.

4.4.6. Detection of DNA by agarose gel electrophoresis

DNA products were mixed with 16x DNA loading buffer (New England BioLabs) and separated in 1% agarose gels. The agarose gel was prepared in 0.5x TAE buffer (20 mM Tris/HCl, pH 8, 0.175 % acetic acid, 0.5 mM EDTA, pH 8) and supplemented with 0.005% ethidium bromide for visualization. A UV-transilluminator was used to detect DNA exposed to UV light. If necessary, DNA products of interest were excised from the gels for further purification.

4.4.7. DNA sequencing

DNA sequencing was performed by Eurofins MWG Operon (Germany). In general, 50-100 ng of DNA products were provided along with suitable oligonucleotides. Sequencing results were analyzed using Vector NTI Advance™ 11 (Invitrogen, Germany) or DNASTAR Navigator.

4.4.8. Transformation of cells

The preparation of chemically competent *E. coli* cells: The overnight cultures of *E. coli* cells were diluted 1: 100 in 250mL LB medium. Cells were grown to an OD600 of 0.6-0.8 and then incubated on ice for 10 min. Cells were then harvested at 4 °C, washed twice with ice cold TSS buffer. After centrifugation, the cells were resuspended in 8 ml of ice-cold TSS buffer supplemented with 15% (v/v) glycerol. Aliquots of competent cells (100 µl each) were snap-frozen in liquid nitrogen and stored at -80 °C for further use.

The transformation of chemically competent *E. coli* cells: The competent cells were mixed with ligation mixtures or plasmid DNA and incubated on ice for 30 min. A heat-shock was then applied for 2 minutes at 42 °C. Cells were then incubated again on ice for 5 min before mixing with 500 µl of LB or SOC medium. The cell suspension was then incubated at 37 °C for 1-2 hours with shaking and spread on LB agar plates supplemented with appropriate antibiotics. Plates were incubated at 37 °C until single colonies were visible.

The preparation of electrocompetent *V. parahaemolyticus* cells: A 5mL culture of the required strain was grown until dense. 1mL of this inoculum was then transferred to 200mL LB and incubated at 37°C until an OD of 1.0. Cells were incubated on ice for 10 min and then harvested at 4700rpm for 20 minutes at 4 °C, washed twice with 25mL ice cold 273 mM sucrose solution (pH7.4, buffered with KOH). After centrifugation, the cells were resuspended in 400uL of same icecold 273 mM sucrose solution + 15% (v/v) glycerol. Aliquots of competent cells (100 µl each) were snap-frozen in liquid nitrogen and stored at -80 °C for further use.

The transformation of electrocompetent *V. parahaemolyticus* cells: 2-5µL of the desired construct was mixed with a 50-100µL of electrocompetant *V. parahaemolyticus* cells, transferred to a pre-cooled 0.2cm electroporation cuvette and incubated on ice for 30 minutes. This was then electroporated at 2400V, 200Ω and 25µF in BioRad. The cells were then transferred to 1mL of LB and incubated at 37°C with shaking for 1 hour and plated in LB agar plates with required antibiotics.

4.4.9. Generation of *V. parahaemolyticus* deletion strains

Gene deletion was achieved by double homologous recombination. In general, plasmids for gene deletion were derived from the suicide vector pDM4 and used for transforming *V. parahaemolyticus* by conjugation. For this, the donor *E. coli* strain harboring the plasmid of interest and the recipient *V. parahaemolyticus* strain were grown to an OD of 0.5. 100µL of each were mixed together and 20µL of this was then spotted on LB agar plates. After incubating the plates for 4-6 hours or overnight, the spots were scrapped off and either resuspended in LB for dilution plating on LB+Amp+Cm plates or restreaked on LB+Amp+Cm agar plates and incubated overnight at 37°C. The colonies were restreaked on LB+Amp+Cm agar plates and incubated at 37°C. The single colonies thus obtained were the single crossovers of pDM4 in *V. parahaemolyticus*. The single crossovers were grown in LB+Amp+Cm broth for 5-6hours with shaking at 37°C. 50µL of this culture was then subcultured into LB with 10% sucrose and incubated with shaking at 20-24 hours. Dilution series (1-10⁸) of this overnight culture were plated on freshly made LB+10% sucrose plates and incubated overnight at 30°C. The colonies thus obtained were patched onto LB+Amp and LB+Amp+Cm agar plates. Genomic DNA were extracted from those colonies sensitive to Cm were checked for deletion with PCR. The PCR positive colonies were restreaked on LB+Amp and incubated at 37°C. The single colonies were again checked for deletion using PCR.

E. coli strains DH5αpir and TOP10 were used for cloning. *E. coli* strain SM10λpir was used to transfer plasmid DNA by conjugation from *E. coli* to *V. cholerae* and *V.*

parahaemolyticus (Miller & Mekalanos, 1988). A comprehensive list of all strains used for this work can be found in Table 8.

Table 8: Strains

STRAINS	DESCRIPTION/GENOTYPE	REFERENCES
<i>E. coli</i> DH5 α pir	<i>sup E44, ΔlacU169 (ΦlacZΔM15), recA1, endA1, hsdR17, thi-1, gyrA96, relA1, λpir phage lysogen</i>	
<i>E. coli</i> SM10 λ pir	KmR, thi-1, thr, leu, tonA, lacY, supE, recA::RP4-2-Tc::Mu, pir	
<i>Saccharomyces cerevisiae</i> AH109	MATa, trp1-901, leu2-3, 112, ura3-52, his3-200, gal4 Δ , gal80 Δ , LYS2 : : GAL1 _{UAS} -GAL1 _{TATA} -HIS3, MEL1 GAL2 _{UAS} -GAL2 _{TATA} -ADE2, URA3::MEL1 _{UAS} -MEL1 _{TATA} -lacZ	Clontech
<i>Vibrio parahaemolyticus</i> RIMD2210633	Clinical isolate, wild-type	(Makino et al., 2003)
MZ01	Δ parC	(Ringgaard et al., 2014)
SM2	Δ parC Δ minCDE	This research
SM3	Δ parB1	This research
SM8	Δ minE	This research
SM9	Δ parB1 Δ slmA	This research
SM10	Δ parC Δ slmA	This research
SM11	Δ minCDE Δ slmA	This research
SM12	Δ minCDE Δ slmA Δ parC	This research
PM19	Δ minCDE	This research
PM27	Δ slmA	This research
PM29	Δ parA1	This research
PM36	Ω vp3077-eyfp (ParB1-eyfp) and Ω vpa1751-mcherry (ParB2-mcherry) in wildtype	This research
PM39	Ω vp3077-eyfp (ParB1-eyfp) and Ω vpa1751-mcherry (ParB2-mcherry) in Δ parA1	This research
AA1	parCG11V	A. Alvarado
AA5	parCK15Q	A. Alvarado
JH5	Δ lafK	J. Heering
CF31	PlafA::mCherry	C. Freitas
<i>E. coli</i> SM10 λ pir	KmR, thi-1, thr, leu, tonA, lacY, supE, recA::RP4-2-Tc::Mu, pir	
<i>E. coli</i> DH5pir	<i>sup E44, ΔlacU169 (ΦlacZΔM15), recA1, endA1, hsdR17, thi-1, gyrA96, relA1, λpir phage lysogen</i>	
<i>E. coli</i> BL21 λ DE3	F ⁻ ompT gal dcm lon hsdS _B (r _B ⁻ m _B ⁻) λ (DE3) pLysS(cm ^R)	

4.4.10. Plasmids and plasmid construction

The list of all plasmids and primers used in this study is given in Table 9 and Table 10 respectively. Relevant information is also provided.

Table 9: Plasmids

PLASMIDS	DESCRIPTION/GENOTYPE	REFERENCES
pBAD33	Cloning vector	(Guzman et al., 1995)
pDM4	Suicide vector for gene deletions and insertions	(Donnenberg & Kaper, 1991)
pGAD424	<i>GAL4</i> ₍₇₆₈₋₈₈₁₎ AD, <i>LEU2</i> amp ^r	Clontech
pGBT9	<i>GAL4</i> ₍₁₋₁₄₇₎ DNA-BD, <i>TRP1</i> , amp ^r	Clontech
pMF390	PBAD:: <i>yfp</i>	(Yamaichi et al., 2007b)
pPM1	PBAD:: <i>yfp-vp0464</i>	This research
pPM6	PBAD:: <i>yfp-vp3077</i>	This research
pPM8	PBAD:: <i>yfp-vpa1751</i>	This research
pPM17	PT7:: <i>vp3077-6HIS</i>	This research
pPM18	PT7:: <i>vpa1751-6HIS</i>	This research
pPM34	Vector for replacing <i>parC</i> at its native site for <i>parCK15Q</i>	This research
pPM35	Vector for replacing <i>parC</i> at its native site for <i>parCG11V</i>	This research
pPM55	PBAD:: <i>yfp-vp0873</i>	This research
pPM56	Vector for deletion of <i>minCDE</i> ($\Delta vp0872 \Delta vp0873 \Delta vp0874$)	This research
pPM72	Vector for deletion of <i>parA1</i> ($\Delta vp3078$)	This research
pPM68	Vector for deletion of <i>slmA</i> ($\Delta vp0810$)	This research
pPM75	Vector for chromosomal integration of <i>vp3077-eyfp</i> and <i>vpa1751-mCherry</i>	This research
pSM8	PBAD:: <i>yfp-vp1105</i>	This research
pSM10	PBAD:: <i>cfp-vpa1751:yfp-vp3077</i>	This research
pSM52	Vector for deletion of <i>parB1</i> ($\Delta vp3077$)	This research
pSM57	pGAD424- <i>vp0464</i>	This research
pSM58	pGBT9- <i>vp0464</i>	This research
pSM59	pGAD424- <i>vp2227</i>	This research
pSM60	pGBT9- <i>vp2227</i>	This research
pCF048	Plasmid for integration of <i>PlafA::mCherry</i> on the chromosome	This research
pSR1035	PBAD:: <i>yfp-vp2227</i>	(Ringgaard et al., 2011)
pSR1084	PBAD:: <i>yfp-vp2227K15Q</i>	(Ringgaard et al., 2014)
pSR1089	PBAD:: <i>yfp-vp2227G11V</i>	(Ringgaard et al., 2014)
pSR1231	PBAD:: <i>PAmCherry-vp2227</i>	This research

Table 10: Primers

PRIMER NAMES	SEQUENCES
VP0464-1-cw	CCCCCTGTACAAGGTCCAGGGCCCATCTTTTGAACCGATGATGGA AATGTCTGA
VP0464-1-ccw	CCCCCGCATGCTTAATCAGCCTGACGACGTAAAAATG CCCC TGTACA AG GTCCAGGGCCCATCT
VP3077-1-cw	TCTAAGCGTGGTCTAGGAAAAGG
VP3077-1-ccw	CCCC GCATGC CTAGGCCTCTAGCTTGCAATTA

VPA1751-1-cw CCCCC TGTACA AG GTCCAGGGCCCATCT
GCTTTGAAAACGTCTGAATTAACGC

VPA1751-1-ccw CCCCC AAGCTT TTATTGCATTTTGCTTTGAACAAAAGTAA
CCCCC TCTAGA GTCCAGGGCCCATCT ATG TTC AAA GAG AAC
GCA AAG AAA GTC

VP1105-cw CCCCC GCATGC TTA ATC TTT TGG TGG CGC TGG

VP1105-ccw CCCCC GCATGC TTA ATC TTT TGG TGG CGC TGG

VP3077 del-a CCCCC TCTAGA GGA AAC CCC ATT TGA TCA AGT G

VP3077 del-b ACC ACG CTT AGA CAT GGA TTG
CAA TCC ATG TCT AAG CGT GGT ATG AGA TAA TTG ATT TAG
GTC AAT TAA

VP3077 del-c CCCCC TCTAGA TGG CGC AGC CAT AAC TCA TC

VP3077 del-d CAAAAACCCAAAAAAGAGATCGAAGCCGCGATGATCGTTTGGAGTG
TAGCT

Y2H ParC
cw_pGAD ACGGATCCCCGGGAATTTTACTGCTCATCGAACGCTAAC
Y2H ParC
ccw_pGAD GTTGACTIONGATCGCCGGAAGCCGCGATGATCGTTTGGAGTG
TAGC
T
Y2H ParC
cw_pGBT9 CAAACCCAAAAAAGAGATCGAAGCCGCGATGTTTGAACCGATGA
TGGAA
Y2H FtsZ
cw_pGAD ACGGATCCCCGGGAATTTTAAATCAGCCTGACGACGTAA
Y2H FtsZ
ccw_pGAD GTTGACTIONGATCGCCGGAAGCCGCGATGTTTGAACCGATGATGGA
A
Y2H FtsZ
ccw_pGBT9 ACGGATCCCCGGGAATTTTAAATCAGCCTGACGACGTAA
CCCCCTCTAGAGACATCCTCGAGCTCATGGCACGCATTATTGTAG
TAACG

vp0873-1-cw CCCCCGCATGCCTAGCCTCCGAACAGTCGTTTAA

vp0873-1-ccw CCCCCGCATGCCTAGCCTCCGAACAGTCGTTTAA

vp0872-74del-a CCCCCCTCGAGAGTGCTTTGGCTTGCTTTACTTTC

vp0872-74del-b TTTAAGGTCTGGTGAATGGGTCAT
ATGACCCATTACCCAGACCTTAAAGTGAAACTGCCTGACGACGAG
A

vp0872-74del-c CCCCCCTCGAGAGACGTTCACTACTTGTGCCAC

vp0872-74del-d CCCCCCTCGAGAGACGTTCACTACTTGTGCCAC

vp0872-74del-a CCCCCCTCTAGATGAAGATATTGCACGTAACCGCG

vp0872-74del-b TTGGTTAGCTACACTCCAAACGAT

vp0872-74del-cc AGGTTAGCGTTTCGATGAGCAGTAA

vp0872-74del-d CCCCCCTCTAGATCTTTGCCGTGCCTTC

vp2227-PMins-cw ATGATCGTTTGGAGTG TAGCTAAC

vp2227-PMins-ccw TTACTIONGCTCATCGAACGCTAAC

del-vp0180-a CCCACTAGTGACGCGTACTATGCACTAGCAAACGCTGCC

del-vp0180-b1 TAGTTACTTCTTTCAAATAC

del-vp0180-c1 GTATTTTGAAGGAAGTAACTAAGATTATGAGTAAAGACAAATAC

del-vp0180-d CGATACCGTCGACCCTCGAGTTGTACAAGCGTCATCAATGG

MATERIALS AND METHODS

VP3077-2-cw	CCCCC CCATGG CA ATGTCTAAGCGTGGTCTAGGAAAAG
VP3077-2-ccw	CCCCC CTCGAG GGCCTCTAGCTTGGCAATTAGT
VPA1751-2-cw	CCCCC CCATGG CA ATGGCTTTGAAAACGTCTGAATTAAC
VPA1751-2-ccw	CCCCC CTCGAG TTGCATTTTGCTTTGAACAAAAGTAAGG
VPA1751-a-cw	CCCCC TCTAGA ATGGCTTTGAAAACGTCTGAAT
vpa 1751 to mcherry-ccw	AT CCT CCT CGC CCT TGC TCA CCA T GACATCCTCGAGCTC TTGCATTTTGCTTTGAACAAAAGT
mcherry-cw	ATGGTGAGCAAGGGCGAGGA
mcherry- ccw with STOP	TCA CTTGTACAGCTCGTCCATGCCG
mCherry to downstr. of vpa1751	CGGCATGGACGAGCTGTACAAG TGA AATTAAGCTTTAACGATAACC
ins-eyfp-C-term- ParB2 ccw	CCCCC TCTAGA GCG GTA AGT AAT ATA CGC AGT GG
parS1-1-cw-Cy3	ACAACCTTTCAAACCGATCAACAC
parS1-1-ccw	TACTTTGATGCCTAAACGACAATC
parS2-123-cw-Cy3	AACATTGAACTTTGTCGGTTCATGAG
parS2-123-ccw	AATTTGGATTATCGGGAAGAAAGC
nc-Vp-S-cw-Cy5	ATAAAGGCGTGTTGAGAGTAGG
nc-Vp-S-ccw	TTAGCAAGCTCGGTTGTGACATC
VP0984-ins-Prom- AQUA-cw-a	AAGCTTGCATGCCTGCAGGTGCGACTAGCCGTTTACCAGGTAAACC
ins-Pvpa1548- VP0984 ccw-b	TTT TAG CGT TAG TTT CCG ATG TGC TAAA GGA GCC TTT TTA TTA ACT GC
VP0985-mCherry- STOP-cw-g	TGGTGGTATGGACGAACACTATACAAATAACATGGAGCCTTTGGCTTT AAGG
VP0985-ins-Prom- AQUA-ccw-h	AGCTCGGTACCCGGGGATCCTCTAGGATGGGCAACGTTCTGGCA
VP0984-ins- Pvpa1548-cw-c	TGCAGTTAATAAAAAGGCTCCTTTAGCACATCGGAAACTAACGC
Pvpa1548- mCherry-Ccw-d	AGTGATAAACTAAGGAGACTAAG
mCherry cw-e	ATGGTTTCTAAAGGTGAAGAAG
mCherry-VP- STOP-ccw-f	TTATTTGTATAGTTCGTCCATA

Plasmid **pPM1** was constructed by PCR amplification of the *vp0464* gene using primers VP0464-1-cw / VP0464-1-ccw and chromosomal DNA from *V. parahaemolyticus* RIMD2210633 as template. The PCR product was digested with BsrGI and SphI and ligated into the equivalent sites of plasmid pMF390 resulting in plasmid pPM1.

Plasmid **pPM17** was constructed by PCR amplification of the *vp3077* gene using primers VP3077-2-cw / VP3077-2-ccw and chromosomal DNA from *V. parahaemolyticus* RIMD2210633 as template. The PCR product was digested with NcoI and XhoI and ligated into the equivalent sites of plasmid pET28b+ resulting in plasmid pPM17.

Plasmid **pPM18** was constructed by PCR amplification of the *vpa1751* gene using primers VPA1751-2-cw / VPA1751-2-ccw and chromosomal DNA from *V. parahaemolyticus* RIMD2210633 as template. The PCR product was digested with NcoI and XhoI and ligated into the equivalent sites of plasmid pET28b+ resulting in plasmid pPM18.

Plasmid **pPM55** was constructed by PCR amplification of the *vp0873* gene using primers VP0873-1-cw / VP0873-1-ccw and chromosomal DNA from *V. parahaemolyticus* RIMD2210633 as template. The PCR product was digested with XbaI and SphI and ligated into the equivalent sites of plasmid pMF390 resulting in plasmid pPM55.

Plasmid pPM75 was constructed by PCR amplification of the *vpa1751-linker* using primers VPA1751-a-cw / vpa 1751 to mCherry-ccw and chromosomal DNA, amplification of mCherry+STOP codon using primers mcherry-cw / mcherry- ccw with STOP and pJH037 as template and amplification of downstream region of *vpa1751* using primers mcherry to downstr. of *vpa1751* / ins-eyfp-C-term-ParB2 ccw and chromosomal DNA from *V. parahaemolyticus* RIMD2210633 as template . The three PCR products were then fused in a fourth PCR reaction using primers VPA1751-a-cw / ins-eyfp-C-term-ParB2 ccw and the products of the previous PCR reactions as templates. The resulted product was digested with XbaI and ligated into the equivalent sites of plasmid pDM4 resulting in plasmid pPM75.

Plasmid **pSM008** was constructed by PCR amplification of the *vp1105* gene using primers VP1105-cw / VP1105-ccw and chromosomal DNA from *V. parahaemolyticus* RIMD2210633 as template. The PCR product was digested with XbaI and SphI and ligated into the equivalent sites of plasmid pMF390 resulting in plasmid pSM008.

Plasmid **pSM57** was constructed by PCR amplification of the *vp0464* gene using primers Y2H FtsZ cw_pGAD / Y2H FtsZ ccw_pGAD and chromosomal DNA from *V. parahaemolyticus* RIMD2210633 as template. The PCR product was mixed with plasmid pGAD424 digested by EcoRI in the presence of SLiCE extract (Zhang et al., 2012) resulting in plasmid pSM57 through Gibson assembly.

Plasmid **pSM58** was constructed by PCR amplification of the *vp0464* gene using primers Y2H FtsZ cw_pGBT9/ Y2H FtsZ ccw_pGBT9 and chromosomal DNA from *V. parahaemolyticus* RIMD2210633 as template. The PCR product was mixed with plasmid

pGBT9 digested by EcoR1 in the presence of SLiCE extract resulting in plasmid pSM58 through Gibson assembly.

Plasmid **pSM59** was constructed by PCR amplification of the *vp2227* gene using primers Y2H ParC cw_pGAD / Y2H ParC ccw_pGAD and chromosomal DNA from *V. parahaemolyticus* RIMD2210633 as template. The PCR product was mixed with plasmid pGAD424 digested by EcoR1 in the presence of SLiCE extract resulting in plasmid pSM59 through Gibson assembly.

Plasmid **pSM60** was constructed by PCR amplification of the *vp2227* gene using primers Y2H ParC cw_pGBT9/ Y2H ParC ccw_pGAD and chromosomal DNA from *V. parahaemolyticus* RIMD2210633 as template. The PCR product was mixed with plasmid pGAD424 digested by EcoR1 in the presence of SLiCE extract resulting in plasmid pSM60 through Gibson assembly.

Plasmid **pSM61** was constructed by PCR amplification of the *vp1105* gene using primers Y2H FtsK cw_pGAD / Y2H FtsK ccw_pGAD and chromosomal DNA from *V. parahaemolyticus* RIMD2210633 as template. The PCR product was mixed with plasmid pGAD424 digested by EcoR1 in the presence of SLiCE extract resulting in plasmid pSM61 through Gibson assembly.

Plasmid **pSM62** was constructed by PCR amplification of the *vp1105* gene using primers Y2H FtsK cw_pGBT9/ Y2H FtsK ccw_pGAD and chromosomal DNA from *V. parahaemolyticus* RIMD2210633 as template. The PCR product was mixed with plasmid pGAD424 digested by EcoR1 in the presence of SLiCE extract resulting in plasmid pSM62 through Gibson assembly.

Plasmid **pPM56** was constructed by PCR amplification of the flanking regions of *vp0872-vp0874* operon using primers vp0872-74del-a / vp0872-74del-b and vp0872-74del-c / vp0872-74del-d and chromosomal DNA from *V. parahaemolyticus* RIMD2210633 as template. The PCR product was digested with XhoI and ligated into the equivalent sites of plasmid pDM4 resulting in plasmid pPM56.

Plasmid **pPM34** was constructed by PCR amplification of the flanking regions of *vp2227* gene using primers vp2227-del-a / vp2227-del-b and vp2227-del-cc / vp2227-del-d , with chromosomal DNA from *V. parahaemolyticus* RIMD2210633 as template and primers vp2227-PM-ins-cw / vp2227-PM-ins-ccw with pSR1084 (plasmid with *vp2227K15Q* point mutation) as template . The final PCR product was digested with XbaI and ligated into the equivalent sites of plasmid pDM4 resulting in plasmid pPM34.

Plasmid **pPM35** was constructed by PCR amplification of the flanking regions of *vp2227* gene using primers *vp2227-del-a* / *vp2227-del-b* and *vp2227-del-cc* / *vp2227-del-d*, with chromosomal DNA from *V. parahaemolyticus* RIMD2210633 as template and primers *vp2227-PM-ins-cw* / *vp2227-PM-ins-ccw* with pSR1089 (plasmid with *vp2227G11V* point mutation) as template. The final PCR product was digested with XbaI and ligated into the equivalent sites of plasmid pDM4 resulting in plasmid pPM35.

Plasmid **pPM068** was constructed by amplification of the flanking regions of gene *vp0180* (*slmA*) using primers *del-vp0180-a* / *del-vp0180-b1* and *del-vp0180-c1* / *del-vp0180-d* and chromosomal DNA from *V. parahaemolyticus* RIMD2210633 as template. In a third PCR reaction the two products were fused using primers *del-vp0180-a* / *del-vp0180-d* and products of the first two PCR reactions as template. The final PCR product was inserted into plasmid pDM4 resulting in plasmid pPM068.

Plasmid **pPM75** was constructed by PCR amplification of the *vpa1751-linker* using primers *VPA1751-a-cw* / *vpa 1751* to mCherry-ccw and chromosomal DNA, amplification of mCherry+STOP codon using primers *mcherry-cw* / *mcherry- ccw* with STOP and pJH037 as template and amplification of downstream region of *vpa1751* using primers *mcherry* to downstr. of *vpa1751* / *ins-eyfp-C-term-ParB2* ccw and chromosomal DNA from *V. parahaemolyticus* RIMD2210633 as template . The three PCR products were then fused in a fourth PCR reaction using primers *VPA1751-a-cw* / *ins-eyfp-C-term-ParB2* ccw and the products of the previous PCR reactions as templates. The resulted product was digested with XbaI and ligated into the equivalent sites of plasmid pDM4 resulting in plasmid pPM75.

Plasmid **pCF048** was constructed by amplification of the intergenic region of gene *vp0984* and *vp0985*, amplification of the promoter region of *vpa1548* (*lafA*) and amplification of *mCherry V. parahaemolyticus* codon optimized sequence. Amplification of the intergenic region of gene *vp0984* and *vp0985* was performed using the pair of primers *VP0984-ins-Prom-AQUA-cw-a* / *ins-Pvpa1548-VP0984* ccw-b and *VP0985-mCherry-STOP-cw-g* / *VP0985-ins-Prom-AQUA-ccw-h*, respectively, and chromosomal DNA from *V. parahaemolyticus* RIMD2210633 as template. Amplification of the promoter region of *vpa1548* (*lafA*) was obtained using the pair of primers *VP0984-ins-Pvpa1548-cw-c* / *Pvpa1548-mCherry-Ccw-d* and chromosomal DNA from *V. parahaemolyticus* RIMD2210633 as template. Amplification of *mCherry V. parahaemolyticus* codon optimized sequence was performed using primers *mCherry cw-e* / *mCherry-VP-STOP-ccw-f*. In a fifth PCR reaction the first product from intergenic region of *vp0984/vp0985* was fused to the promoter of *vpa1548*, using primers *VP0984-ins-Prom AQUA cw-a* /

Pvpa1548-mCherry-Ccw-d and the products of the PCR reactions as template. In a sixth PCR reaction the mCherry product was fused to the second product from intergenic region of *vp0984/vp0985*, using primers mCherry cw-e / VP0985-ins-Prom-AQUA-ccw-h and the products of the PCR reactions as template. In a final PCR reaction the products of both fifth and sixth PCR reactions were fused using primers VP0984-ins-Prom AQUA cw-a VP0985-ins-Prom-AQUA-ccw-h and the products of the fifth and sixth PCR reactions as template. The final PCR product was inserted into plasmid pJH081 (pDM4 derivative) resulting in plasmid pCF041.

4.5. Microscopic methods

4.5.1. Nucleoid staining

100 μ L *V. parahaemolyticus* swimmer cells grown to required OD were incubated with 0.5 μ g/ml 4', 6-diamidino-2-phenylindole (DAPI) for 5 min in the dark with shaking at 37 °C. The swarmer cells grown on HI agar plates were cut out and imprinted on microscopy agarose pad spotted with 10 μ L of 0.05 μ g/ml DAPI and incubated for 2 minutes. Stained samples were then processed for further imaging.

4.5.2. Fluorescent Microscopy

For imaging of swimmer cells five milliliters culture of *V. parahaemolyticus* swimmer cells harboring the relevant plasmid was grown in LB medium to OD₆₀₀ \approx 0.1 at which expression of fluorescent fusion proteins was induced by addition of L-arabinose to a final concentration of 0.2% w/v. The cultures were incubated for an additional 2 hours. Cells were then mounted on 1% agarose in PBS buffer (containing 10% LB medium) on microscope slides, and microscopy was performed. Same conditions were used for time-lapse microscopy.

For imaging of swarmer cells, a culture of swimmer cells was grown in LB to an OD₆₀₀ \approx 0.1 and subsequently spotted on swarm agar additionally supplemented with 0.5% w/v L-arabinose. The plates were then incubated overnight at 24°C. The edge of the swarm colony was excised from the swarm agar, imprinted on 1 % agarose in PBS on microscopy slide and mounted with cover slip.

All the microscopy was performed using Nikon eclipse Ti inverted Andor spinning-disc confocal microscope equipped with a 100x lens and an Andor Zyla sCMOS cooled camera and an Andor FRAPPA system. Microscopy images were analyzed using ImageJ imaging software (<http://rsbweb.nih.gov/ij>) and Metamorph Offline (version 7.7.5.0, Molecular Devices).

FRAP and photoactivation were performed using the Andor FRAPPA system. Cells were treated and mounted on agarose pads as described for time-lapse fluorescence microscopy. For FRAP experiments, areas of interest were bleached with five pulses using a 515-nm laser at 7% intensity. For photoactivation, a point of interest was activated with a 9 second pulse using a 405-nm laser at 9 % intensity.

4.5.3. Image analysis

Images generated using Nikon NIS-Elements AR were first separated into single channels using Fiji/ImageJ 1.49j10 and saved as tiff images. DIC and the corresponding fluorescent channel were loaded in MetaMorph Offline (version 7.7.5.0, Molecular Devices) for analysis. An overlay of both channels was generated and the cells were marked using the Multi-line tool. The regions were then transferred to the fluorescent channel image. Distances of foci from the cell poles in *V. parahaemolyticus* cells were enumerated by hand. These measurements were then plotted in Microsoft Excel.

In generation of demographs the fluorescence intensity profiles of cells were measured in Fiji/ImageJ, version 1.49j10. The generated data was then processed in R (version 3.0.1; (R Development Core Team, 2008)) with a script (Cameron et al., 2014a) that sorts cells by length and normalizes the generated intensity profiles as an average of each cell's fluorescence. The ggplot2 package (version 1.0.0; (Wickham, 2009)) was used to produce the demographs. For demographic analysis three independent experiments were performed and for each experiment the localization pattern of YFP-FtsZ or YFP-ParC was determined in a total of 200-300 cells. The data for each experiment was pooled in generation of the demograph, resulting in the fluorescence profile of a total of 600-900 cells displayed in each demograph.

The distance of division sites to the cell pole was enumerated by hand; the distance of visible invaginations transverse to the cell length in the DIC channel was measured and plotted as a function of cell length.

For calculation of the percentage of cells with distinct FtsZ localization patterns, three independent experiments were performed and for each experiment the localization pattern of FtsZ was determined in a total of 200-300 cells. The average percentage of the three experiments was then calculated for each FtsZ localization pattern and plotted as stacked bar-graphs including error bars depicting the SEM. The percentage of mini-cells in a population was determined the same way.

Swarm colonies for stereomicroscopy was prepared as described above. Stereomicroscopy was carried out using a Leica M205 FA stereomicroscope equipped with a Hamamatsu ORCA-Flash 4.0 digital camera C11440.

In order to measure expression of mCherry from the *lafA* promoter (*PlafA*), the gene encoding mCherry was translationally fused to *PlafA*. The fusion construct was then integrated into the intergenic region between *vp0984* and *vp0985* on the *V. parahaemolyticus* chromosome, resulting in strain CF31 (*PlafA::mCherry*). CF31 cells from swarm-colony flares or planktonic cells from liquid culture (grown in LB to OD600 ~ 0.5) were then analyzed by fluorescence microscopy to test for expression of mCherry protein. The average fluorescence intensity of swarmer and planktonic cells was then measured and correlated with cell length. The average intensity was plotted with error bars indicating the standard-error-mean (SEM).

For the analysis of localization of ParB1 and ParB2, images generated using Nikon NIS-Elements AR and Zeiss Axio Imager were first separated into single channels using Fiji/ImageJ 1.49j10 and saved as tiff images. DIC and the corresponding fluorescent channel were loaded in MetaMorph Offline (version 7.7.5.0, Molecular Devices) for analysis. An overlay of both channels was generated and the cells were marked using the Multi-line tool. The regions were then transferred to the fluorescent channel image. Distances of foci from the cell poles in *V. parahaemolyticus* cells were enumerated by hand. These measurements were sorted on increasing cell lengths. The average position of each foci for every 0.5 μ m of the cell lengths were calculated and the distance of foci from the cell pole were plotted as a function of cell length in Microsoft Excel.

To plot the number of ParB1 and ParB2 foci as a function of cell length, the total number of foci in each cell were counted and plotted against corresponding cell lengths in Microsoft Excel.

4.5.4. Transmission Electron Microscopy

Transmission electron microscopy (TEM) was performed to check the mini-cell formation in *V. parahaemolyticus* deletion strains in comparison to wildtype. The cells of interest were mounted on an electron microscopy (EM) grid, fixed and stained using the negative stain method with uranyl acetate. In brief, uranyl acetate stock solution was prepared by solving 4 % (w/v) uranyl acetate in ddH₂O. This solution was diluted to 2 % with ddH₂O. 2 % uranyl acetate solution was spun down prior to usage for 10 min at 20000 g at room temperature. Uranyl acetate solution was stored at room temperature in the dark for several months. For fixation and negative staining of the cells, 10 μ L of the culture was

mounted on a charged EM grid and incubated for 3 minutes. The excess liquid was blotted out from the grid by touching the grid vertically on a Whatman paper. Grid was washed twice with ddH₂O and once with 1 % Uranyl acetate solution with the same technique. Then 10 μ L of 1% uranyl acetate was applied on the grid for 1 minutes and dried by blotting. This was then followed by washing with ddH₂O and subsequent drying. The finished grids were stored in a grid holder for several months at room temperature. Electron microscopy was performed with a JEM-1400 Plus (Jeol).

4.6. Biochemical methods

4.6.1. Protein detection

SDS-PAGE (SDS-Polyacrylamide gel electrophoresis) was used for the separation of proteins (Laemmli, 1970). Protein samples of cell lysates were obtained as follows: *V. parahaemolyticus* cells were harvested at 9000 rpm and 4 °C for 10 min. The cells were then resuspended in 2 \times SDS (sodium dodecyl sulphate) sample buffer. The suspension was then heated at 95 °C for 10 minutes. Protein samples from biochemical assays were diluted with SDS sample buffer and heated at 95 °C for 10 min. Protein samples were then loaded to an SDS gel consisting of a 5% stacking gel and 11% resolving gel (Table 11), along with a molecular mass marker (Color Prestained Protein Standard Broad Range, NewEngland BioLabs). Proteins were separated at 150-165V in SDS running buffer (TGS buffer from Bio-Rad), using a Bio-Rad MiniPROTEAN 3 Cell or MiniPROTEAN TetraCell. Proteins separated by SDS-PAGE were stained with Instant Blue™ (Expedeon, UK) for 10 minutes. The composition for the buffers used for SDS-PAGE are listed in Table 12.

Table 11: Composition of SDS-PAGE gels.

Reagents	11% Resolving gel (10mL)	5% Stacking gel (5mL)
Resolving gel buffer	3.8mL	-
Stacking gel buffer	-	2.8mL
30% Acrylamide	2.5mL	1.25mL
ddH ₂ O	3.7mL	825 μ L
TEMED	80 μ L	50 μ L
10% APS	6 μ L	3.75 μ L

Table 12: Composition of SDS-PAGE buffers.

Buffer	Composition
Resolving gel buffer	1.5M Tris-HCl pH 8.8 0.4% (w/v) SDS
Stacking gel buffer	1.5M Tris-HCl pH 6.8

2x SDS sample buffer	0.4% (w/v) SDS 120mM Tris pH 6.8 20% (w/v) glycerol 4% (w/v) SDS 0.02% bromophenol blue
----------------------	---

4.6.2. Immunoblot analysis

Immunoblot analysis was performed to detect proteins of interest with specific antibodies. First proteins from cell lysates or samples from biochemical assays were separated by SDS-PAGE as described earlier. Proteins were transferred to a methanol-activated 0.2 μ m PVDF membrane (GE healthcare Europe GmbH) using the semi-dry Trans-Blot Turbo™ Transfer System (BioRad, München) with a buffer containing 300 mM glycine and 300 mM Tris base with a pH around 9-10. Transfer was performed using 1.3 A, 25 V for 7 minutes.

Membranes were transferred into a clean plastic container and blocked for 1 hour shaking at room temperature in 5 % dried non-fat milk powder (w/v) in 1xTBST (50 mM Tris-HCl pH 7.5; 150 mM NaCl, 0.1% (v/v) Tween20). After blocking the membrane, primary antibody was added to the blot in 1 % dried non-fat milk powder (w/v) prepared in 1 x TBS at the corresponding dilution (Table 13) and incubated overnight, shaking at 4 °C. After washing 3 times with 1x TBST (50 mM Tris-HCl pH 7.5; 150 mM NaCl; 0.1 % (v/v) Tween20) the horseradish peroxidase-coupled α -rabbit/ α -mouse immunoglobulin G secondary antibody was applied to the blot at a given dilution in 1% dried non-fat milk powder (w/v) in 1x TBS for 1 hour at room-temperature shaking. The membrane was washed again thrice with 1x TBST.

The blot was then developed with the Luminata™ Forte Western HRP Substrate (Millipore Merck, Schwalbach) and visualized with the luminescent image analyzer LAS-4000 (Fujifilm, Düsseldorf). FtsZ specific primary antibodies was produced by Eurogentec (Seraing, Belgium), using rabbits as production host and YFP specific antibody was from Clotech.

Table 13: Antibodies used for immunoblot analysis

Antibodies	Dilution
α -FtsZ	1:25,000
α -YFP (JL-8)	1:4,000
Goat α -rabbit IgG	1:15,000
Sheep α -mouse IgG	1:10,000

4.6.3. Protein purification of ParB1 and ParB2

C-terminal 6HIS tagged ParB1 and ParB2 were purified from pPM17 and pPM18 respectively. Both ParB1 and ParB2 were expressed individually in BL21 λ DE3-RIL cells grown in 100mL LB with 50 μ g/mL Kanamycin and 34 μ g/mL Chloramphenicol at 37°C and incubated to an OD of 0.5. Expression was induced by adding IPTG to 0.5mM and growing the cells at 37°C for 2hours. The harvested cells were pelleted and resuspended in 30mL lysis buffer (300mM KCl, 50mM KH_2PO_4 , 5mM imidazol, 3mM DTT, pH=7.5) and lysed by French press. The resulting extract was centrifuged to pellet cell debris and membranes. The clarified supernatant was then loaded onto 1mL Bio-scale Mini Profinity IMAC cartridge (Biorad) in PROFINIA-system (Biorad). The column was washed with 6mL wash buffer (300mM KCl, 50mM KH_2PO_4 , 10mM imidazol, 3mM DTT, pH=7.5) and eluted in 4mL elution buffer (300mM KCl, 50mM KH_2PO_4 , 250mM imidazol, 3mM DTT, pH=7.5). The elute was then dialyzed into 100mM Tris, 250mM NaCl, 1mM MgCl_2 , 10% Glycerol, 250mM KCl, 3mM DTT, pH=7.5 at 4°C.

4.6.4. Electron Mobility Shift Assay

Cy3- and Cy5-endlabelled PCR fragments were used throughout and were obtained by using either a 5'-Cy3 or 5'Cy5 end labelled oligonucleotide in a PCR reaction with additional oligonucleotide designed to obtain the construct of interest. The reaction mixture containing water, salmon sperm DNA, reaction buffer (100mM Tris, 250mM NaCl, 1mM MgCl_2 , 10% Glycerol, 250mM KCl, 3mM DTT, pH=7.5), purified DNA and varying concentrations of proteins (0 μ M to 5.6 μ M) were incubated for 15 minutes at room temperature. After incubation, glycerol was added to a concentration of 5% and reactions were analyzed by electrophoresis on a 0.5X TBE, 5% polyacrylamide gel in 1X TBE buffer (0.89M Tris-base, 0.89M boric acid, 0.02 M EDTA, pH 8.3) at 125V for 2 hours. A concentration of 5nM DNA fragments were used throughout. The gel was scanned on a Typhoon Trio instrument.

4.6.5. Co-Immunoprecipitation

V. parahaemolyticus cells harboring the required plasmids for expression of YFP, YFP-FtsZ, and YFP-ParC respectively, were grown to an OD600 of 1.0 at 37°C in 200mL LB containing Chloramphenicol at 5 μ g/mL and 0.2 % w/v L-arabinose. Subsequently, 2% formaldehyde was added to the cultures, which were incubated additional 50 minutes at 30°C. This was followed by an addition of Glycine to a final concentration of 0.2M (Glycine stock solution of 2 M) and the cultures were incubated additional 15 minutes. One milliliter of each was then collected to check for induction of tagged proteins. The rest of the

cultures were harvested, washed twice with cold PBS and subsequently resuspended in 10mL lysis buffer (50mM Tris-HCl, 50mM KCl, pH = 8.0). The cells were disrupted by bead beating. The lysed samples were further centrifuged at 8000 rpm for 20 minutes and the supernatant was collected. Subsequently, 100 μ L of GFP-Trap beads (Chromotek), equilibrated in lysis buffer was added to the supernatant of each sample, which were then incubated at 4°C overnight. Beads were collected by centrifugation at 8000 rpm for 15 minutes at 4°C, washed twice with 1 mL cold lysis buffer and resuspended in 50 μ L of lysis buffer and 50 μ L of 2 \times SDS sample loading buffer. The samples were boiled at 95°C for 10minutes and centrifuged. The supernatants were used for SDS-PAGE and subsequent western blotting.

4.6.6. Liquid Chromatography-Mass Spectrometry (LC-MS)

Sample preparation for LC-MS

Planktonic cells were grown in 20 mL LB to an OD600 of 0.6. To perform aztreonam treatment, planktonic cells were grown to an OD600 of 0.5 and aztreonam was added to a final concentration of 60 μ g/mL and cell were incubated for an additional hour at 37 °C. Cells were then harvested. The swarmer cells from swarm flares were collected by flushing the periphery of the swarm colony with water. Subsequently the liquid was collected and swarmer cells harvested by centrifugation. The cell pellets from all samples were washed with water. The final pellet was then resuspended in lysis buffer (1 % Sodium lauryl sulphate in 0.1 M NH_4HCO_3) and boiled for 5 minutes. Following ultrasonification (2x20 seconds) and a short centrifugation spin, the samples were incubated at 90 °C and shaking for 15 minutes. A 40X dilution of Tris carboxyethyl phosphine (TCEP) was added to the sample and incubated again at 90 °C and shaking for 15 minutes. After cooling down, a 40X dilution of 0.1M Iodoacetamide were added to the sample followed at incubation in dark for 40 minutes. The protein concentration of the samples were then determined by performing a BCA assay. Samples equivalent to 50 μ g of protein were digested with trypsin in presence of 1 % SLS overnight at 30 °C. Following digestion, the SLS was precipitated out adding TFA (Trifluoroacetic acid) to a final concentration of 1.5 % and C-18 purification of peptides was performed to concentrate and desalt the samples. The C18 columns were equilibrated in 300 μ l 100 % Acetonitrile, followed by 300 μ l 0.1 % TFA. The samples were then loaded and bound to these columns. Following two washes with wash buffer (5 % acetonitrile (v/v), 0.1% TFA (v/v)), the peptides were eluted in 300 μ L elution buffer 4 (50 % acetonitrile (v/v), 0.1 % TFA (v/v)) and concentrated in a vacuum press. Finally, the peptides were dissolved in 100 μ L 0.1 % TFA. These peptide samples were then analyzed by LC-MS.

Quantification of protein level using liquid chromatography-mass spectrometry (LC-MS)

LC-MS and data analysis was carried out as described previously (Glatter et al., 2015; Yuan et al., 2017), with the following modifications. For each strain three or four biological samples were analyzed. Purified peptides were analyzed using liquid-chromatography-mass spectrometry (LC-MS) carried out on a Q-Exactive Plus instrument connected to an Ultimate 3000 RSLC nano and a nanospray flex ion source (all Thermo Scientific). Peptide separation was performed on a reverse phase HPLC column (75 μm x 42 cm) packed in-house with C18 resin (2.4 μm ; Dr. Maisch). The following separating gradient was used: 98% solvent A (0.15% formic acid) and 2% solvent B (99.85% acetonitrile, 0.15% formic acid) to 32% solvent B over 60 minutes at a flow rate of 300 nl/min. For label-free quantification (LFQ) the raw data was loaded into Progenesis (Version 2.0, Nonlinear Dynamics) and exported mgf files searched by MASCOT (Version 2.5, Matrix Science) using the uniprot database for *V. parahaemolyticus*. Progenesis peptide measurement exports were then further evaluated using SafeQuant (SQ) and LFQ values from the SQ output were used to determine protein abundance changes.

REFERENCES

- Aarsman, M. E. G., Piette, A., Fraipont, C., Vinkenvleugel, T. M. F., Nguyen-Distèche, M., & Den Blaauwen, T. (2005). Maturation of the *Escherichia coli* divisome occurs in two steps. *Molecular Microbiology*, *55*(6), 1631–1645. <https://doi.org/10.1111/j.1365-2958.2005.04502.x>
- Adams, D. W., Juan Wu, L., & Errington, J. (2015). Nucleoid occlusion protein Noc recruits DNA to the bacterial cell membrane. *The EMBO Journal*, *34*(4), 491–501. <https://doi.org/10.15252/embj>
- Addinall, S. G., Cao, C., & Lutkenhaus, J. (1997). FtsN, a late recruit to the septum in *Escherichia coli*. *Molecular Microbiology*, *25*(2), 303–309. <https://doi.org/10.1046/j.1365-2958.1997.4641833.x>
- Alberti, L., & Harshey, R. M. (1990). Differentiation of *Serratia marcescens* 274 into swimmer and swarmer cells. *Journal of Bacteriology*, *172*(8), 4322–4328. <https://doi.org/10.1128/jb.172.8.4322-4328.1990>
- Alvarado, A., Kjæ, A., Yang, W., Mann, P., Briegel, A., Waldor, M. K., & Ringgaard, S. (2017). Coupling chemosensory array formation and localization. *eLife*, *6*, 1–29. <https://doi.org/10.7554/eLife.31058>
- Arjes, H. A., Kriel, A., Sorto, N. A., Shaw, J. T., Wang, J. D., & Levin, P. A. (2014). Failsafe mechanisms couple division and DNA replication in bacteria. *Current Biology*, *24*(18), 2149–2155. <https://doi.org/10.1016/j.cub.2014.07.055>
- Ausubel, F. M., Brent, R., Kingston, R. E., Moore, D. D., Seidman, J. G., Smith, J. a, & Struhl, K. (2002). *Short Protocols in Molecular Biology*. Wiley (Vol. 1&2). <https://doi.org/10.1002/mrd.1080010210>
- Baumann, P., & Baumann, L. (1977). Biology of the marine Enterobacteria: Genera *Beneckea* and *Photobacterium*.
- Begg, K. J., Dewar, S. J., & Donachie, W. D. (1995). A new *E. coli* cell division gene, *ftsK*. *J. Bacteriol.*, *177*(21), 6211–6222.
- Beilharz, K., Novakova, L., Fadda, D., Branny, P., Massidda, O., & Veening, J.-W. (2012). Control of cell division in *Streptococcus pneumoniae* by the conserved Ser/Thr protein kinase StkP. *Proceedings of the National Academy of Sciences*, *109*(15), E905–E913. <https://doi.org/10.1073/pnas.1119172109>
- Belas, R., Simon, M., & Silverman, M. (1986). Regulation of Lateral Flagella Gene-Transcription in *Vibrio parahaemolyticus*. *J Bacteriol*, *167*(1), 210–218. Retrieved from <http://jb.asm.org/content/167/1/210.full.pdf>
- Bernhardt, T. G., & De Boer, P. A. J. (2004). Screening for synthetic lethal mutants in *Escherichia coli* and identification of EnvC (YibP) as a periplasmic septal ring factor with murein hydrolase activity. *Molecular Microbiology*, *52*(5), 1255–1269. <https://doi.org/10.1111/j.1365-2958.2004.04063.x>
- Bernhardt, T. G., & De Boer, P. A. J. (2005). SlmA, a nucleoid-associated, FtsZ binding protein required for blocking septal ring assembly over chromosomes in *E. coli*. *Molecular Cell*, *18*(5), 555–564. <https://doi.org/10.1016/j.molcel.2005.04.012>
- Bi, E. F., & Lutkenhaus, J. (1991). FtsZ ring structure associated with division in *Escherichia coli*. *Nature*, *354*(6349), 161–164. <https://doi.org/10.1038/354161a0>
- Bigot, S., Saleh, O. A., Lesterlin, C., Pages, C., El Karoui, M., Dennis, C., ... Cornet, F. (2005). KOPS: DNA motifs that control *E. coli* chromosome segregation by orienting the FtsK translocase. *EMBO Journal*, *24*(21), 3770–3780. <https://doi.org/10.1038/sj.emboj.7600835>
- Bisson Filho, A. W., Hsu, Y.-P., Squyres, G., Kuru, E., Wu, F., Jukes, C., ... Garner, E. (2016). Treadmilling by FtsZ filaments drives peptidoglycan synthesis and bacterial cell division. *Science*. <https://doi.org/10.1101/077560>
- Böttcher, T., Elliott, H. L., & Clardy, J. (2016). Dynamics of snake-like swarming behavior of *Vibrio alginolyticus*. *Biophysical Journal*, *110*(4), 981–992. <https://doi.org/10.1016/j.bpj.2015.12.037>
- Bowman, G. R., Comolli, L. R., Gaietta, G. M., Fero, M., Hong, S. H., Jones, Y., ... Shapiro, L. (2010). *Caulobacter* PopZ forms a polar subdomain dictating sequential changes in pole composition and function. *Molecular Microbiology*, *76*(1), 173–189. <https://doi.org/10.1111/j.1365-2958.2010.07088.x>
- Bramkamp, M., Emmins, R., Weston, L., Donovan, C., Daniel, R. A., & Errington, J. (2008). A novel component of the division-site selection system of *Bacillus subtilis* and a new mode of action for the division inhibitor MinCD. *Molecular Microbiology*, *70*(6), 1556–1569. <https://doi.org/DOI.10.1111/j.1365-2958.2008.06501.x>

- Buske, P. J., & Levin, P. A. (2013). A flexible C-terminal linker is required for proper FtsZ assembly in vitro and cytokinetic ring formation in vivo. *Molecular Microbiology*, *89*(2), 249–263. <https://doi.org/10.1111/mmi.12272>
- Bussiere, D. E., & Bastia, D. (1999). Termination of DNA replication of bacterial and plasmid chromosomes. *Molecular Microbiology*, *31*(6), 1611–1618. <https://doi.org/10.1046/j.1365-2958.1999.01287.x>
- Cameron, T. A., Anderson-Furgeson, J., Zupan, J. R., Zik, J. J., & Zambryski, P. C. (2014a). Peptidoglycan synthesis machinery in *Agrobacterium tumefaciens* during unipolar growth and cell division. *mBio*, *5*(3), e01219-14. <https://doi.org/10.1128/mBio.01219-14>
- Cameron, T. A., Anderson-Furgeson, J., Zupan, J. R., Zik, J. J., & Zambryski, P. C. (2014b). Peptidoglycan synthesis machinery in *Agrobacterium tumefaciens* during unipolar growth and cell division. *mBio*, *5*(3), e01219-14. <https://doi.org/10.1128/mBio.01219-14>
- Caspi, Y., & Dekker, C. (2016). Mapping out min protein patterns in fully confined fluidic chambers. *eLife*, *5*(e19271), 1–27. <https://doi.org/10.7554/eLife.19271>
- Castillo, D. E., Yang, D., Siopsis, G., & Männik, J. (2016). The role of MatP, ZapA and ZapB in chromosomal organization and dynamics in *Escherichia coli*. *Nucleic Acids Research*, *44*(3), 1216–1226. <https://doi.org/10.1093/nar/gkv1484>
- Cho, H., McManus, H. R., Dove, S. L., & Bernhardt, T. G. (2011a). Nucleoid occlusion factor SlmA is a DNA-activated FtsZ polymerization antagonist. *Proceedings of the National Academy of Sciences*, *108*(9), 3773–3778. <https://doi.org/10.1073/pnas.1018674108>
- Cho, H., McManus, H. R., Dove, S. L., & Bernhardt, T. G. (2011b). Nucleoid occlusion factor SlmA is a DNA-activated FtsZ polymerization antagonist. *Proceedings of the National Academy of Sciences*, *108*(9), 3773–3778. <https://doi.org/10.1073/pnas.1018674108>
- Coltharp, C., Buss, J., Plumer, T. M., & Xiao, J. (2016). Defining the rate-limiting processes of bacterial cytokinesis. *Proceedings of the National Academy of Sciences*, *113*(8), E1044–E1053. <https://doi.org/10.1073/pnas.1514296113>
- Dai, K., & Lutkenhaus, J. (1992). The proper ratio of FtsZ to FtsA is required for cell division to occur in *Escherichia coli*. *Journal of Bacteriology*, *174*(19), 6145–6151.
- Dajkovic, A., Lan, G., Sun, S. X., Wirtz, D., & Lutkenhaus, J. (2008). MinC spatially controls bacterial cytokinesis by antagonizing the scaffolding function of FtsZ. *Current Biology*, *18*(4), 235–244. <https://doi.org/DOI 10.1016/j.cub.2008.01.042>
- David, A., Demarre, G., Muresan, L., Paly, E., Barre, F. X., & Possoz, C. (2014). The Two Cis-Acting Sites, parS1 and oriC1, Contribute to the Longitudinal Organisation of *Vibrio cholerae* Chromosome I. *PLoS Genetics*, *10*(7). <https://doi.org/10.1371/journal.pgen.1004448>
- de Boer, P. A. J., Crossley, R. E., & Rothfield, L. I. (1989). A division inhibitor and a topological specificity factor coded for by the minicell locus determine proper placement of the division septum in *E. coli*. *Cell*, *56*(4), 641–649. [https://doi.org/10.1016/0092-8674\(89\)90586-2](https://doi.org/10.1016/0092-8674(89)90586-2)
- De Boer, P., Crossley, R., & Rothfield, L. (1992). The essential bacterial cell-division protein FtsZ is a GTPase. *Nature*, *359*(6392), 254–256. <https://doi.org/10.1038/359254a0>
- Demarre, G., Galli, E., Muresan, L., Paly, E., David, A., Possoz, C., & Barre, F. X. (2014). Differential Management of the Replication Terminus Regions of the Two *Vibrio cholerae* Chromosomes during Cell Division. *Plos Genetics*, *10*(9). <https://doi.org/ARTN e1004557DOI 10.1371/journal.pgen.1004557>
- Denk, J., Kretschmer, S., Halatek, J., Hartl, C., Schwille, P., & Frey, E. (2018). MinE conformational switching confers robustness on self-organized Min protein patterns. *Proceedings of the National Academy of Sciences*, *115*(18), 201719801. <https://doi.org/10.1073/pnas.1719801115>
- Din, N., Quardokus, E. M., Sackett, M. J., & Brun, Y. V. (1998). Dominant C-terminal deletions of FtsZ that affect its ability to localize in *Caulobacter* and its interaction with FtsA. *Molecular Microbiology*, *27*(5), 1051–1063. <https://doi.org/10.1046/j.1365-2958.1998.00752.x>
- Donachie, W. D., & Begg, K. J. (1970). Growth of the Bacterial Cell. *Nature*, *227*, 561.
- Donnenberg, M. S., & Kaper, J. B. (1991). Construction of an *ea*e deletion mutant of enteropathogenic *Escherichia coli* by using a positive-selection suicide vector. *J Bacteriol*, *59*(12), 4310–4317.
- Dryselius, R., Izutsu, K., Honda, T., & Iida, T. (2008). Differential replication dynamics for large and small *Vibrio* chromosomes affect gene dosage, expression and location. *BMC Genomics*, *9*, 1–16.

<https://doi.org/10.1186/1471-2164-9-559>

- Du, S., & Lutkenhaus, J. (2014). SlmA Antagonism of FtsZ Assembly Employs a Two-pronged Mechanism like MinCD. *PLoS Genetics*, *10*(7). <https://doi.org/10.1371/journal.pgen.1004460>
- Duderstadt, K. E., Mott, M. L., Crisona, N. J., Chuang, K., Yang, H., & Berger, J. M. (2010). Origin remodeling and opening in bacteria rely on distinct assembly states of the DnaA initiator. *Journal of Biological Chemistry*, *285*(36), 28229–28239. <https://doi.org/10.1074/jbc.M110.147975>
- Duman, R., Ishikawa, S., Celik, I., Strahl, H., Ogasawara, N., Troc, P., ... Hamoen, L. W. (2013). Structural and genetic analyses reveal the protein SepF as a new membrane anchor for the Z ring. *Proceedings of the National Academy of Sciences*, *110*(48), E4601–E4610. <https://doi.org/10.1073/pnas.1313978110>
- Durand-Heredia, J. M., Yu, H. H., De Carlo, S., Lesser, C. F., & Janakiraman, A. (2011). Identification and characterization of ZapC, a stabilizer of the FtsZ ring in Escherichia coli. *Journal of Bacteriology*, *193*(6), 1405–1413. <https://doi.org/10.1128/JB.01258-10>
- Ebersbach, G., Briegel, A., Jensen, G. J., & Jacobs-Wagner, C. (2008). A Self-Associating Protein Critical for Chromosome Attachment, Division, and Polar Organization in Caulobacter. *Cell*, *134*(6), 956–968. <https://doi.org/10.1016/j.cell.2008.07.016>
- Edwards, D. H., Thomaidis, H. B., & Errington, J. (2000). Promiscuous targeting of Bacillus subtilis cell division protein DivIVA to division sites in Escherichia coli and fission yeast. *The EMBO Journal*, *19*(11), 2719–2727. <https://doi.org/10.1093/emboj/19.11.2719>
- Egea-Cortines, M., Saedler, H., & Sommer, H. (1999). Ternary complex formation between the MADS-box proteins SQUAMOSA, DEFICIENS and GLOBOSA is involved in the control of floral architecture in *Antirrhinum majus*. *EMBO Journal*, *18*(19), 5370–5379. <https://doi.org/10.1093/emboj/18.19.5370>
- Erickson, H. P. (1995). FtsZ, a prokaryotic homolog of tubulin? *Cell*, *80*(3), 367–370. [https://doi.org/10.1016/0092-8674\(95\)90486-7](https://doi.org/10.1016/0092-8674(95)90486-7)
- Espeli, O., Borne, R., Dupaigne, P., Thiel, A., Gigant, E., Mercier, R., & Boccard, F. (2012). A MatP-divisome interaction coordinates chromosome segregation with cell division in E. coli. *EMBO Journal*, *31*(14), 3198–3211. <https://doi.org/10.1038/emboj.2012.128>
- Espinosa, E., Barre, F.-X., & Galli, E. (2017). Coordination between replication, segregation and cell division in multi-chromosomal bacteria: lessons from *Vibrio cholerae*. *International Microbiology*, *20*(3), 121–129. <https://doi.org/10.2436/20.1501.01.293>
- Eswaramoorthy, P., Erb, M. L., Gregory, J. A., Silverman, J., Pogliano, K., Pogliano, J., & Ramamurthi, K. S. (2011). Cellular architecture mediates DivIVA ultrastructure and regulates min activity in Bacillus subtilis. *mBio*, *2*(6), 1–9. <https://doi.org/10.1128/mBio.00257-11>
- Fiebig, A., Keren, K., & Theriot, J. A. (2006). Fine-scale time-lapse analysis of the biphasic, dynamic behaviour of the two Vibrio cholerae chromosomes. *Molecular Microbiology*, *60*(5), 1164–1178. <https://doi.org/10.1111/j.1365-2958.2006.05175.x>
- Fleurie, A., Lesterlin, C., Manuse, S., Zhao, C., Cluzel, C., Lavergne, J.-P., ... Grangeasse, C. (2014). MapZ marks the division sites and positions FtsZ rings in Streptococcus pneumoniae. *Nature*, *516*(7530), 259–262. <https://doi.org/10.1038/nature13966>
- Fogel, M. A., & Waldor, M. K. (2005). Distinct segregation dynamics of the two Vibrio cholerae chromosomes. *Molecular Microbiology*, *55*(1), 125–136. <https://doi.org/10.1111/j.1365-2958.2004.04379.x>
- Fogel, M. A., & Waldor, M. K. (2006). A dynamic, mitotic-like mechanism for bacterial chromosome segregation. *Genes and Development*, *20*(23), 3269–3282. <https://doi.org/10.1101/gad.1496506>
- Frey, E., Halatek, J., Kretschmer, S., & Schwille, P. (2018). Protein Pattern Formation, 1–17. Retrieved from <http://arxiv.org/abs/1801.01365>
- Fu, X., Shih, Y. L., Zhang, Y., & Rothfield, L. I. (2001). The MinE ring required for proper placement of the division site is a mobile structure that changes its cellular location during the Escherichia coli division cycle. *Proceedings of the National Academy of Sciences of the United States of America*, *98*(3), 980–985. <https://doi.org/10.1073/pnas.98.3.980>
- Galli, E., Paly, E., & Barre, F.-X. (2017). Late assembly of the Vibrio cholerae cell division machinery postpones septation to the last 10% of the cell cycle. *Scientific Reports*, *7*(February), 44505. <https://doi.org/10.1038/srep44505>

- Galli, E., Poidevin, M., Le Bars, R., Desfontaines, J.-M., Muresan, L., Paly, E., ... Barre, F.-X. (2016a). Cell division licensing in the multi-chromosomal *Vibrio cholerae* bacterium. *Nature Microbiology*, *1*(9), 16094. <https://doi.org/10.1038/nmicrobiol.2016.94>
- Galli, E., Poidevin, M., Le Bars, R., Desfontaines, J.-M., Muresan, L., Paly, E., ... Barre, F.-X. (2016b). Cell division licensing in the multi-chromosomal *Vibrio cholerae* bacterium. *Nature Microbiology*, *1*(9), 16094. <https://doi.org/10.1038/nmicrobiol.2016.94>
- Gamba, P., Veening, J. W., Saunders, N. J., Hamoen, L. W., & Daniel, R. A. (2009). Two-step assembly dynamics of the *Bacillus subtilis* divisome. *Journal of Bacteriology*, *191*(13), 4186–4194. <https://doi.org/10.1128/JB.01758-08>
- Gerdes, K., Howard, M., & Szardenings, F. (2010). Pushing and pulling in prokaryotic DNA segregation. *Cell*, *141*(6), 927–942. <https://doi.org/10.1016/j.cell.2010.05.033>
- Gerding, M. A., Liu, B., Bendezú, F. O., Hale, C. A., Bernhardt, T. G., & De Boer, P. A. J. (2009). Self-enhanced accumulation of FtsN at division sites and roles for other proteins with a SPOR domain (DamX, DedD, and RlpA) in *Escherichia coli* cell constriction. *Journal of Bacteriology*, *191*(24), 7383–7401. <https://doi.org/10.1128/JB.00811-09>
- Gilpin, R. W., & Nagy, S. S. (1976). Time-Lapse Photography of *Bacillus subtilis* L-Forms Replicating in Liquid Medium Time-Lapse Photography of *Bacillus subtilis* L-Forms Replicating in Liquid Medium, *127*(2), 1018–1021.
- Glatter, T., Ahrné, E., & Schmidt, A. (2015). Comparison of different sample preparation protocols reveals lysis buffer-specific extraction biases in gram-negative bacteria and human cells. *Journal of Proteome Research*, *14*(11), 4472–4485. <https://doi.org/10.1021/acs.jproteome.5b00654>
- Gode-Potratz, C. J., Kustus, R. J., Breheny, P. J., Weiss, D. S., & McCarter, L. L. (2011). Surface sensing in *Vibrio parahaemolyticus* triggers a programme of gene expression that promotes colonization and virulence. *Molecular Microbiology*, *79*(1), 240–263. <https://doi.org/10.1111/j.1365-2958.2010.07445.x>
- Green, M. ., & Sambrook D.W., J. (2012). *Molecular Cloning: A laboratory manual* (Fourth Edition).
- Gregory, J. A., Becker, E. C., & Pogliano, K. (2008). *Bacillus subtilis* MinC destabilizes FtsZ-rings at new cell poles and contributes to the timing of cell division. *Genes Dev*, *22*(24), 3475–3488. <https://doi.org/10.1101/Gad.1732408>
- Gruber, S., & Errington, J. (2009). Recruitment of Condensin to Replication Origin Regions by ParB/SpoOJ Promotes Chromosome Segregation in *B. subtilis*. *Cell*, *137*(4), 685–696. <https://doi.org/10.1016/j.cell.2009.02.035>
- Gueiros-filho, F. J., & Losick, R. (2002). Assembly of the tubulin-like protein FtsZ A widely conserved bacterial cell division protein that promotes assembly of the tubulin-like protein FtsZ. *Genes & Development*, *25*44–2556. <https://doi.org/10.1101/gad.1014102>
- Guzman, L., Belin, D., Carson, M. J., & Beckwith, J. (1995). Tight regulation, modulation, and high-level expression by vectors containing the arabinose PBAD promoter. *J Bacteriol*, *177*(14), 4121–4130.
- Hale, C. A., & De Boer, P. A. J. (1997). Direct binding of FtsZ to ZipA, an essential component of the septal ring structure that mediates cell division in *E. coli*. *Cell*, *88*(2), 175–185. [https://doi.org/10.1016/S0092-8674\(00\)81838-3](https://doi.org/10.1016/S0092-8674(00)81838-3)
- Hale, C. A., Shiomi, D., Liu, B., Bernhardt, T. G., Margolin, W., Niki, H., & De Boer, P. A. J. (2011). Identification of *Escherichia coli* ZapC (YcbW) as a component of the division apparatus that binds and bundles FtsZ polymers. *Journal of Bacteriology*, *193*(6), 1393–1404. <https://doi.org/10.1128/JB.01245-10>
- Harms, A., Treuner-Lange, A., Schumacher, D., & Søgaard-Andersen, L. (2013). Tracking of Chromosome and Replisome Dynamics in *Myxococcus xanthus* Reveals a Novel Chromosome Arrangement. *PLoS Genetics*, *9*(9), 19–23. <https://doi.org/10.1371/journal.pgen.1003802>
- Harshey, R. M. (1994). Bees aren't the only ones: swarming in gram-negative bacteria. *Mol Microbiol*, *13*(3), 389–394. Retrieved from <http://www.ncbi.nlm.nih.gov/pubmed/7997156>
- Hatano, T., Yamaichi, Y., & Niki, H. (2007). Oscillating focus of SopA associated with filamentous structure guides partitioning of F plasmid. *Molecular Microbiology*, *64*(5), 1198–1213. <https://doi.org/10.1111/j.1365-2958.2007.05728.x>
- Heering, J., Alvarado, A., & Ringgaard, S. (2017). Induction of Cellular Differentiation and Single Cell Imaging of *Vibrio parahaemolyticus* Swimmer and Swarmer Cells. *Journal of Visualized Experiments*,

e55842(123), 1–8. <https://doi.org/10.3791/55842>

- Heering, J., & Ringgaard, S. (2016). Differential localization of chemotactic signaling arrays during the lifecycle of *Vibrio parahaemolyticus*. *Frontiers in Microbiology*, 7(NOV), 1–12. <https://doi.org/10.3389/fmicb.2016.01767>
- Holečková, N., Doubravová, L., Massidda, O., Molle, V., Buriánková, K., Benada, O., ... Branny, P. (2014). LocZ is a new cell division protein involved in proper septum placement in *Streptococcus pneumoniae*. *mBio*, 6(1), 1–13. <https://doi.org/10.1128/mBio.01700-14>
- Hu, Z. L., Mukherjee, A., Pichoff, S., & Lutkenhaus, J. (1999). The MinC component of the division site selection system in *Escherichia coli* interacts with FtsZ to prevent polymerization. *Proceedings of the National Academy of Sciences of the United States of America*, 96(26), 14819–14824. <https://doi.org/DOI.10.1073/pnas.96.26.14819>
- Hu, Z., & Lutkenhaus, J. (2000). Analysis of MinC reveals two independent domains involved in interaction with MinD and FtsZ. *Journal of Bacteriology*, 182(14), 3965–3971. <https://doi.org/10.1128/JB.182.14.3965-3971.2000>
- Hu, Z., & Lutkenhaus, J. (2003). A conserved sequence at the C-terminus of MinD is required for binding to the membrane and targeting MinC to the septum. *Molecular Microbiology*, 47(2), 345–355. <https://doi.org/10.1046/j.1365-2958.2003.03321.x>
- Huang, K. C., Meir, Y., & Wingreen, N. S. (2003). Dynamic structures in *Escherichia coli*: spontaneous formation of MinE rings and MinD polar zones. *Proceedings of the National Academy of Sciences of the United States of America*, 100(22), 12724–12728. <https://doi.org/10.1073/pnas.2135445100>
- Huitema, E., Pritchard, S., Matteson, D., Radhakrishnan, S. K., & Viollier, P. H. (2006). Bacterial birth scar proteins mark future flagellum assembly site. *Cell*, 124(5), 1025–1037. <https://doi.org/10.1016/j.cell.2006.01.019>
- Huls, P. G., Vischer, N. O. E., & Woldringh, C. L. (1999). Delayed nucleoid segregation in *Escherichia coli*. *Molecular Microbiology*, 33(5), 959–970. <https://doi.org/10.1046/j.1365-2958.1999.01535.x>
- Ireton, K., Iv, N. W. G., & Grossman, A. D. (1994). *spoOJ* is required for normal chromosome segregation as well as the initiation of sporulation in *Bacillus subtilis*. *Microbiology*, 176(17), 5320–5329. <https://doi.org/10.1128/jb.176.17.5320-5329.1994>
- Jensen, L. J., Kuhn, M., Stark, M., Chaffron, S., Creevey, C., Muller, J., ... von Mering, C. (2009). STRING 8—a global view on proteins and their functional interactions in 630 organisms. *Nucleic Acids Res*, 37(Database issue), D412–6. <https://doi.org/10.1093/nar/gkn760>
- Jensen, M. H., Morris, E. J., & Weitz, D. A. (2015). Mechanics and dynamics of reconstituted cytoskeletal systems. *Biochimica et Biophysica Acta - Molecular Cell Research*, 1853(11), 3038–3042. <https://doi.org/10.1016/j.bbamcr.2015.06.013>
- Juarez, J. R., & Margolin, W. (2010). Changes in the min oscillation pattern before and after cell birth. *Journal of Bacteriology*, 192(16), 4134–4142. <https://doi.org/10.1128/JB.00364-10>
- Katayama, T., Ozaki, S., Keyamura, K., & Fujimitsu, K. (2010). Regulation of the replication cycle: Conserved and diverse regulatory systems for DnaA and *oriC*. *Nature Reviews Microbiology*, 8(3), 163–170. <https://doi.org/10.1038/nrmicro2314>
- Kibbe, W. A. (2007). OligoCalc: An online oligonucleotide properties calculator. *Nucleic Acids Research*. <https://doi.org/10.1093/nar/gkm234>
- Kiekebusch, D., Michie, K. A., Essen, L. O., Löwe, J., & Thanbichler, M. (2012). Localized Dimerization and Nucleoid Binding Drive Gradient Formation by the Bacterial Cell Division Inhibitor MipZ. *Molecular Cell*, 46(3), 245–259. <https://doi.org/10.1016/j.molcel.2012.03.004>
- Kiekebusch, D., & Thanbichler, M. (2014). Spatiotemporal organization of microbial cells by protein concentration gradients. *Trends in Microbiology*, 22(2), 65–73. <https://doi.org/DOI.10.1016/j.tim.2013.11.005>
- Kirov, S. M., Tassell, B. C., Semmler, A. B. T., Donovan, L. A. O., Rabaan, A. A., & Shaw, J. G. (2002). Lateral flagella and swarming motility in *Aeromonas* species. *Journal of Bacteriology*, 184(2), 547–555. <https://doi.org/10.1128/JB.184.2.547>
- Kretschmer, S., & Schwille, P. (2016). Pattern formation on membranes and its role in bacterial cell division. *Current Opinion in Cell Biology*, 38, 52–59. <https://doi.org/10.1016/j.ceb.2016.02.005>

- Król, E., van Kessel, S. P., van Bezouwen, L. S., Kumar, N., Boekema, E. J., & Scheffers, D. J. (2012). *Bacillus subtilis* SepF binds to the C-terminus of FtsZ. *PLoS ONE*, 7(8). <https://doi.org/10.1371/journal.pone.0043293>
- Laemmli, U. K. (1970). Cleavage of Structural Proteins during the Assembly of the Head of Bacteriophage T4. *Nature*, 227(5259), 680–685. <https://doi.org/10.1038/227680a0>
- Lam, H., Schofield, W. B., & Jacobs-Wagner, C. (2006). A landmark protein essential for establishing and perpetuating the polarity of a bacterial cell. *Cell*, 124(5), 1011–1023. <https://doi.org/10.1016/j.cell.2005.12.040>
- Leaver, M., Domínguez-Cuevas, P., Coxhead, J. M., Daniel, R. A., & Errington, J. (2009). Life without a wall or division machine in *Bacillus subtilis*. *Nature*, 457(7231), 849–853. <https://doi.org/10.1038/nature07742>
- Lee, P. S., & Grossman, A. D. (2006). The chromosome partitioning proteins Soj (ParA) and Spo0J (ParB) contribute to accurate chromosome partitioning, separation of replicated sister origins, and regulation of replication initiation in *Bacillus subtilis*. *Molecular Microbiology*, 60(4), 853–869. <https://doi.org/10.1111/j.1365-2958.2006.05140.x>
- Leipe, D. D., Wolf, Y. I., Koonin, E. V., & Aravind, L. (2002). Classification and evolution of P-loop GTPases and related ATPases. *Journal of Molecular Biology*, 317(1), 41–72. <https://doi.org/10.1006/jmbi.2001.5378>
- Letchumanan, V., Chan, K. G., & Lee, L. H. (2014). *Vibrio parahaemolyticus*: A review on the pathogenesis, prevalence, and advance molecular identification techniques. *Frontiers in Microbiology*, 5(DEC), 1–13. <https://doi.org/10.3389/fmicb.2014.00705>
- Letunic, I., & Bork, P. (2018). 20 years of the SMART protein domain annotation resource. *Nucleic Acids Research*. <https://doi.org/10.1093/nar/gkx922>
- Liu, B., Persons, L., Lee, L., & de Boer, P. A. J. (2015). Roles for both FtsA and the FtsBLQ subcomplex in FtsN-stimulated cell constriction in *Escherichia coli*. *Molecular Microbiology*, 95(6), 945–970. <https://doi.org/10.1111/mmi.12906>
- Loose, M., Fischer-F, Riedrich, E., Ries, J., Kruse, K., & Schwille, P. (2008). Spatial Regulators for Bacterial Cell. *Science*, 320(May), 789–792. <https://doi.org/DOI:10.1126/science.1154413>
- Löwe, J., & Amos, L. a. (1998). Crystal structure of the bacterial cell-division protein FtsZ. *Nature*, 391(6663), 203–206. <https://doi.org/10.1038/34472>
- Lu, C., Stricker, J., & Erickson, H. P. (2001). Site-specific mutations of FtsZ--effects on GTPase and in vitro assembly. *BMC Microbiology*, 1, 7. <https://doi.org/10.1186/1471-2180-1-1>
- Lutkenhaus, J., Pichoff, S., & Du, S. (2012). Bacterial cytokinesis: From Z ring to divisome. *Cytoskeleton*, 69(10), 778–790. <https://doi.org/10.1002/cm.21054>
- Lutkenhaus, J., Wolf-Watz, H., & Donachie, W. D. (1980). Organization of genes in the ftsA-envA region of the *Escherichia coli* genetic map and identification of a new fts locus (ftsZ). *Journal of Bacteriology*, 142(2), 615–620. <https://doi.org/10.1016/j.fct.2004.09.005>
- Ma, X., & Margolin, W. (1999). Genetic and functional analyses of the conserved C-terminal core domain of *Escherichia coli* FtsZ. *J Bacteriol*, 181(24), 7531–7544.
- Makino, K., Oshima, K., Kurokawa, K., & Yokoyama, K. (2003). Genome sequence of *Vibrio parahaemolyticus*: a pathogenic mechanism distinct from that of *V. cholerae*. *Lancet*, 361(9359), 743–749.
- McCarter, L. (1999). The multiple identities of *Vibrio parahaemolyticus*. *Journal of Molecular Microbiology and Biotechnology*, 1(1), 51–57.
- McCarter, L., Hilmen, M., & Silverman, M. (1988). Flagellar dynamometer controls swarmer cell differentiation of *V. parahaemolyticus*. *Cell*, 54(3), 345–351. [https://doi.org/10.1016/0092-8674\(88\)90197-3](https://doi.org/10.1016/0092-8674(88)90197-3)
- McCarter, L. L. (2004). Dual flagellar systems enable motility under different circumstances. *Journal of Molecular Microbiology and Biotechnology*. <https://doi.org/10.1159/000077866>
- McCarter, L. L. (2010). Bacterial acrobatics on a surface: swirling packs, collisions, and reversals during swarming. *Journal of Bacteriology*, 192(13), 3246–3248. <https://doi.org/10.1128/JB.00434-10>

- McCarter, L., & Silverman, M. (1989). Iron regulation of swarmer cell differentiation of *Vibrio parahaemolyticus*. *Journal of Bacteriology*, *171*(2), 731–736. <https://doi.org/10.1128/jb.171.2.731-736.1989>
- McCarter, L., & Silverman, M. (1990). Surface induced swarmer cell differentiation of *Vibrio parahaemolyticus*. *Molecular Microbiology*, *4*(7), 1057–1062. <https://doi.org/10.1111/j.1365-2958.1990.tb00678.x>
- Meinhardt, H., & de Boer, P. A. J. (2001). Pattern formation in *Escherichia coli*: A model for the pole-to-pole oscillations of Min proteins and the localization of the division site. *Proceedings of the National Academy of Sciences*, *98*(25), 14202–14207. <https://doi.org/10.1073/pnas.251216598>
- Mercier, R., Domínguez-Cuevas, P., & Errington, J. (2012). Crucial Role for Membrane Fluidity in Proliferation of Primitive Cells. *Cell Reports*, *1*(5), 417–423. <https://doi.org/10.1016/j.celrep.2012.03.008>
- Mercier, R., Petit, M. A., Schbath, S., Robin, S., El Karoui, M., Bocard, F., & Espéli, O. (2008). The MatP/matS Site-Specific System Organizes the Terminus Region of the *E. coli* Chromosome into a Macrodomain. *Cell*, *135*(3), 475–485. <https://doi.org/10.1016/j.cell.2008.08.031>
- Miller, V. L., & Mekalanos, J. J. (1988). A novel suicide vector and its use in construction of insertion mutations: osmoregulation of outer membrane proteins and virulence determinants in *Vibrio cholerae* requires *toxR*. *J Bacteriol*, *170*(6), 2575–2583.
- Modell, J. W., Kambara, T. K., Perchuk, B. S., & Laub, M. T. (2014). A DNA Damage-Induced, SOS-Independent Checkpoint Regulates Cell Division in *Caulobacter crescentus*. *PLoS Biology*, *12*(10). <https://doi.org/10.1371/journal.pbio.1001977>
- Mohammadi, T., Van Dam, V., Sijbrandi, R., Vernet, T., Zapun, A., Bouhss, A., ... Breukink, E. (2011). Identification of FtsW as a transporter of lipid-linked cell wall precursors across the membrane. *EMBO Journal*, *30*(8), 1425–1432. <https://doi.org/10.1038/emboj.2011.61>
- Moriya, S., Rashid, R. A., Rodrigues, C. D. A., & Harry, E. J. (2010). Influence of the nucleoid and the early stages of DNA replication on positioning the division site in *Bacillus subtilis*. *Molecular Microbiology*, *76*(3), 634–647. <https://doi.org/10.1111/j.1365-2958.2010.07102.x>
- Mukherjee, A., Dai, K., & Lutkenhaus, J. (1993). *Escherichia coli* cell division protein FtsZ is a guanine nucleotide binding protein. *Proceedings of the National Academy of Sciences of the United States of America*, *90*(3), 1053–1057. <https://doi.org/10.1073/pnas.90.3.1053>
- Mulder, E., & Woldringh, C. L. (1989). Actively replicating nucleoids influence positioning of division sites in *Escherichia coli* filaments forming cells lacking DNA. *Journal of Bacteriology*, *171*(8), 4303–4314.
- Nam K. Tonthat, Sara L. Milam, Nagababu Chinnam, Travis Whitfill, William Margolin, and M. A. S. (2013). SlmA forms a higher-order structure on DNA that inhibits cytokinetic Z-ring formation over the nucleoid. *Proceedings of the National Academy of Sciences*, *110*(37), 15163–15163. <https://doi.org/10.1073/pnas.1314920110>
- Nielsen, H. J., Ottesen, J. R., Youngren, B., Austin, S. J., & Hansen, F. G. (2006). The *Escherichia coli* chromosome is organized with the left and right chromosome arms in separate cell halves. *Molecular Microbiology*, *62*(2), 331–338. <https://doi.org/10.1111/j.1365-2958.2006.05346.x>
- Niki, H., Yamaichi, Y., & Hiraga, S. (2000). Dynamic organization of chromosomal DNA in *Escherichia coli*. *Genes & Development*, *14*(2), 212–223. <https://doi.org/10.1101/GAD.14.2.212>
- Nogales, E., Wolf, S. G., & Downing, K. H. (1998). Structure of the $\alpha\beta$ tubulin dimer by electron crystallography. *Nature*, *391*(January), 199–204. <https://doi.org/10.1007/1-4020-3920-4>
- Oliva, M. A., Cordell, S. C., & Löwe, J. (2004). Structural insights into FtsZ protofilament formation. *Nature Structural and Molecular Biology*, *11*(12), 1243–1250. <https://doi.org/10.1038/nsmb855>
- Ortiz, C., Natale, P., Cueto, L., & Vicente, M. (2015). The keepers of the ring : regulators of FtsZ assembly. *FEMS Microbiology Reviews*, (August), 1–11. <https://doi.org/10.1093/femsre/fuv040>
- Osawa, M., Anderson, D. E., & Erickson, H. P. (2008). Reconstitution of contractile FtsZ rings in liposomes. *Science*, *320*(5877), 792–794. <https://doi.org/10.1126/science.1154520>
- Osawa, M., Anderson, D. E., & Erickson, H. P. (2009). Curved FtsZ protofilaments generate bending forces on liposome membranes. *EMBO Journal*, *28*(22), 3476–3484. <https://doi.org/10.1038/emboj.2009.277>
- Osawa, M., & Erickson, H. P. (2013). Liposome division by a simple bacterial division machinery.

- Proceedings of the National Academy of Sciences*, 110(27), 11000–11004.
<https://doi.org/10.1073/pnas.1222254110>
- Park, K. T., Dajkovic, A., Wissel, M., Du, S., & Lutkenhaus, J. (2018). MinC and FtsZ mutant analysis provides insight into MinC/ MinD-mediated Z ring disassembly. *Journal of Biological Chemistry*, 293(16), 5834–5846. <https://doi.org/10.1074/jbc.M117.815894>
- Park, K. T., Villar, M. T., Artigues, A., & Lutkenhaus, J. (2017). MinE conformational dynamics regulate membrane binding, MinD interaction, and Min oscillation. *Proceedings of the National Academy of Sciences*, 114(29), 7497–7504. <https://doi.org/10.1073/pnas.1707385114>
- Pende, N., Leisch, N., Gruber-Vodicka, H. R., Heindl, N. R., Ott, J., Den Blaauwen, T., & Bulgheresi, S. (2014). Size-independent symmetric division in extraordinarily long cells. *Nature Communications*, 5. <https://doi.org/10.1038/ncomms5803>
- Pogliano, J., Pogliano, K., Weiss, D. S., Losick, R., & Beckwith, J. (1997). Inactivation of FtsI inhibits constriction of the FtsZ cytokinetic ring and delays the assembly of FtsZ rings at potential division sites. *Proceedings of the National Academy of Sciences of the United States of America*, 94(2), 559–564. <https://doi.org/10.1073/pnas.94.2.559>
- R Development Core Team, R. F. F. S. C. (2008). R: A Language and Environment for Statistical Computing. *R Foundation for Statistical Computing*. <https://doi.org/10.1007/978-3-540-74686-7>
- Raskin, D. M., & de Boer, P. A. (1999a). MinDE-dependent pole-to-pole oscillation of division inhibitor MinC in *Escherichia coli*. *J Bacteriol*, 181(20), 6419–6424. Retrieved from <http://www.ncbi.nlm.nih.gov/pubmed/10515933>
- Raskin, D. M., & de Boer, P. A. (1999b). Rapid pole-to-pole oscillation of a protein required for directing division to the middle of *Escherichia coli*. *Proceedings of the National Academy of Sciences of the United States of America*, 96(April), 4971–4976.
- Raskin, D. M., & de Boer, P. A. (1999c). Rapid pole-to-pole oscillation of a protein required for directing division to the middle of *Escherichia coli*. *Proceedings of the National Academy of Sciences of the United States of America*, 96(9), 4971–4976. <https://doi.org/10.1073/pnas.96.9.4971>
- Raskin, D. M., & De Boer, P. A. J. (1997). The MinE ring: An FtsZ-independent cell structure required for selection of the correct division site in *E. coli*. *Cell*, 91(5), 685–694. [https://doi.org/10.1016/S0092-8674\(00\)80455-9](https://doi.org/10.1016/S0092-8674(00)80455-9)
- RayChaudhuri, D., & Park, J. T. (1992). *Escherichia coli* cell-division gene *ftsZ* encodes a novel GTP-binding protein. *Nature*, 359(6392), 251–254. <https://doi.org/10.1038/359251a0>
- Reinhardt, J. M., & Bardy, S. L. (2018). Partitioning protein ParP directly links chemotaxis to biofilm dispersal in *Pseudomonas aeruginosa*. *bioRxiv*. <https://doi.org/10.1101/330878>
- Rico, A. I., García-Ovalle, M., Palacios, P., Casanova, M., & Vicente, M. (2010). Role of *Escherichia coli* FtsN protein in the assembly and stability of the cell division ring. *Molecular Microbiology*, 76(3), 760–771. <https://doi.org/10.1111/j.1365-2958.2010.07134.x>
- Ringgaard, S., Schirner, K., Davis, B. M., & Waldor, M. K. (2011). A family of ParA-like ATPases promotes cell pole maturation by facilitating polar localization of chemotaxis proteins. *Genes Dev*, 25(14), 1544–1555. <https://doi.org/10.1101/gad.2061811>
- Ringgaard, S., van Zon, J., Howard, M., & Gerdes, K. (2009). Movement and equipositioning of plasmids by ParA filament disassembly. *Proceedings of the National Academy of Sciences*, 106(46), 19369–19374. <https://doi.org/10.1073/pnas.0908347106>
- Ringgaard, S., Zepeda-Rivera, M., Wu, X., Schirner, K., Davis, B. M., & Waldor, M. K. (2014). ParP prevents dissociation of CheA from chemotactic signaling arrays and tethers them to a polar anchor. *Proceedings of the National Academy of Sciences*, 111(2), E255–E264. <https://doi.org/10.1073/pnas.1315722111>
- Sar, N., McCarter, L., Simon, M., & Silverman, M. (1990). Chemotactic control of the two flagellar systems of *Vibrio parahaemolyticus*. *Journal of Bacteriology*, 172(1), 334–341. <https://doi.org/10.1128/jb.172.1.334-341.1990>
- Schindelin, J., Arganda-Carreras, I., Frise, E., Kaynig, V., Longair, M., Pietzsch, T., ... Cardona, A. (2012). Fiji: An open-source platform for biological-image analysis. *Nature Methods*. <https://doi.org/10.1038/nmeth.2019>
- Schofield, W. B., Lim, H. C., & Jacobs-Wagner, C. (2010). Cell cycle coordination and regulation of bacterial

- chromosome segregation dynamics by polarly localized proteins. *EMBO Journal*, 29(18), 3068–3081. <https://doi.org/10.1038/emboj.2010.207>
- Schumacher, D., Bergeler, S., Harms, A., Vonck, J., Huneke-Vogt, S., Frey, E., & Søgaard-Andersen, L. (2017). The PomXYZ Proteins Self-Organize on the Bacterial Nucleoid to Stimulate Cell Division. *Developmental Cell*, 41(3), 299–314.e13. <https://doi.org/10.1016/j.devcel.2017.04.011>
- Schumacher, M. A., & Zeng, W. (2016). Structures of the nucleoid occlusion protein SImA bound to DNA and the C-terminal domain of the cytoskeletal protein FtsZ. *Proceedings of the National Academy of Sciences*, 113(18), 4988–4993. <https://doi.org/10.1073/pnas.1602327113>
- Schwarz, U., Asmus, A., & Frank, H. (1969). Autolytic enzymes and cell division of *Escherichia coli*. *Journal of Molecular Biology*, 41(3), 419–429. [https://doi.org/10.1016/0022-2836\(69\)90285-X](https://doi.org/10.1016/0022-2836(69)90285-X)
- Schweizer, J., Loose, M., Bonny, M., Kruse, K., Monch, I., & Schwille, P. (2012). Geometry sensing by self-organized protein patterns. *Proceedings of the National Academy of Sciences*, 109(38), 15283–15288. <https://doi.org/10.1073/pnas.1206953109>
- Sengupta, S., & Rutenberg, A. (2007). Modeling partitioning of Min proteins between daughter cells after septation in *Escherichia coli*. *Physical Biology*, 4(3), 145–153. <https://doi.org/10.1088/1478-3975/4/3/001>
- Sham, L. T., Butler, E. K., Lebar, M. D., Kahne, D., Bernhardt, T. G., & Ruiz, N. (2014). MurJ is the flippase of lipid-linked precursors for peptidoglycan biogenesis. *Science*, 345(6193), 220–222. <https://doi.org/10.1126/science.1254522>
- Shebelut, C. W., Guberman, J. M., van Teeffelen, S., Yakhnina, A. a, & Gitai, Z. (2010). Caulobacter chromosome segregation is an ordered multistep process. *Proceedings of the National Academy of Sciences of the United States of America*, 107(32), 14194–14198. <https://doi.org/10.1073/pnas.1005274107>
- Shen, B., & Lutkenhaus, J. (2009). The conserved C-terminal tail of FtsZ is required for the septal localization and division inhibitory activity of MinCC/MinD. *Molecular Microbiology*, 72(2), 410–424. <https://doi.org/10.1111/j.1365-2958.2009.06651.x>
- Shen, B., & Lutkenhaus, J. (2010). Examination of the interaction between FtsZ and MinCN in *E. coli* suggests how MinC disrupts Z rings. *Molecular Microbiology*, 75(5), 1285–1298. <https://doi.org/10.1111/j.1365-2958.2010.07055.x>
- Shinoda, S., & Okamoto, K. (1977). Formation and function of *Vibrio parahaemolyticus* Formation and Function of *Vibrio parahaemolyticus* Lateral Flagella. *Microbiology*, 129(3), 1266–1271.
- Shiomi, D., & Margolin, W. (2007). The C-terminal domain of MinC inhibits assembly of the Z ring in *Escherichia coli*. *Journal of Bacteriology*, 189(1), 236–243. <https://doi.org/10.1128/JB.00666-06>
- Skarstad, K., Steen, H. B., & Boye, E. (1985). *Escherichia coli* DNA distributions measured by flow cytometry and compared with theoretical computer simulations. *Journal of Bacteriology*, 163(2), 661–668. Retrieved from <http://jb.asm.org.ep.fjernadgang.kb.dk/content/163/2/661.full.pdf>
- Specht, M., Dempwolff, F., Schätzle, S., Thomann, R., & Waidner, B. (2013). Localization of FtsZ in *helicobacter pylori* and consequences for cell division. *Journal of Bacteriology*, 195(7), 1411–1420. <https://doi.org/10.1128/JB.01490-12>
- Spratt, B. G. (1975). Distinct penicillin binding proteins involved in the division, elongation, and shape of *Escherichia coli* K12. *Proceedings of the National Academy of Sciences*, 72(8), 2999–3003. <https://doi.org/10.1073/pnas.72.8.2999>
- Srivastava, P., Fekete, R. A., & Chattoraj, D. K. (2006). Segregation of the replication terminus of the two *Vibrio cholerae* chromosomes. *Journal of Bacteriology*, 188(3), 1060–1070. <https://doi.org/10.1128/JB.188.3.1060-1070.2006>
- Stewart, B. J., & McCarter, L. L. (2003). Lateral flagellar gene system of *Vibrio parahaemolyticus*. *Journal of Bacteriology*, 185(15), 4508–4518. <https://doi.org/10.1128/JB.185.15.4508-4518.2003>
- Stokke, C., Waldminghaus, T., & Skarstad, K. (2011). Replication patterns and organization of replication forks in *Vibrio cholerae*. *Microbiology*, 157(3), 695–708. <https://doi.org/10.1099/mic.0.045112-0>
- Sullivan, N. L., Marquis, K. A., & Rudner, D. Z. (2009). Recruitment of SMC by ParB-parS Organizes the Origin Region and Promotes Efficient Chromosome Segregation. *Cell*, 137(4), 697–707. <https://doi.org/10.1016/j.cell.2009.04.044>

- Sundararajan, K., & Goley, E. D. (2017). The intrinsically disordered C-terminal linker of FtsZ regulates protofilament dynamics and superstructure in vitro. *Journal of Biological Chemistry*, 292(50), 20509–20527. <https://doi.org/10.1074/jbc.M117.809939>
- Sundararajan, K., Miguel, A., Desmarais, S. M., Meier, E. L., Casey Huang, K., & Goley, E. D. (2015). The bacterial tubulin FtsZ requires its intrinsically disordered linker to direct robust cell wall construction. *Nature Communications*, 6, 1–14. <https://doi.org/10.1038/ncomms8281>
- Surovtsev, I. V., Campos, M., & Jacobs-Wagner, C. (2016). DNA-relay mechanism is sufficient to explain ParA-dependent intracellular transport and patterning of single and multiple cargos. *Proceedings of the National Academy of Sciences*, 113(46), E7268–E7276. <https://doi.org/10.1073/pnas.1616118113>
- Surovtsev, I. V., & Jacobs-Wagner, C. (2018). Subcellular Organization: A Critical Feature of Bacterial Cell Replication. *Cell*, 172(6), 1271–1293. <https://doi.org/10.1016/j.cell.2018.01.014>
- Szeto, J., Eng, N. F., Acharya, S., Rigden, M. D., & Dillon, J. A. R. (2005). A conserved polar region in the cell division site determinant MinD is required for responding to MinE-induced oscillation but not for localization within coiled arrays. *Research in Microbiology*, 156(1), 17–29. <https://doi.org/10.1016/j.resmic.2004.07.009>
- Szeto, T. H., Rowland, S. L., Habrukowich, C. L., & King, G. F. (2003). The MinD membrane targeting sequence is a transplantable lipid-binding helix. *Journal of Biological Chemistry*, 278(41), 40050–40056. <https://doi.org/10.1074/jbc.M306876200>
- Takekawa, N., Kwon, S., Nishioka, N., Kojima, S., & Homma, M. (2016). HubP, a polar landmark protein, regulates flagellar number by assisting in the proper polar localization of FlhG in *Vibrio alginolyticus*. *Journal of Bacteriology*, 198(22), 3091–3098. <https://doi.org/10.1128/JB.00462-16>
- Taschner, P. E., Huls, P. G., Pas, E., & Woldringh, C. L. (1988). Division behavior and shape changes in isogenic ftsZ, ftsQ, ftsA, pbpB, and ftsE cell division mutants of *Escherichia coli* during temperature shift experiments. *Journal of Bacteriology*, 170(4), 1533–1540. <https://doi.org/10.1128/jb.170.4.1533-1540.1988>
- Thanbichler, M., & Shapiro, L. (2006). MipZ, a spatial regulator coordinating chromosome segregation with cell division in *Caulobacter*. *Cell*, 126(1), 147–162. <https://doi.org/10.1016/j.cell.2006.05.038>
- Tonthat, N. K., Arold, S. T., Pickering, B. F., Van Dyke, M. W., Liang, S., Lu, Y., ... Schumacher, M. A. (2011). Molecular mechanism by which the nucleoid occlusion factor, SlmA, keeps cytokinesis in check. *The EMBO Journal*, 30(1), 154–164. <https://doi.org/10.1038/emboj.2010.288>
- Toro, E., Hong, S. H., McAdams, H. H., & Shapiro, L. (2008). *Caulobacter* requires a dedicated mechanism to initiate chromosome segregation. *Proc Natl Acad Sci U S A*, 105(40), 15435–15440. <https://doi.org/10.1073/pnas.0807448105>
- Tostevin, F., & Howard, M. (2006). A stochastic model of Min oscillations in *Escherichia coli* and Min protein segregation during cell division. *Physical Biology*, 3(1), 1–12. <https://doi.org/10.1088/1478-3975/3/1/001>
- Treuner-Lange, A., Aguiluz, K., van der Does, C., G??mez-Santos, N., Harms, A., Schumacher, D., ... S??gaard-Andersen, L. (2013). PomZ, a ParA-like protein, regulates Z-ring formation and cell division in *Myxococcus xanthus*. *Molecular Microbiology*, 87(2), 235–253. <https://doi.org/10.1111/mmi.12094>
- Tsang, M. J., & Bernhardt, T. G. (2015). A role for the FtsQLB complex in cytokinetic ring activation revealed by an ftsL allele that accelerates division. *Molecular Microbiology*, 95(6), 925–944. <https://doi.org/10.1111/mmi.12905>
- Turner, R. D., Ratcliffe, E. C., Wheeler, R., Golestanian, R., Hobbs, J. K., & Foster, S. J. (2010). Peptidoglycan architecture can specify division planes in *Staphylococcus aureus*. *Nature Communications*, 1(3), 1–9. <https://doi.org/10.1038/ncomms1025>
- Valens, M., Penaud, S., Rossignol, M., Cornet, F., & Boccard, F. (2004). Macrodome organization of the *Escherichia coli* chromosome. *EMBO Journal*, 23(21), 4330–4341. <https://doi.org/10.1038/sj.emboj.7600434>
- Varma, A., Huang, K. C., & Young, K. D. (2008). The Min system as a general cell geometry detection mechanism: Branch lengths in Y-shaped *Escherichia coli* cells affect Min oscillation patterns and division dynamics. *Journal of Bacteriology*, 190(6), 2106–2117. <https://doi.org/10.1128/JB.00720-07>
- Viollier, P. H., Thanbichler, M., McGrath, P. T., West, L., Meewan, M., McAdams, H. H., & Shapiro, L. (2004). Rapid and sequential movement of individual chromosomal loci to specific subcellular locations during bacterial DNA replication. *Proceedings of the National Academy of Sciences of the United States of*

- America, 101(25), 9257–9262. <https://doi.org/10.1073/pnas.0402606101>
- Wang, X., Huang, J., Mukherjee, A., Cao, C., & Lutkenhaus, J. (1997). Analysis of the interaction of FtsZ with itself. *Journal of Bacteriology*, 179(17), 5551–5559. <https://doi.org/10.1128/jb.179.17.5551-5559.1997>
- Wang, X., Liu, X., Possoz, C., & Sherratt, D. J. (2006). The two Escherichia coli chromosome arms locate to separate cell halves. *Journal of Bacteriology*, 179(17), 5551–5559. <https://doi.org/10.1128/jb.179.17.5551-5559.1997>
- Wang, X., Montero Llopis, P., & Rudner, D. Z. (2014). Bacillus subtilis chromosome organization oscillates between two distinct patterns. *Proceedings of the National Academy of Sciences*, 111(35), 12877–12882. <https://doi.org/10.1073/pnas.1407461111>
- Wehrens, M., Ershov, D., Rozendaal, R., Walker, N., Schultz, D., Kishony, R., ... Tans, S. J. (2018). Size Laws and Division Ring Dynamics in Filamentous Escherichia coli cells. *Current Biology*, 28(6), 972–978.e5. <https://doi.org/10.1016/j.cub.2018.02.006>
- Wickham, H. (2009). Hadley Wickham. *Media*, 35(July), 211. <https://doi.org/10.1007/978-0-387-98141-3>
- Willemse, J., Borst, J. W., Waal, E. De, Willemse, J., Borst, J. W., Waal, E. De, ... Wezel, G. P. Van. (2011). Positive control of cell division : FtsZ is recruited by SsgB during sporulation of Streptomyces Positive control of cell division : FtsZ is recruited by SsgB during sporulation of Streptomyces, 89–99. <https://doi.org/10.1101/gad.600211>
- Williams, B., Bhat, N., Chien, P., & Shapiro, L. (2014). ClpXP and ClpAP proteolytic activity on divisome substrates is differentially regulated following the Caulobacter asymmetric cell division. *Molecular Microbiology*, 93(5), 853–866. <https://doi.org/10.1111/mmi.12698>
- Woldringh, C. L. (1989). ROLE OF THE NUCLEOID IN THE TOPOREGULATION OF DIVISION.
- Wu, L. J., & Errington, J. (2004). Coordination of cell division and chromosome segregation by a nucleoid occlusion protein in Bacillus subtilis. *Cell*, 117(7), 915–925. <https://doi.org/10.1016/j.cell.2004.06.002>
- Wu, L. J., Ishikawa, S., Kawai, Y., Oshima, T., Ogasawara, N., & Errington, J. (2009). Noc protein binds to specific DNA sequences to coordinate cell division with chromosome segregation. *EMBO Journal*, 28(13), 1940–1952. <https://doi.org/10.1038/emboj.2009.144>
- Wu, W., Park, K. T., Holyoak, T., & Lutkenhaus, J. (2011). Determination of the structure of the MinD-ATP complex reveals the orientation of MinD on the membrane and the relative location of the binding sites for MinE and MinC. *Molecular Microbiology*, 79(6), 1515–1528. <https://doi.org/10.1111/j.1365-2958.2010.07536.x>
- Yamaichi, Y., Bruckner, R., Ringgaard, S., Möll, A., Ewen Cameron, D., Briegel, A., ... Waldor, M. K. (2012). A multidomain hub anchors the chromosome segregation and chemotactic machinery to the bacterial pole. *Genes and Development*, 26(20), 2348–2360. <https://doi.org/10.1101/gad.199869.112>
- Yamaichi, Y., Fogel, M. A., & Waldor, M. K. (2006). par genes and the pathology of chromosome loss in Vibrio cholerae.
- Yamaichi, Y., Fogel, M. a, McLeod, S. M., Hui, M. P., & Waldor, M. K. (2007a). Distinct centromere-like parS sites on the two chromosomes of Vibrio spp. *Journal of Bacteriology*, 189(14), 5314–5324. <https://doi.org/10.1128/JB.00416-07>
- Yamaichi, Y., Fogel, M., & Waldor, M. K. (2007b). par genes and the pathology of chromosome loss in Vibrio cholerae. *Proc Natl Acad Sci U S A*, 104(2), 630–635. <https://doi.org/10.1073/pnas.0608341104>
- Yang, X., Lyu, Z., Miguel, A., McQuillen, R., Huang, K. K. C., & Xiao, J. (2016). GTPase activity-coupled treadmilling of the bacterial tubulin FtsZ organizes septal cell-wall synthesis. *Science*, 747(February), 744–747. <https://doi.org/10.1101/077610>
- Youngren, B., Nielsen, H. J., Jun, S., & Austin, S. (2014). The multifork Escherichia coli chromosome is a self-duplicating and self-segregating thermodynamic ring polymer. *Genes and Development*, 28(1), 71–84. <https://doi.org/10.1101/gad.231050.113>
- Yu, X. C., & Margolin, W. (1999). FtsZ ring clusters in min and partition mutants: Role of both the Min system and the nucleoid in regulating FtsZ ring localization. *Molecular Microbiology*, 32(2), 315–326. <https://doi.org/10.1046/j.1365-2958.1999.01351.x>
- Yuan, J., Jin, F., Glatter, T., & Sourjik, V. (2017). Osmosensing by the bacterial PhoQ/PhoP two-component system. *Proceedings of the National Academy of Sciences*, E10792–E10798.

<https://doi.org/10.1073/pnas.1717272114>

Zhang, Y., Werling, U., & Edelman, W. (2012). SLiCE: A novel bacterial cell extract-based DNA cloning method. *Nucleic Acids Research*, *40*(8), 1–10. <https://doi.org/10.1093/nar/gkr1288>

Zhou, H., & Lutkenhaus, J. (2005). MinC mutants deficient in MinD- and DicB-mediated cell division inhibition due to loss of interaction with MinD, DicB, or a septal component. *Journal of Bacteriology*, *187*(8), 2846–2857. <https://doi.org/10.1128/JB.187.8.2846-2857.2005>

Zieske, K., & Schwille, P. (2013). Reconstitution of pole-to-pole oscillations of min proteins in microengineered polydimethylsiloxane compartments. *Angewandte Chemie - International Edition*, *52*(1), 459–462. <https://doi.org/10.1002/anie.201207078>

Zieske, K., & Schwille, P. (2014). Reconstitution of self-organizing protein gradients as spatial cues in cell-free systems. *eLife*, *3*(e03949), 1–19. <https://doi.org/10.7554/eLife.03949>

ACKNOWLEDGEMENTS

The last 4 years had been a true roller-coaster ride. Looking back, I almost cannot believe that I survived the graduate life! It would not have been possible without the love, motivation and guidance of a whole bunch of lovely people.

Firstly, I thank Dr. Simon Ringgaard, for entrusting me with this project. Thank you very much for all the fruitful discussions and guidance during the past four years. If at all my research has contributed anything to the scientific field, it is with your support. Thank you!

Ale, Rehab and Petra, I don't know the right words to thank you guys for being the wonderful people you are. Ale, you are one of a kind! The dedication, hardwork, craziness...I could go on! Most amazingly, you are a hell of a friend! I am so glad that this graduate life paved the way for both of us to come all the way from two corners of the world, so that I could befriend you. Rehab, I can already hear you complain because I didn't write about you first. It is just because this is the order I met you guys ;) You are the most amazing multi-tasker I have met in all these years! I would dearly miss all the moments we spent making fun of you. Thank you for showing me how to keep going forward even when all the odds are against you!

Petra! You are my magic genie! You have always solved all my worries. All the stories and advices of wisdom you passed on have changed for good the way I looked at life and people. I am sure I could never meet another Petra on this planet! Wherever I go, I will fondly cherish our times together.

Jan, thank you so much for being a great friend whom I could always count on. I would never forget your love for wasps. I know you will hate me for bringing it up, again! :D Shankar and Carolina, I wish we had met sooner. Nevertheless you guys made every single day in the lab more fun and bearable. Stephan, Barbara, Karo, Marco-in spite of the short times you guys spent in the Ringgaard lab, all the days we spent together are close to my heart and will be cherished forever. Especially Barbara, I am so proud of the researcher you have become.

Emöke, Dorota, Yacine, Andrea, Tristan, Maria, Lin, Jörg...the list of people who helped me in various stages of my doctoral research is way too long. I extend my sincere appreciation to you guys for sparing your time for me.

All the past and present staff of Max Planck Institute for Terrestrial Microbiology, thank you all for your support and assistance. Our awesome IT support team, a big thanks to you! Life here would have been much difficult without your help.

Dear Reinhard, your hearty smile and radiant energy have always been a motivation. I am very grateful for all the help you extended since my day 1 here. You will be missed! I would also like to extend my sincere acknowledgement to the past and present MPI

international office-Simone Hain and Zrinka Gattin. You guys made the paperwork, and hence my life, so much easier! Thank you!

My dear friends from IISER, in spite of the distance, time zones and your busy schedule, you guys have always stayed in touch. Our Skype sessions and hangouts were real stress busters-Thank you ☺

Dr. Sunish Radhakrishnan, your words of advice and encouragement helped me overcome some of the most difficult periods of my graduate life. You are the one who paved my interest for Microbiology and who instilled the confidence in me to attempt this doctoral research. You continue to be a big source of inspiration and someone whom I count on for inputs. I am glad and proud that I was your student. Thank you!

And finally, my heartfelt gratitude to the people in my life who stay by my side no matter what. I don't know the language to pen down my love and appreciation for you ♥

CURRICULUM VITAE

SAMADA MURALEEDHARAN

DATE OF BIRTH 09.02.1991

NATIONALITY INDIAN

EDUCATION

- Oct 2014-Oct 2018 **PhD (Dr.rer.nat)**
Max Planck Institute for Terrestrial Microbiology, Marburg &
Philipps Universität Marburg, Germany.
Doctoral thesis: Understanding cell division and its regulation in
the human pathogenic bacterium, *Vibrio parahaemolyticus*
- May 2013-May 2014 **Master thesis:** A genetic screen to analyze the asymmetric
spatial regulation of SpmX in *Caulobacter crescentus*
- Aug 2009-May 2014 **Dual degree of Bachelor of Science-Master of Science**
Indian Institute of Science Education and Research (IISER)
Thiruvananthapuram, India.
Major: Biological Sciences
Minor: Chemical Sciences

PUBLICATIONS

Muraleedharan, S., Freitas, C., Mann, P., Glatter, T. and Ringgaard, S. (2018). A cell length-dependent transition in MinD-dynamics promotes a switch in division-site placement and preservation of proliferating elongated *Vibrio parahaemolyticus* swarmer cells. *Molecular Microbiology* 109(3): 365-384

Muraleedharan, S., Heering, J. and Ringgaard, S. ParA-like protein, ParC regulates cell division in swarmer cells of *Vibrio parahaemolyticus* (in preparation).

Kumar, L., **Muraleedharan, S.** and Radhakrishnan, S. K. Dissection of a signaling mechanism that couples polar structural morphogenesis to cell division in *Caulobacter crescentus*. (in preparation).

____. _____. _____, Marburg

ERKLÄRUNG

Hermit versichere ich, dass ich die vorliegende Dissertation mit dem **Titel „Understanding cell division and its regulation in the human pathogenic bacterium, *Vibrio parahaemolyticus*“** selbstständig verfasst, keine anderen als die Text angegebenen Hilfsmittel verwendet und sämtliche Stellen, die im Wortlaut oder dem Sinn nach anderen Werken entnommen sind, mit Quellenangaben kenntlich gemachth habe.

Die Dissertation wurde in der jetzigen oder einer ähnlichen Form noch bei keiner anderen Hochschule eingereicht und hat noch keinen sonstigen Prüfungswegjen gedient.

Ort, Datum

Samada Muraleedharan

EINVERSTÄNDNISERKLÄRUNG

Ich erkläre mich dem einverstanden, dass die vorliegende Dissertation,

**„ Understanding cell division and its regulation in the human pathogenic
bacterium, *Vibrio parahaemolyticus* “**

in Bibliotheken allgemein zugänglich gemacht wird. Dazu gehört, dass sie

- von der Bibliothek der Einrichtung, in der meine Dissertation angefertigt wurde, zur Benutzung in ihren Räumen bereitgehalten wird;
- in konventionellen und maschinenlesbaren Katalogen, Verzeichnissen und Datenbanken verzeichnet wird;
- im Rahmen der urheberrechtlichen Bestimmungen für Kopierzwecke benutzt werden kann.

Marburg, den ____ . ____ . ____

Samada Muraleedharan

Dr. Simon Ringgaard